

INFORMATION TO USERS

This manuscript has been reproduced from the microfilm master. UMI films the text directly from the original or copy submitted. Thus, some thesis and dissertation copies are in typewriter face, while others may be from any type of computer printer.

The quality of this reproduction is dependent upon the quality of the copy submitted. Broken or indistinct print, colored or poor quality illustrations and photographs, print bleedthrough, substandard margins, and improper alignment can adversely affect reproduction.

In the unlikely event that the author did not send UMI a complete manuscript and there are missing pages, these will be noted. Also, if unauthorized copyright material had to be removed, a note will indicate the deletion.

Oversize materials (e.g., maps, drawings, charts) are reproduced by sectioning the original, beginning at the upper left-hand corner and continuing from left to right in equal sections with small overlaps.

Photographs included in the original manuscript have been reproduced xerographically in this copy. Higher quality 6" x 9" black and white photographic prints are available for any photographs or illustrations appearing in this copy for an additional charge. Contact UMI directly to order.

**ProQuest Information and Learning
300 North Zeeb Road, Ann Arbor, MI 48106-1346 USA
800-521-0600**

UMI[®]

The Paleomagnetic Field's Long-term Mean Intensity and
Secular Variation

Rainer Heller

A dissertation submitted in partial fulfillment of
the requirements for the degree of

Doctor of Philosophy

University of Washington

2001

Program Authorized to Offer Degree: Department of Earth and Space Sciences

UMI Number: 3036479

**Copyright 2001 by
Heller, Rainer**

All rights reserved.

UMI[®]

UMI Microform 3036479

**Copyright 2002 by ProQuest Information and Learning Company.
All rights reserved. This microform edition is protected against
unauthorized copying under Title 17, United States Code.**

**ProQuest Information and Learning Company
300 North Zeeb Road
P.O. Box 1346
Ann Arbor, MI 48106-1346**

©Copyright 2001

Rainer Heller

In presenting this dissertation in partial fulfillment of the requirements for the Doctorial degree at the University of Washington, I agree that the Library shall make its copies freely available for inspection. I further agree that extensive copying of this thesis is allowable only for scholarly purposes, consistent with "fair use" as prescribed in the U.S. Copyright Law. Requests for copying or reproduction of this dissertation may be referred to University Microfilms, 1490 Eisenhower Place, P.O. Box 975, Ann Arbor, MI 48106, to whom the author has granted "the right to reproduce and sell (a) copies of the manuscript in microform and/or (b) printed copies of the manuscript made from microform."

Signature Rainier Helle

Date Dec 20, 01

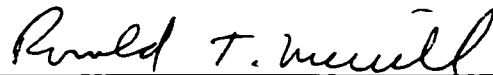
University of Washington
Graduate School

This is to certify that I have examined this copy of a doctoral dissertation by

Rainer Heller

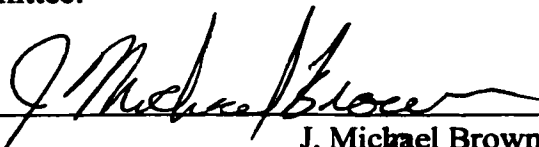
and have found that it is complete and satisfactory in all respects,
and that any and all revisions required by the final
examining committee have been made.

Chair of Supervisory Committee:

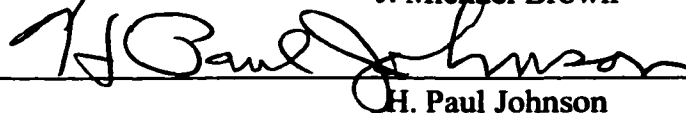


Ronald T. Merrill

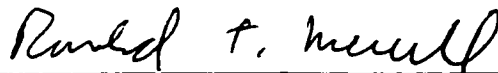
Reading Committee:



J. Michael Brown



H. Paul Johnson



Ronald T. Merrill

Date: Dec 18, 2001

University of Washington

Abstract

The Paleomagnetic Field's Long-term Mean Intensity and Secular
Variation

by Rainer Heller

Chair of Supervisory Committee

Professor Ronald T. Merrill
Department of Earth and Space Sciences

VGP and VDM data are widely used in paleomagnetism to describe paleofield behavior, during times of stable magnetic polarity as well as during reversal transitions. Both of these concepts neglect non-dipole fields and, thus, the presence of non-dipole fields will lead to uncertainties. We introduce a new method, based on geomagnetic intensities, to calculate what percentage of the field is due to non-dipole fields, and find a value of 20–25% for the present and 17–18% a century ago. A model, based on the present field, is then used to investigate how VGP and VDM are affected by a relative increase of the non-dipole field. For a decreasing dipole, the VGP scatter increases while, surprisingly, the VDM scatter generally does not. The spatial distribution of VGP is used to simulate a magnetic reversal transition. There is large spatial variation in transitional VGP suggesting that reversal transitions and their duration, if defined by VGP latitude, depend on location; furthermore, the Brunhes reverse VGP are unlikely to have occurred from a simple reduction of the dipole moment with all other factors kept invariant.

An existing paleointensity database is expanded by about 30% and used to explore

questions regarding the long-term paleointensity and paleosecular variation during the last 320 Myr. We introduce a method to use VDM scatter as a proxy for long-term paleosecular variation from intensities, which might help to constrain geodynamo modeling. An analysis of the VDM data suggests a correlation between the mean intensity and the VDM scatter which could be due either to a bias in the data (e.g. a rock magnetic artifact) or reflect true paleofield behavior. We find evidence for bimodality in the evolution of the VDM histograms. Surprisingly, the two peaks are almost constant with time, at around $4\text{--}5 \times 10^{22} \text{ Am}^2$ and a value close to the present field. The bimodality might be the result of paleofield behavior, suggesting the presence of local energy minimum (LEM) states in the geodynamo, or could be due to a bias in the data. At present we cannot distinguish between these two possibilities.

TABLE OF CONTENTS

List of Figures	iv
Chapter 1: Introduction	1
1.1 Geomagnetic and Paleomagnetic Data	2
1.2 Paleointensity Methods	5
1.2.1 The Thellier Method	6
1.2.2 The Shaw Method	8
1.3 Comparing Paleomagnetic Directions and Intensities from Different Locations	10
1.4 Paleosecular Variation and the Mean Paleointensity	11
Chapter 2: Non-dipole Field Ratio and Intensity and Directional Scatter for a Decreasing Dipole	15
2.1 Summary	15
2.2 Introduction	15
2.3 A Non-Dipole Field Ratio from Intensities	16
2.4 VGP and VDM Scatter as a Function of Dipole Intensity	20
2.5 Discussion and Conclusions	26
Chapter 3: The Variation of Intensity of Earth's Magnetic Field with Time	29
3.1 Summary	29
3.2 Introduction	29

3.3	Rock Magnetism: a Lesson from Mineralogy	33
3.4	The Database	37
3.5	Data Analyses and Results	40
3.6	Discussion	44
3.7	Conclusions	48
 Chapter 4: Short-term and Long-term Variation of the Intensity of Earth's Magnetic Field		50
4.1	Summary	50
4.2	Introduction	50
4.3	Paleomagnetic Proxies for Secular Variation	53
4.4	Data Analyses	57
4.5	Potential Statistical Artifacts	58
4.6	Paleointensity Variation	63
4.7	Interpretations	68
4.8	Conclusions	71
 Chapter 5: Conclusions		72
 Chapter 6: Future Research		79
 Bibliography		84
 Appendix A: Kolmogorov-Smirnov Tests		95
 Appendix B: Code for Rotating a Given Magnetic Field in Spherical Coordinates		97
 Appendix C: Kolmogorov-Smirnov Two-sample Test Results		111

**Appendix D: VDM Distributions and Bimodal and Unimodal Mean
VDM**

120

LIST OF FIGURES

2.1	Non-dipole field ratios during the last century	19
2.2	Non-dipole field ratios for a decreasing dipole and constant non-dipole field	22
2.3	Global VGP scatter σ_{VGP} for a decreasing dipole and constant non-dipole field	23
2.4	Global distribution of VGP for constant non-dipole field and variable dipole strength	24
2.5	VDM and VADM means for a decreasing dipole and constant non-dipole field	25
2.6	VDM and VADM scatter for a decreasing dipole and constant non-dipole field	27
3.1	Mean paleointensity models	32
3.2	Solvus and Néel temperature for the magnetite-ulvöspinel system . .	35
3.3	Spatial and temporal distribution of VDM data	41
3.4	Long-term paleointensity means for 0–320 Ma	42
3.5	Distribution of VDM data with ages between 0–5 Ma and 5–320 Ma .	44
3.6	VADM data distribution for database 2	45
3.7	Distribution of VDM data with ages between 5 and 65 Ma from database 1	48
4.1	VGP scatter σ_{VGP} for a decreasing dipole and constant non-dipole field	54
4.2	Global distribution of VGP for constant non-dipole field and variable dipole strength	55

4.3	VDM scatter for a decreasing dipole and constant non-dipole field . .	57
4.4	Means and standard deviations of VDM data as a function of time for 0–320 Ma	59
4.5	Triangular distribution as approximation for a zero-bound distribution	61
4.6	Monte Carlo procedure to test whether $\mu^2 = k\sigma^2$ is a statistical artifact	62
4.7	Evolution of VDM data distribution for ages 5–320 Ma	65
4.8	Mean paleointensity as a function of time for 0–320 Ma	66
4.9	Mean paleointensity and scatter for unimodal normal distributions and unimodal and bimodal distributions	67
5.1	Long-term mean paleointensity, PSVI, reversal rate and directional PSV	75
6.1	Arai plot with ‘concave’ NRM–TRM curve	81
6.2	Spences Bridge intensity data	82
C.1	Kolmogorov-Smirnov two-sample test for Thellier and Shaw data with ages between 5–320 Ma	113
C.2	Kolmogorov-Smirnov two-sample test for Thellier and Shaw data with ages between 0–5 Ma	114
C.3	Kolmogorov-Smirnov two-sample test for Thellier and Shaw data with ages between 5–65 Ma	115
C.4	Kolmogorov-Smirnov two-sample test for Thellier data with and with- out pTRM checks and ages between 5–320 Ma	116
C.5	Kolmogorov-Smirnov two-sample test for Thellier data with and with- out pTRM checks and ages between 0–5 Ma	117
C.6	Kolmogorov-Smirnov two-sample test for Thellier data with and with- out pTRM checks and ages between 5–65 Ma	118

C.7	Kolmogorov-Smirnov two-sample test for VDM data from the Kiaman and the KNS	119
D.1	Evolution of VDM data distribution for ages 5–320 Ma	121
D.2	Evolution of VDM data distribution for ages 5–320 Ma, $N_{\min} = 50$, $\Delta t_{\min} = 40$ Myr	122
D.3	Evolution of VDM data distribution for ages 0–320 Ma, $\Delta t = 20$ Myr	123
D.4	Evolution of VDM data distribution for ages 0–320 Ma, $\Delta t = 40$ Myr	124
D.5	Individual VDM data and corresponding age distributions 1–4	125
D.6	Individual VDM data and corresponding age distributions 5–8	126
D.7	Individual VDM data and corresponding age distributions 9–12 . . .	127
D.8	Individual VDM data and corresponding age distributions 13–16 . . .	128
D.9	Individual VDM data and corresponding age distributions 17	129

ACKNOWLEDGMENTS

I would like to thank Ron Merrill for his inspiration and enthusiasm – and for many stimulating, exciting and often interdisciplinary discussions. I am particularly grateful for his support during the year when my father was ill. And I would like to thank my wife Corey for her love and friendship, for the many sacrifices she made, and for her unrelenting support throughout.

DEDICATION

**To the memory of my father
and
the promise of my son**

Chapter 1

INTRODUCTION

Magnus magnes ipse est globus terrestris.

(W. Gilbert, *De Magnete*, 1600)

Centuries of intense research since the days of Gilbert have provided us with a wealth of knowledge of our planet's magnetic field, with progress being made on both the theoretical as well as the experimental front, and, more recently, through computer modeling. The field of study has grown to such an extent that several subfields have emerged, including geomagnetism, the study of the origin, history and properties of Earth's magnetic field, paleomagnetism, the study of the magnetization of ancient rocks and their interpretation in terms of plate tectonics and properties of the paleomagnetic field, rock magnetism, the study of the origin, stability and properties of magnetization in rocks, and even more curiously, biomagnetism, the study of magnetism in and its use by organisms. The research presented in this thesis is concerned with questions in three of these, geomagnetism, paleomagnetism and rock magnetism. Chapter 2 introduces a new method to calculate the ratio of non-dipole to total field, based on intensities, and investigates some of the limitations paleomagnetists should be aware of when using virtual dipole moments (VDM) and virtual geomagnetic poles (VGP) to compare paleomagnetic intensities and directions from different sampling localities. In chapter 3, we present a new paleointensity database and use it to investigate long-term trends and statistical distributions of paleointensity data spanning the past 320 Myr. We contend that absolute paleointensity estimates obtained from

submarine basaltic glasses (SBG) are likely to be systematically biased toward low values and provide a good lower bound for the paleointensity, and evaluate paleointensity models put forward in the past (e.g., *Prévot et al.*, 1990; *Selkin and Tauze*, 2000; *Tarduno et al.*, 2001) in light of the new database. Chapter 4 extends the concepts of chapter 3 and introduces a method to estimate long-term paleosecular variation from paleointensities. Averaging paleointensity data over several tens of millions of years we find persistent bimodal distributions during the Cenozoic but not during the Mesozoic and discuss possible interpretations. Chapters 2 to 4 evolved as individual projects and have the format of papers. This necessitates the use of appendices in cases when for this dissertation more detailed information is required. Furthermore, some minor repetition will be caused by the fact that some of the results from chapter 2 are used in chapter 4. In the remainder of this chapter I will give an overview of where this research fits into the bigger framework of the field and describe the more relevant concepts necessary for its understanding.

1.1 Geomagnetic and Paleomagnetic Data

A multitude of different sources of information on the geomagnetic and paleomagnetic field is available to geomagnetists, each having their advantages and limitations. The following description of the kinds of data most commonly used in studying Earth's magnetic field contains many generalities and oversimplifications. However, its purpose is to provide a brief overview of the data and to describe where the paleointensity data used in this dissertation fit into the broader perspective. Earth's magnetic field, being a time-variable three-dimensional vector field, is fully characterized by its intensity and direction at a given location and at a specified time. Paleomagnetists and geomagnetists typically use surface spherical harmonics with time-dependent Gauss coefficients to describe the field (for more details on this, see, for example, *Merrill et al.* (1996)). Obviously, the higher the desired precision the more data are required.

Broadly speaking, the farther back in time one ventures the sparser become the data and the more difficult their interpretation.

The data available to geomagnetists can be broadly classified into two categories: direct and indirect observations. Today, direct measurements of Earth's magnetic field are made continuously by satellite and fixed magnetic observatories on land, as well as by magnetic surveys, permitting a detailed description of the present field as well as the determination not only of the field in historical times but also the evolution of both dipole and non-dipole fields over this period. Satellite data have an excellent spatial and temporal distribution but have only been made during the past few decades. Magnetic observatory data, on the other hand, are available from the middle of the 19th century onward but lack the spatial distribution of satellite data. In addition to this, even ancient mariners' charts have been analyzed to extend our knowledge of the geomagnetic field back to 1715 (*Bloxham and Gubbins, 1985, 1986*). For information on the field prior to that, however, one has to resort to indirect measurements and deduce paleointensities and paleodirections from archeomagnetic and paleomagnetic samples. Indirect measurements are based on the observation that rocks containing ferromagnetic minerals carry a natural remanent magnetization, NRM, which, under favorable conditions, contains a record of the paleomagnetic field. The NRM consists of a primary RM, the RM acquired during rock formation, and a secondary RM, acquired subsequent to formation. Examples of a primary RM include thermal RM, TRM, detrital RM, DRM, post-depositional RM, pDRM, and chemical RM, CRM. Igneous rocks, as they cool to ambient temperatures in the presence of a magnetic field, acquire a TRM. DRM is produced when magnetic grains are oriented as they settle in water and become incorporated in sedimentary rocks. A pDRM results when the magnetic grains in sediments are reoriented after deposition, by processes such as compaction and bioturbation. Chemical reactions such as the alteration of minerals to different ferromagnetic minerals or the precipitation of ferromagnetic minerals from solution produce a CRM, for example in metamorphic rocks. A few examples of

secondary RM are chemical changes that affect the rock's ferromagnetic minerals, a remanent magnetization acquired by exposure to nearby lightning strikes or a viscous RM (VRM) caused by long-term exposure to the field subsequent to rock formation.

If the primary RM can be distinguished from the secondary RM and if the rock's age can be determined a paleomagnetic sample can provide a record of the paleofield at one location and time. Paleointensity measurements of Earth's magnetic field are much more difficult to make than paleodirections and subsequently, the amount of data is an order of magnitude smaller, making their interpretation more difficult and speculative. There are two main categories of paleointensity determinations made at present; relative paleointensities are obtained from marine and lacustrine sedimentary cores while absolute paleointensities are determined from igneous rocks. Sedimentary rocks have the advantage that they can provide a continuous record of the paleofield, however, they only allow the determination of the relative paleointensity since it is difficult to separate the NRM into its primary and secondary components. The typical procedure is to measure the NRM along the length of the drilled core and then normalize it, for example by the isothermal remanent magnetization (IRM), the low field magnetic susceptibility, or the anhysteretic remanent magnetization (ARM). This normalization is necessary since the NRM depends strongly on the magnetic mineralogy, the concentration of magnetic material, grain size etc., which may all have varied during core formation. An excellent review of this subject can be found in *Tauxe* (1993). In contrast to the relative paleointensities from sedimentary cores, igneous rocks can be used to obtain absolute paleointensity estimates. These are the only rocks for which the magnetization acquisition can be reasonably well duplicated in the laboratory. Extrusive igneous rocks such as lava flows, as they cool to ambient temperatures in the presence of a (weak) magnetic field, acquire a remanent magnetization that is typically parallel and proportional to the inducing field. Thus, they provide only a spot reading of the field, in contrast to the continuous record of sedimentary cores. However, a variety of paleointensity techniques have been developed

to separate primary and secondary RM in these rocks and to thus obtain an absolute and reliable intensity estimate. The two most widely used methods, the Thellier and Shaw methods will be explained in more detail in the following section. Compared to some of the other kinds of geomagnetic and paleomagnetic data described above, paleointensity data have a number of characteristic problems that make their interpretation more difficult; for example, age uncertainties vary greatly between studies, paleointensity estimates vary greatly in terms of their reliability (necessitating a careful choice of selection criteria) and the temporal data distribution is inhomogeneous during the past 320 Myr, with significant age intervals having poor or no data coverage. Despite all these problems paleointensity along with paleodirectional data provide us with the only direct evidence of processes and properties of Earth's deep interior on timescales of tens to hundreds of millions of years and may help constrain future geodynamo modeling.

1.2 Paleointensity Methods

Rocks containing ferromagnetic minerals have the ability to carry a remanent magnetization which, in principle, can be used to extract information on the paleomagnetic field. The total NRM of a rock is the vector sum of its primary and secondary remanent magnetizations. When an igneous rock forms and cools to ambient temperatures in a magnetic field H_{anc} , the primary RM it acquires is a thermoremanent magnetization (TRM). In most cases there is a linear relationship between the TRM, M_{TRM} , and the inducing (ancient) field strength H_{anc} :

$$M_{\text{TRM}} = C_1 H_{\text{anc}} \quad (1.1)$$

provided H_{anc} is sufficiently weak (magnetic induction $B \sim 10^{-4}\text{T}$). The constant C_1 in Equation 1.1 is unknown, as it depends on the rock's magnetic properties such as composition as well as the grain size and shape of the magnetic minerals. In principle,

the ancient field strength H_{anc} can be determined by first demagnetizing the rock and then remagnetizing it in a known laboratory field H_{lab} . The laboratory TRM, M_{lab} , and H_{lab} , are also linearly proportional

$$M_{\text{lab}} = C_2 H_{\text{lab}} \quad (1.2)$$

and can be used to solve for H_{anc} :

$$H_{\text{anc}} = \frac{M_{\text{TRM}}}{M_{\text{lab}}} H_{\text{lab}} \quad (1.3)$$

Equation 1.3, first used by *Koenigsberger* (1938a,b), assumes $C_1 = C_2$, i.e. that the rock magnetic properties have not changed since formation or during laboratory treatment. Unfortunately, for most rocks, this is not the case. The rock may have acquired a secondary RM, for example, through chemical alteration, in the field or the laboratory. In order to obtain confidence in a particular paleointensity estimate it is crucial to assess whether the assumption $C_1 = C_2$ can be made or not. Several paleointensity techniques have been developed to address this problem. Their basic approach is to obtain several independent paleointensity estimates from the same sample. A reliable paleointensity determination then requires consistency between such estimates.

1.2.1 *The Thellier Method*

The Thellier method and modifications thereof (*Thellier and Thellier*, 1959; *Coe*, 1967a; *Kono and Ueno*, 1977) aims at reliably determining absolute paleointensities from rocks which acquired their magnetization as a TRM. The method attempts to duplicate in the laboratory the cooling process that occurred during rock formation. The single domain theory developed by *Néel* (1949) illustrates that different grains in the rock will block their magnetization at different temperatures, depending on mineralogy, grain size and shape. The Thellier method relies on ‘the law of additivity

of pTRM' (Thellier, 1938) which states that the partial TRM (pTRM) acquired in a given temperature interval is uniquely associated with and is independent of the state of magnetization outside of that interval. The basic idea of the Thellier method is to obtain estimates as in Equation 1.3 for many segments of pTRM. If different temperature intervals yield the same paleointensity there is a greater likelihood of having found the true paleointensity since the factors that change the NRM or the TRM spectrum usually affect the various pTRM segments to different degrees. A typical procedure during a Thellier experiment involves a series of double heatings and coolings. The sample is heated from room temperature T_r to some higher temperature T_1 and cooled to T_r in the absence of a field. This destroys the NRM associated with the temperature interval (T_r, T_1) and the remaining NRM is measured. The sample is then reheated to T_1 and cooled to T_r in a known magnetic field. This will remagnetize the grains with blocking temperatures between T_r and T_1 and the new RM is measured. By repeating this process for successively higher temperatures (until the Curie temperature is reached), different pTRM segments are tapped. When the NRM remaining after each zero-field cooling is plotted against the NRM gained after each laboratory field cooling (Arai plot) one should ideally obtain a straight line the slope of which can be used to estimate the paleointensity. Ideal Thellier behavior suggests the following:

1. The NRM is a pure, unaltered TRM.
2. Thellier's additivity law is satisfied.
3. The TRM is linearly proportional to the inducing field.
4. No physico-chemical changes in the TRM properties occurred since rock formation (and, in particular, during laboratory treatment).

Most samples fail at least one of the criteria above and exhibit non-ideal Thellier behavior, i.e. deviations from a straight line. A good discussion of mechanisms causing non-ideal Thellier behavior was given by *Coe (1967a)*. The paleointensity database used in this dissertation contains data obtained with a number of different modifications of the original Thellier method. In the full Thellier method checks for changes in the TRM spectrum due to laboratory heating induced chemical changes are made by performing so-called pTRM checks. After having completed measurements at some temperature, a lower temperature step is repeated and consistency between the new and previously obtained results is required. Since heating and cooling cycles are very time-consuming some studies do without pTRM checks. We will refer to this as the modified Thellier method. In our database there are roughly equal numbers of data obtained with the full and the modified Thellier method.

1.2.2 The Shaw Method

A major disadvantage of the Thellier method is the length of time required for heating and cooling the sample. To overcome this drawback, attempts have been made to use AF demagnetization methods, which only require one heating (*Shaw, 1974; Kono, 1978; Rolph and Shaw, 1985*). *Shaw (1974)* suggested a method which would also detect any alteration of the sample on heating. In this method four series of AF demagnetization measurements with successively increasing peak alternating fields are made: on the original NRM, on an anhysteretic RM (ARM1) before heating, on a TRM given to the sample by heating it above its Curie temperature and letting it cool in a known field, and on an ARM after heating (ARM2). A plot of ARM1 versus ARM2 for successive demagnetization fields will give a straight line of unit slope if there has been no alteration. The peak alternating field values that fall on a unit-slope line in the ARM1/ARM2 plot are then used to determine the paleointensity from the NRM/TRM plot. Thus the coercive force spectrum obtained on AF demagnetization is used to obtain the paleointensity estimate, rather than the blocking temperature

spectrum as used in the Thellier method. The criteria for success are analogous to those for the Thellier method:

1. The NRM is a pure, unaltered TRM.
2. The NRM lost in an interval (H_i, H_{i+1}) of peak alternating fields is independent of the NRM lost in a non-overlapping interval.
3. The RM acquired in each interval (H_i, H_{i+1}) is linearly proportional to the inducing field.

Although both the Thellier and the Shaw method offer significant improvement over older techniques that had no consistency checks there are still significant uncertainties. For once, the criteria stated above are a necessary, but not sufficient condition for successful measurements. It is possible to obtain ideal Thellier behavior or unit slope in the ARM1/ARM2 plot even though some of the criteria for success are not met. In particular, it has not yet been fully investigated whether Shaw's method can distinguish between a CRM and a TRM in all cases. Intuitively, Thellier's method is more appealing as it more realistically duplicates in the laboratory the TRM acquisition.

There has been much debate as to which intensity method is to be preferred. It appears that overall the Thellier method works better than the Shaw method (e.g., *Prévot and Perrin, 1992; Goguitchaichvili et al., 1999*) although numerous studies have reported similar intensities from Shaw and Thellier methods (e.g., *Senanayake et al., 1982; Tanaka et al., 1997*). Currently, the use of the Thelliers' method (with pTRM checks) is preferred by most in the field. However, one should note that the increased number of heatings due to pTRM checks increases the risk of chemical alteration in the laboratory and might therefore decrease the already low success rate of paleointensity determinations. Moreover, *McClelland and Briden (1996)* have

shown that failure of pTRM checks does not necessarily indicate that alteration of high-blocking temperature material has occurred.

1.3 Comparing Paleomagnetic Directions and Intensities from Different Locations

Determining a sample's paleodirection, paleointensity and age gives a spot reading of the paleofield at one location. For any reasonable field geometry, however, the field will vary depending on where on the surface of Earth the measurement is made. In order to compare paleodirections from different locations, paleomagnetists commonly use virtual geomagnetic poles (VGP). A VGP is the position of the pole of a geocentric dipole that can account for the observed magnetic field at the sampling site. It can be calculated from an observation of the magnetic field direction and the sampling site coordinates. A detailed description of the trigonometry involved can be found elsewhere (e.g., *Butler*, 1992). The important thing to note here is that in the calculation of a VGP one assumes that the paleodirection was produced by a geocentric dipole field. In general, however, a rock records the total field, i.e. the sum of both dipole and non-dipole fields, and, therefore, the use of VGP will introduce a certain amount of error. Similarly, paleointensities from different locations can be compared by using virtual dipole moments, or VDM (*Smith*, 1967a). A VDM is the moment of the geocentric dipole that can account for the observed intensity at the sampling site. It can be calculated from the sample's inclination I and its intensity F :

$$\text{VDM} = \frac{4\pi a^3 F}{2\mu_0} (1 + 3 \cos^2 I)^{\frac{1}{2}} \quad (1.4)$$

where a is Earth's radius and μ_0 the free-air permeability ($\mu_0 = 4\pi \times 10^{-7} \text{Hm}^{-1}$). If the paleohorizontal is unobtainable, a VDM cannot be calculated; however, it is possible to determine a virtual axial dipole moment (VADM) instead. A VADM is

the geocentric axial dipole (i.e. it is aligned with the axis of rotation) that can account for the observed intensity at a specified site. For a geocentric axial dipole field, the inclination and the site colatitude θ are related by $\tan I = 2 \cot \theta$. Hence, if the sample's paleosite is known the inclination in Equation 1.4 can be expressed in terms of the paleocolatitude θ , yielding a VADM. The obvious advantage of using VADM data is that more data are available, in particular, *Selkin and Tauxe* (2000) have substantially increased their paleointensity database by including VADM data obtained from submarine basaltic glasses where inclination information was unobtainable. On the other hand, the use of the inclination in Equation 1.1 guards against the effect of a tilted dipole to which VADM data are sensitive. Similar to VGP, VDM and VADM both assume an underlying dipole field. The presence of non-dipole fields will thus result in a certain amount of error. Some of the consequences of using these approximations will be investigated further in chapter 2.

1.4 Paleosecular Variation and the Mean Paleointensity

To first order Earth has a magnetic field with a dipolar structure, a fact that has been used for navigational purposes for many centuries. Interpretation of paleomagnetic data would be the most straightforward if the field were stationary and identical to the field of a geocentric axial dipole, i.e. a dipole located at the center of Earth and aligned with the rotational axis. If this were the case any deviation from the expected direction could be directly interpreted in terms of tectonic movement of the sample. However, the geomagnetic field is far from a perfect, stationary, geocentric axial dipole field. For instance, the present dipole moment is not aligned with Earth's axis of rotation, but is tilted at an angle of about 10.5 degrees. The field exhibits non-dipole fields, i.e. deviations from a perfect dipole field, in intensity as well as directions. Both dipole and non-dipole fields have varied significantly during historic times; for example, in London, the declination, the angle between geographic north

and the horizontal component of the field, has changed at a rate of more than 10 degrees/century for at least the past 400 years, and the global dipole moment has decreased by about 5% during the last century (e.g., *Merrill et al.*, 1996). Temporal variations of the geomagnetic field, including the examples above, occur on a wide range of time scales, with periods ranging from milliseconds to millions of years. The shortest period transient variations arise mostly from causes outside the Earth and will not be considered here. Field changes at the surface of Earth with periods greater than about a year are generally referred to as geomagnetic secular variation. They typically have their origin within the interior of Earth, except possibly for some variations that have periods close to fundamental solar periods (e.g., *Barton*, 1989). Almost certainly the geomagnetic field at the core-mantle boundary (CMB) also exhibits changes on time scales less than a year; however, due to the screening effect of the lowermost electrically conducting mantle (e.g., *Backus*, 1991), these are not observable at Earth's surface. The term paleosecular variation (PSV) commonly refers to geomagnetic secular variation of the paleomagnetic field. It can be investigated only through the use of paleomagnetic data. Chapter 4 will address questions regarding PSV obtained from paleointensity data spanning the past 320 Myr. To provide a framework for this and to give some insight into the variety and time scales involved I will briefly touch upon a few examples of geomagnetic and paleosecular variation. A more extensive summary can be found in *Merrill et al.* (1996). The phenomenon with the shortest observed period that is believed to be of internal origin is the so-called magnetic jerk of 1969, a sudden change in the secular variation found in the eastward component of the magnetic field (e.g., *Courtillot et al.*, 1978; *Ducruix et al.*, 1980). Estimates of its period vary from approximately one year (e.g., *Courtillot and LeMouél*, 1984; *Backus et al.*, 1987) to one or two decades (*Allredge*, 1984). Other examples include the westward shift of various isoporic foci during the last century of about 0.18° per year (translating to a period of about 2000 years), known as the westward drift of the non-dipole field (e.g., *Bullard et al.*, 1950), and magnetic field reversal transitions which

are estimated to have durations between 1-10 kyr (e.g., *Merrill and McFadden, 1999*). The above are examples of secular variation with periods less than or comparable to time scales on which the geodynamo is believed to operate (several tens of thousands of years (e.g., *Merrill et al., 1996*)), suggesting that they are a manifestation of dynamo processes. Secular variation with periods of 1 Myr or less will be referred to as short-term PSV, in contrast to long-term PSV which will be used to describe temporal variations of the field with periods greater than ~ 10 Myr. Changes on these time-scales are less likely to be due to dynamo processes since this would require the geodynamo to have a memory of its past state. Instead, long-term PSV is more likely a manifestation of changing CMB conditions. For instance, the reversal rate of Earth's magnetic field as a function of time has been shown to vary between zero and six per million years (e.g., *McFadden et al., 1991*), and has a period on the order of 10^8 years, a time-scale suggestive of CMB changes. *McFadden et al. (1991)* used VGP scatter as a proxy for the long-term paleosecular variation from lavas (PSVL) during the past 190 Myr and found a correlation between this and the reversal rate during this period. While paleodirections have been investigated in terms of long-term PSV, paleointensities have not. In chapter 4 we propose a method using VDM scatter as a proxy for long-term PSV from intensities and apply it to our paleointensity database.

Long-term trends of the mean paleointensity, in the strict sense of our definition another manifestation of long-term PSV, have been addressed in a number of studies in the past. *Prévot et al. (1990)* analyzed Thellier data of Triassic and younger ages. They found large, long-term changes in the strength of the field and an average VDM during the Cenozoic close to the present field strength. However, during most of the Mesozoic the intensity was significantly lower, about 1/3 of the present value. The intensity increases again prior to about 185 Ma ago. *Perrin and Shcherbakov (1997)* analyze Shaw and Thellier data from the past 400 Myr, confirming the Mesozoic dipole low and suggesting a bimodal distribution for all of the VDM data. They also report a correlation between VDM scatter and the mean VDM but suspect that

this might be an artifact as they also find a similar relation between the number of determinations and the VDM scatter. *Tanaka et al.* (1995), analyzing Thellier and Shaw data older than 0.03 Ma, find a broad low intensity between 180 and 120 Ma, also confirming the Mesozoic dipole low. *Juarez et al.* (1998), using VADM data from submarine basaltic glasses with ages between 5 and 160 Ma, report a significantly lower mean paleointensity, about half of the present field, for this period. Expanding on this, *Selkin and Tauze* (2000) combine SBG data with other paleointensity data and find that if only data obtained with the full Thellier method are considered the field intensity was dramatically higher during the most recent 0.3 Myr than during the preceding 300 Myr. There has been much controversy as to whether the intensity during superchrons is systematically high or low. While most authors report low paleointensities during the Cretaceous Normal Superchron (KNS), *Tarduno et al.* (2001) report values higher than the present field. In chapters 3 and 4 we present a new paleointensity database and use it to evaluate the above models as well as investigate the variation of VDM data distributions with time. We find persistent bimodal distributions during at least the Cenozoic and part of the Mesozoic and discuss possible interpretations.

Chapter 2

NON-DIPOLE FIELD RATIO AND INTENSITY AND DIRECTIONAL SCATTER FOR A DECREASING DIPOLE

2.1 Summary

The intensity of the present non-dipole field at Earth's surface has been estimated to be anywhere between 5% and 25% of the total field. Although some of the differences reflect semantic problems, we show that a value between 20 to 25% is the appropriate percentage for the 1995 IGRF. We also show that paleomagnetic excursion data cannot have occurred solely as a result of the dipole intensity having been lower in the past. Lastly, VGP and VDM scatter are calculated based on a model that starts with the 1995 IGRF and assumes a decrease in dipole intensity. VGP scatter increases with a decrease in the dipole strength, as intuitively expected. Somewhat surprisingly, this is not the case for VDM scatter, which initially decreases until it reaches a minimum and then increases again.

2.2 Introduction

The purpose of this chapter is to use the properties of Earth's present magnetic field to examine a host of issues paleomagnetists face. Although such approaches have been used for nearly a half century (e.g., *Cox*, 1962; *McElhinny and McFadden*, 1999), there remain at least three issues that are unsettled.

The first issue addresses the apparently inconsistent estimates of the ratio of the

present non-dipole field to the dipole field at Earth's surface. For example, the rms intensity of the present non-dipole field to dipole field has been estimated to be anywhere from 5% (*Irving, 1964, p. 40*) to 25% (*Stacey, 1992, p. 346*). If we cannot distinguish between such estimates, can we reasonably expect to be able to estimate the relative roles of the non-dipole and dipole fields in the paleofield record?

The second issue concerns the nature of the scatter of virtual geomagnetic poles, VGP, virtual dipole moments, VDM, and virtual axial dipole moments, VADM, when the dipole field is reduced. It may seem intuitively obvious that the scatter would increase if the non-dipole field were kept invariant while the dipole moment is decreased. However, some of our results suggest that this may not always be the case.

The third issue concerns transitional VGP (with paleocolatitude greater than 45° (*Verosub and Banerjee, 1977*)) and reverse transitional VGP (with paleocolatitude greater than 90° , (*Merrill and McFadden, 1994*)). It is commonly believed that excursions and reverse excursions occur when the dipole intensity is low (e.g., *Valet and Meynadier, 1993; Merrill and McFadden, 1994*) and that there are at least eight reverse excursions or reversal events (subchrons) in the Brunhes (e.g., *Champion et al., 1988; Spell and McDougall, 1992; Merrill and McFadden, 1994*). We show that the Brunhes reverse VGP are unlikely to have occurred from a simple reduction of the dipole moment with all other factors kept invariant.

2.3 A Non-Dipole Field Ratio from Intensities

Several estimates of what percentage of the geomagnetic field is due to its non-dipole components have been published, typically falling between 5 and 25% (for a summary see *Merrill et al., 1998*). We calculated a non-dipole field intensity ratio in four different ways that use two different methods. Each of the two methods employed yields an upper and a lower estimate.

The geomagnetic scalar potential is given by

$$\Psi = \frac{a}{\mu_0} \sum_{n=1}^{\infty} \sum_{m=0}^n \left(\frac{a}{r}\right)^{n+1} P_n^m(\cos \theta) (g_n^m \cos m\phi + h_n^m \sin m\phi) \quad (2.1)$$

where a is Earth's radius, μ_0 the magnetic free-air permeability, $P_n^m(\cos \theta)$ are the partially normalized Schmidt functions, g_n^m and h_n^m are the Gauss coefficients, and θ and ϕ are the colatitude and longitude. n and m are referred to as degree and order, respectively. Naturally, the field is obtained by taking the negative gradient of the potential. Using the Gauss coefficients of the most recent international reference field, or IGRF 1995 (obtained online from the National Geophysical Data Center at www.ngdc.noaa.gov, for background information see (Langel, 1987)) we first calculated the intensity of the resulting geomagnetic field at Earth's surface on a latitude-longitude grid with a spacing of two degrees. The intensity was determined for the total field, F_t , the dipole field, F_d , only and the non-dipole field, F_{nd} , only. This was done by including all Gauss coefficients (degrees $n = 1$ to 10), dipole Gauss coefficients only (degree $n = 1$, or g_1^0 , g_1^1 , and h_1^1), and non-dipole Gauss coefficients only (degrees $n = 2$ to 10).

In method 1 the intensities (weighted by equal area) were first averaged globally (step 1). The resulting global averages of total field $\langle F_t \rangle$, dipole field $\langle F_d \rangle$, and non-dipole field $\langle F_{nd} \rangle$ were then used to calculate an upper and a lower estimate of the non-dipole field ratio (step 2) from

$$r_{\text{low}}^{(1)} = 1 - \frac{\langle F_d \rangle}{\langle F_t \rangle} \quad (2.2)$$

and

$$r_{\text{up}}^{(1)} = \frac{\langle F_{nd} \rangle}{\langle F_t \rangle} \quad (2.3)$$

Method 2 differs from method 1 in that steps 1 and 2 above were reversed. For every location a lower ratio $(1 - F_d/F_t)$ and an upper ratio (F_{nd}/F_t) were determined first,

then the global average of these ratios was taken, yielding overall lower and upper estimates, $r_{\text{low}}^{(2)}$ and $r_{\text{up}}^{(2)}$ given by

$$r_{\text{low}}^{(2)} = 1 - \left\langle \frac{F_d}{F_t} \right\rangle \quad (2.4)$$

and

$$r_{\text{up}}^{(2)} = \left\langle \frac{F_{\text{nd}}}{F_t} \right\rangle \quad (2.5)$$

For the present geomagnetic field, the values obtained with methods 1 and 2 are: $r_{\text{low}}^{(1)} = 2.4\%$, $r_{\text{up}}^{(1)} = 22.5\%$, $r_{\text{low}}^{(2)} = -0.5\%$, and $r_{\text{up}}^{(2)} = 24.6\%$. It is a simple matter to use Equations 2.2 – 2.5 for past epochs. For example, we find that the geomagnetic field's non-dipole field content was about 17–18% a century ago and has increased since to the present values, as is shown in Figure 2.1.

The fact that the methods used yield both an upper and a lower limit highlights a semantic problem in determining a “non-dipole field ratio”. At some arbitrary location on the surface of Earth, the total field vector is the vector sum of the dipole field $\mathbf{B}_{\text{dipole}}$ and the non-dipole field $\mathbf{B}_{\text{non-dipole}}$. Of course, both $\mathbf{B}_{\text{dipole}}$ and $\mathbf{B}_{\text{non-dipole}}$ are themselves vector sums. However, while the components of $\mathbf{B}_{\text{dipole}}$ are mutually orthogonal, this is not the case for $\mathbf{B}_{\text{non-dipole}}$. Thus, if one were to calculate a non-dipole field ratio based on energies the result would be biased towards non-dipole fields. Using intensities that effect is decreased. In principle, both the upper and the lower ratios in methods 1 and 2 are technically correct: the upper ratios overestimate the non-dipole contribution to the total field while the lower ratios overestimate the dipole contribution and, therefore, underestimate the non-dipole one. The lower estimates are expected to be close to zero considering that on the global average non-dipole fields will almost equally decrease and increase the total field. However, because of the non-linearity in combining the dipole and non-dipole fields, they need not be exactly equal to zero and may even be less than zero, as is the case for $r_{\text{low}}^{(2)}$.

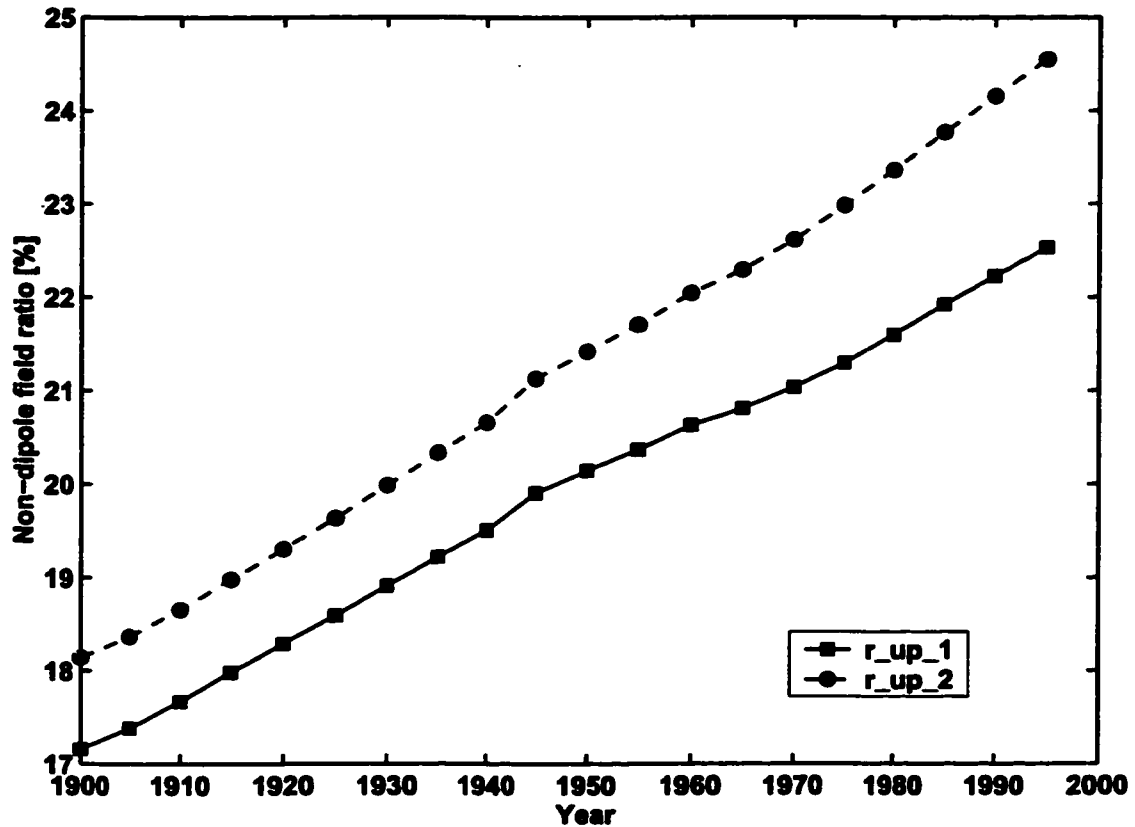


Figure 2.1: Non-dipole field ratios $r_{up}^{(1)}$ and $r_{up}^{(2)}$ (see Equations 2.3 and 2.5) during the last century. $r_{up}^{(1)}$ is shown as squares, $r_{up}^{(2)}$ as circles.

The percentage of the non-dipole field to total field usually referred to is the upper value given; it lies between 20 and 25% depending on the specific definition used.

Magnetic field directions cannot be used to calculate a percentage value to estimate how much of the field is non-dipolar. An ideal geocentric axial dipole field, for example, would have zero declination everywhere. Adding a non-dipole field would result in non-zero declinations but without a reference value this does not yield a percentage ratio. However, one can use statistical moments of global direction anomaly data or VGP distributions to compare different field configurations. We opted for VGP since they are most commonly used to represent statistical properties of

the non-dipole field. The sampling sites in our model were located symmetrically with respect to the axis of rotation. To avoid a sampling bias due to the presence of equatorial dipole fields in the present magnetic field (IGRF 1995) we first rotated the geomagnetic field to align the geomagnetic with the geographic north pole. We then calculated field directions and VGP for 10000 sites on the surface of Earth. The number of sites for a given latitude were adjusted such that each site represented the same surface area. Using Fisher statistics, for the IGRF 1995, the VGP scatter is $\sigma_{\text{VGP, equator}} = 8.6^\circ$ at the equator and $\sigma_{\text{VGP}} = 12.2^\circ$ globally. These values are consistent with previous estimates (e.g., *Cox, 1962; Merrill et al., 1998*).

2.4 VGP and VDM Scatter as a Function of Dipole Intensity

In this section we consider a simple model to obtain various statistical properties of VGP, VDM and VADM. In general, for any given instant in time, the spatial distribution of samples is poor, and, therefore, the paleofield's spectral content cannot be resolved. In addition, there are uncertainties in age determination which can result in significant errors because both the intensity and directions are known to vary by several percent and degrees, respectively, just within the past century (e.g., *Merrill et al., 1998*). This leads to a variety of methods to determine the time derivative of the paleofield, that is, the paleosecular variation. For example, VGP scatter is often used as a proxy for secular variation. The term 'proxy' is used deliberately here, as the quantity measured, VGP scatter, has three different sources: experimental error, spatial field variability and temporal variability. It does not include any intensity variations. Typically, spatial variability (due to non-dipole fields and dipole variation) and temporal variability are grouped together in a mixed average over time (for further discussion, see *Merrill and McElhinny (1983)*). To investigate the effect of the spatial variability on VGP scatter we used a straightforward model with variable dipole and constant non-dipole content.

The present field dipole is tilted with respect to the axis of rotation by 10.5° . To avoid introducing a bias due to this tilted dipole we first rotated all Gauss coefficients such that dipole and axis of rotation are aligned. Intensities F , declinations D , inclinations I , VGP, VDM and VADM were then calculated a) for a latitude/longitude grid with a spacing of 2 or 5° for plotting data globally and b) for 10,000 sites each representing the same amount of surface area whenever global distributions and their statistical properties were of interest. This procedure was performed for a series of calculations in which the dipole components were gradually reduced in strength (in 5% steps) from the present value to zero while the non-dipole Gauss coefficients were held constant. The data generated were then used for analyses.

Figure 2.2 shows the non-dipole field ratio dependence on dipole strength for $r_{\text{up}}^{(1)}$ and $r_{\text{up}}^{(2)}$ (as introduced in the previous section). As expected both non-dipole field ratios increase as the dipole is reduced in strength. For a vanishing dipole (dipole strength=0%) in Figure 2.2 non-dipole field and total field are identical and both $r_{\text{up}}^{(1)}$ and $r_{\text{up}}^{(2)}$ are equal to 1. Method 2 (in which ratios are taken first and global averaging follows) appears to be more sensitive to local effects.

The quantity most relevant for paleomagnetic work is the angular standard deviation of the VGP distribution, or VGP scatter (Figure 2.3). As expected, it increases with decreasing dipole strength. The mean VGP in all cases lies well within one angular standard deviation of the geomagnetic pole. Note that σ_{VGP} has small values initially ($\sim 10^\circ$) but can become fairly large when the dipole is weak ($\sim 35^\circ$). We will return to this in the next section.

Figure 2.4 shows, for various dipole strengths how the field polarity, as determined from VGP, varies on the surface of Earth. The VGP data were separated into normal, normal transitional, reverse transitional, and reverse. The present geomagnetic field has no transitional VGP (Figure 2.4a). The first transitional VGP in our calculations appear when the dipole has been reduced by roughly 25% (Figure 2.4b). The area with transitional VGP grows gradually as the dipole is reduced in size. For a dipole strength

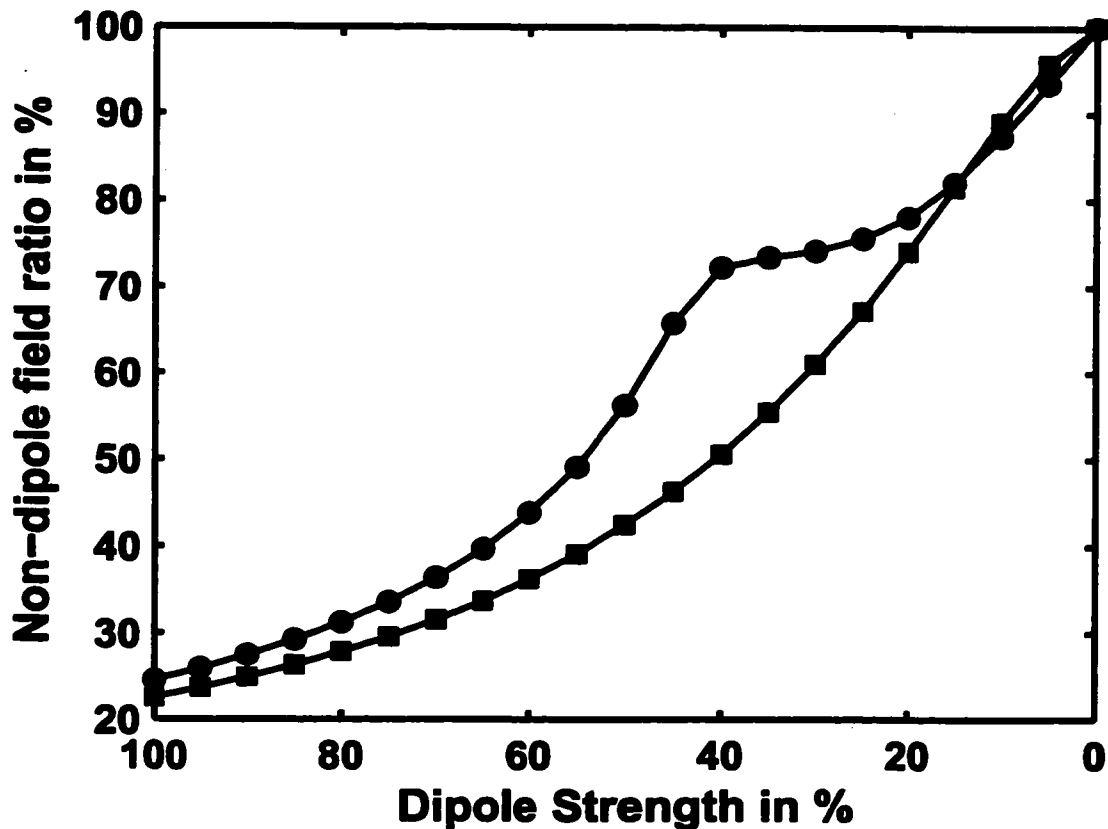


Figure 2.2: Non-dipole field ratios $r_{up}^{(1)}$ and $r_{up}^{(2)}$ (see Equations 2.3 and 2.5) for a decreasing dipole and constant non-dipole field, based on the IGRF 1995. $r_{up}^{(1)}$ is shown as squares, $r_{up}^{(2)}$ as circles.

of 25%, about 40% of the area has transitional or reverse polarity (Figure 2.4d). During geomagnetic reversals the field intensity tends to decrease to a minimum near 25% of its previous state (e.g., *Tanaka et al.*, 1995). However, both absolute and relative paleointensity data indicate that excursions occurred during the Brunhes when the dipole intensity was about half of the usual value (e.g., *Merrill et al.*, 1998; *Guyodo and Valet*, 1999). Figure 2.4d shows both transitional regions and regions of local reversals (as determined from VGP). The phenomenon of producing local reversals from the non-dipole field was first suggested by *Whitney et al.* (1971) and

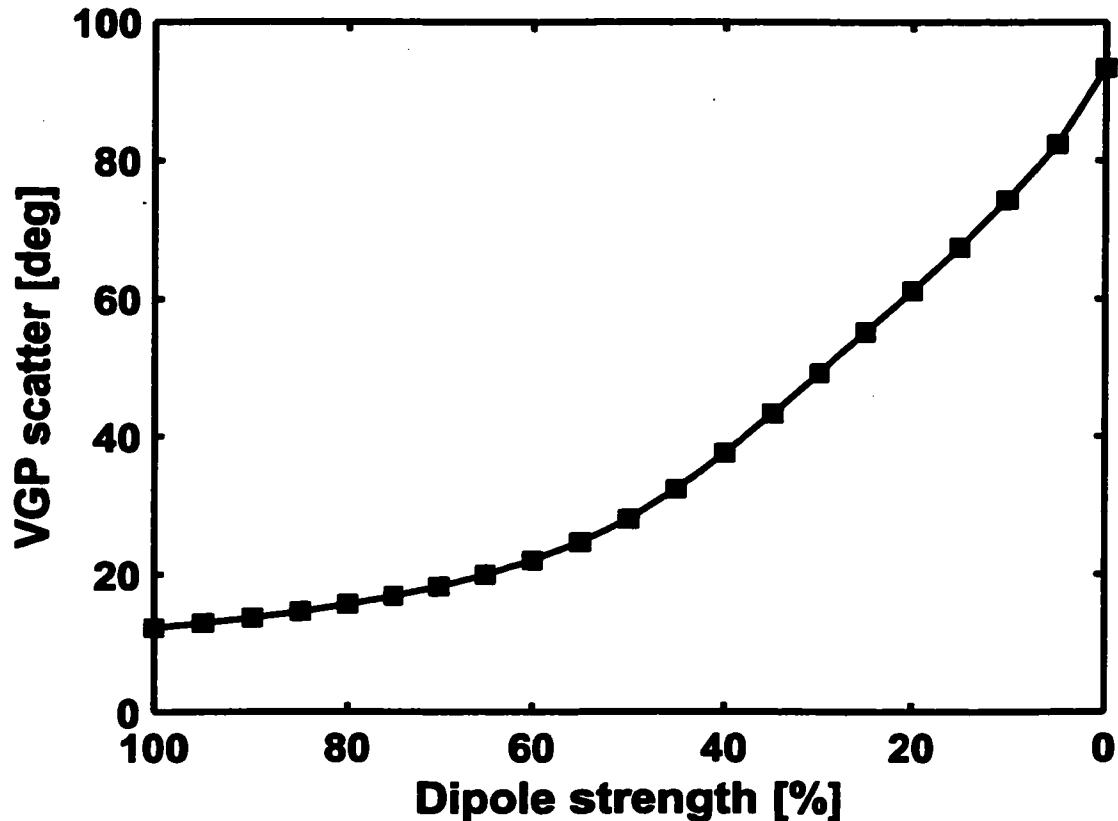


Figure 2.3: Global VGP scatter σ_{VGP} for a decreasing dipole and constant non-dipole field, based on the IGRF 1995.

is now well recognized. Our results suggest that major excursions (showing reverse directions) require that either the non-dipole field intensity increases while the dipole intensity decreases or that the dipole deviates substantially from a geocentric axial dipole one during an excursion. This follows because the dipole intensity had to be reduced by more than 60% to produce any reverse directions.

Finally, the VDM and VADM data from our model were generated following the same procedure as for the VGP analyses above, i.e. each point represents the same surface area, to allow for straightforward statistical treatment. Means and standard deviations of global VDM and VADM distributions were then determined as a func-

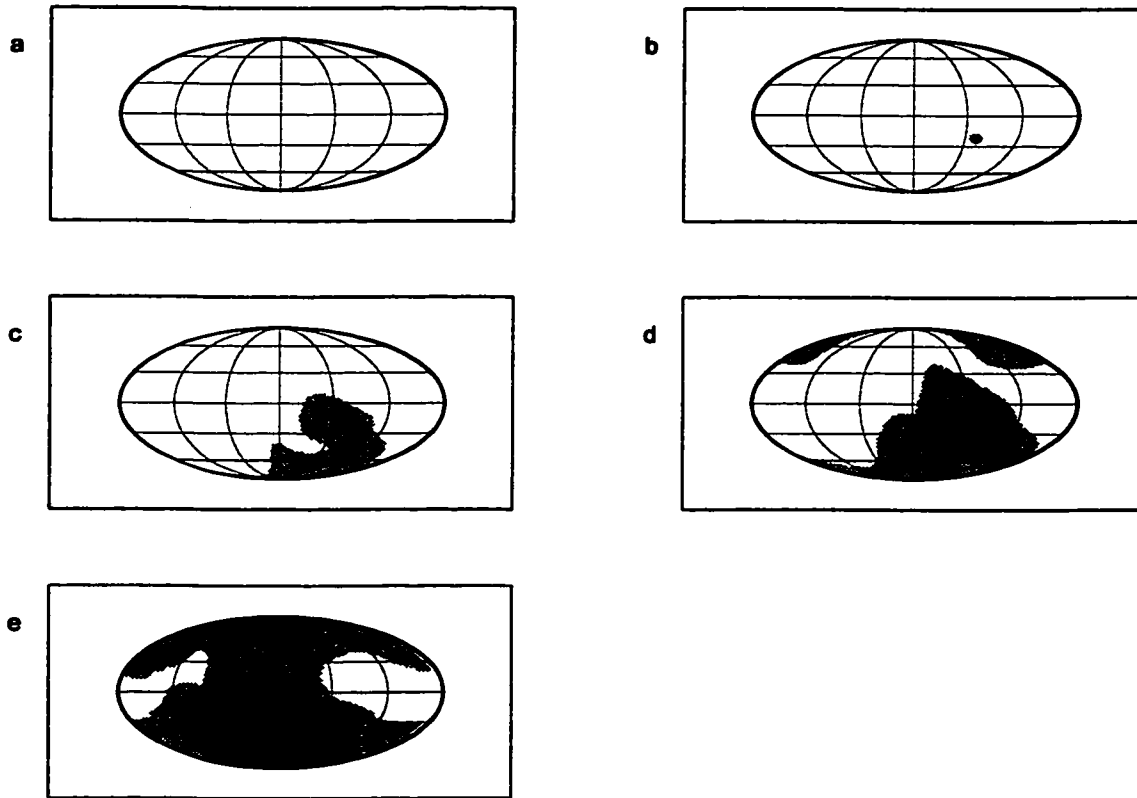


Figure 2.4: Global distribution of VGP for constant non-dipole field and dipole strength a) 100%, b) 75%, c) 50%, d) 25%, and e) zero. The VGP data were separated into normal (white, VGP latitude $\lambda_{\text{VGP}} > 45^\circ$), normal transitional (light gray, $0^\circ < \lambda_{\text{VGP}} < 45^\circ$), reverse transitional (dark gray, $-45^\circ < \lambda_{\text{VGP}} < 0^\circ$), and reverse (black, $\lambda_{\text{VGP}} < -45^\circ$).

tion of dipole strength. The purpose was twofold: to investigate the sensitivity of VDM (and VADM) means and standard deviations to a decreasing dipole field and to explore similarities and differences of VDM and VADM, both of which are widely used in paleomagnetism. The determination of a VDM requires knowledge of both the paleointensity F and the inclination I ; a VADM, on the other hand, can be calculated even if I is unknown, which often is the case. For a geocentric dipole field, $\tan I = 2 \cot \theta$ where θ is the paleosite colatitude; this relationship can be used to substitute θ for I . Since for the calculation of a VADM the field is assumed to be

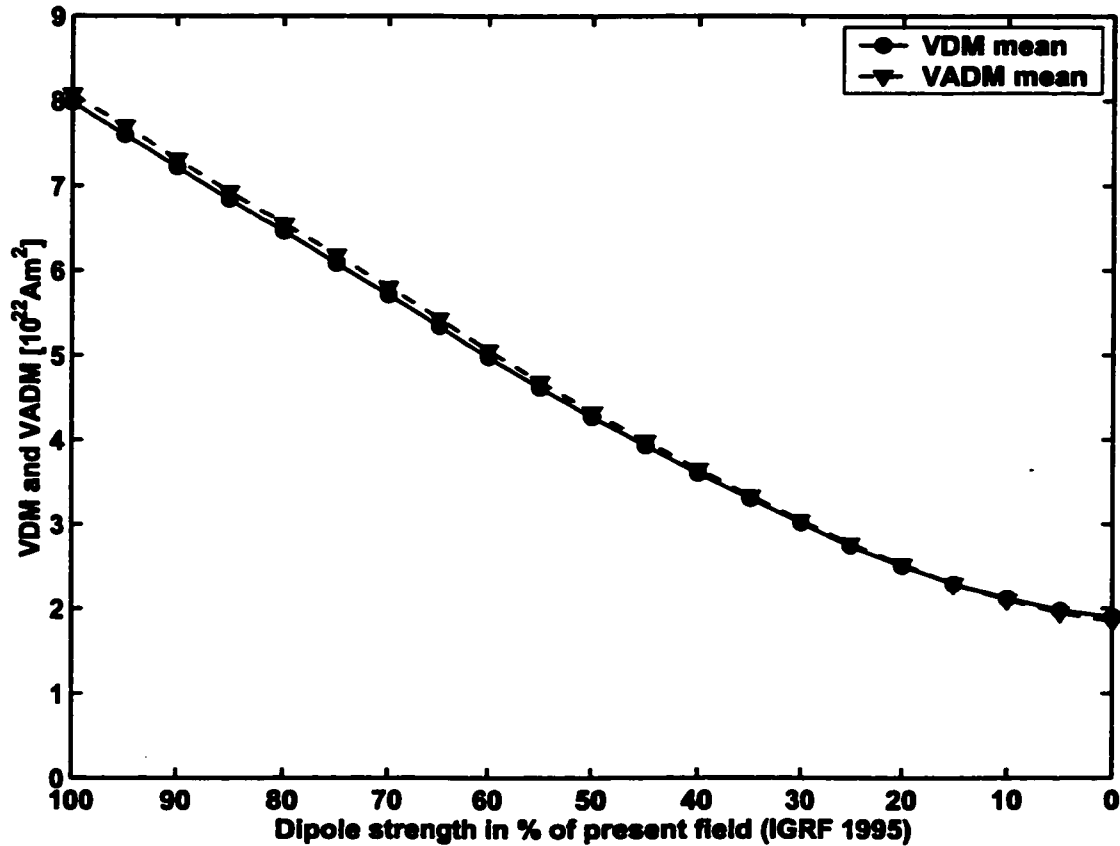


Figure 2.5: VDM and VADM means μ_{VDM} and μ_{VADM} for a decreasing dipole and constant non-dipole field, based on the IGRF 1995. μ_{VDM} are shown by circles and a solid line, and μ_{VADM} by triangles and a dashed line.

that of a geocentric axial dipole, VADM have the disadvantage that they are sensitive to an equatorial dipole while VDM are not. Results for VDM and VADM means, shown in Figure 2.5, are almost identical; this is not surprising because VDM and VADM were globally averaged. As expected the means decrease from their present day values ($\mu_{\text{VDM}} = 8 \times 10^{22} \text{Am}^2$ and $\mu_{\text{VADM}} = 8.1 \times 10^{22} \text{Am}^2$) as the dipole is reduced in strength. The slope is almost constant until the dipole is reduced to about 2/3 of its initial value, the percentage reduction in mean VDM in that part of the curve is close to that in dipole strength. The curve gradually levels off as non-dipole fields

become more significant. VDM and VADM scatter as a function of dipole strength are shown in Figure 2.6. The slightly higher VADM scatter can be attributed to equatorial dipole fields. Note that unlike the standard deviation of the VGP distribution, the VDM (and VADM) standard deviation decreases initially until it reaches a minimum (for dipole strength $\sim 15\%$) and then increases again. So, while VGP scatter increases with decreasing dipole strength that is not the case for the VDM scatter in this model. This result indicates that the decrease in dipole field strength does not imply that the scatter in VDM (and VADM) will increase. Although it may increase or decrease depending on the properties of the non-dipole field, it would decrease if the paleofield resembles that of the present field.

2.5 Discussion and Conclusions

There is not a simple answer to the simple question: what is the percentage of the present dipole and non-dipole fields at Earth's surface? If one is referring to the average ratio of local non-dipole to total field intensities, this ratio is roughly 20 to 25%, as is more fully discussed in section 2.3. A century ago this value was approximately 17–18%, which is significantly lower. The intensity of the paleomagnetic field appears to have varied substantially in the past (e.g., *McElhinny and Senanayake, 1982; Guyodo and Valet, 1999*). It is thought that magnetic field excursions are more common when the dipole intensity is relatively low (*Valet and Meynadier, 1993; Merrill and McFadden, 1994*). A simple model of keeping the present non-dipole field invariant while decreasing the intensity, but not the direction, of the dipole field has been used in this paper to investigate possible statistical properties of VGP, VDM and VADM for low values of dipole intensity. In spite of the oversimplified model, it illustrates some likely properties of the paleofield. No reversal excursions are evident when the dipole intensity is reduced in half. Yet reversal excursions appear to often occur in the paleomagnetic data when the dipole field is reduced by this much. Evidently, in

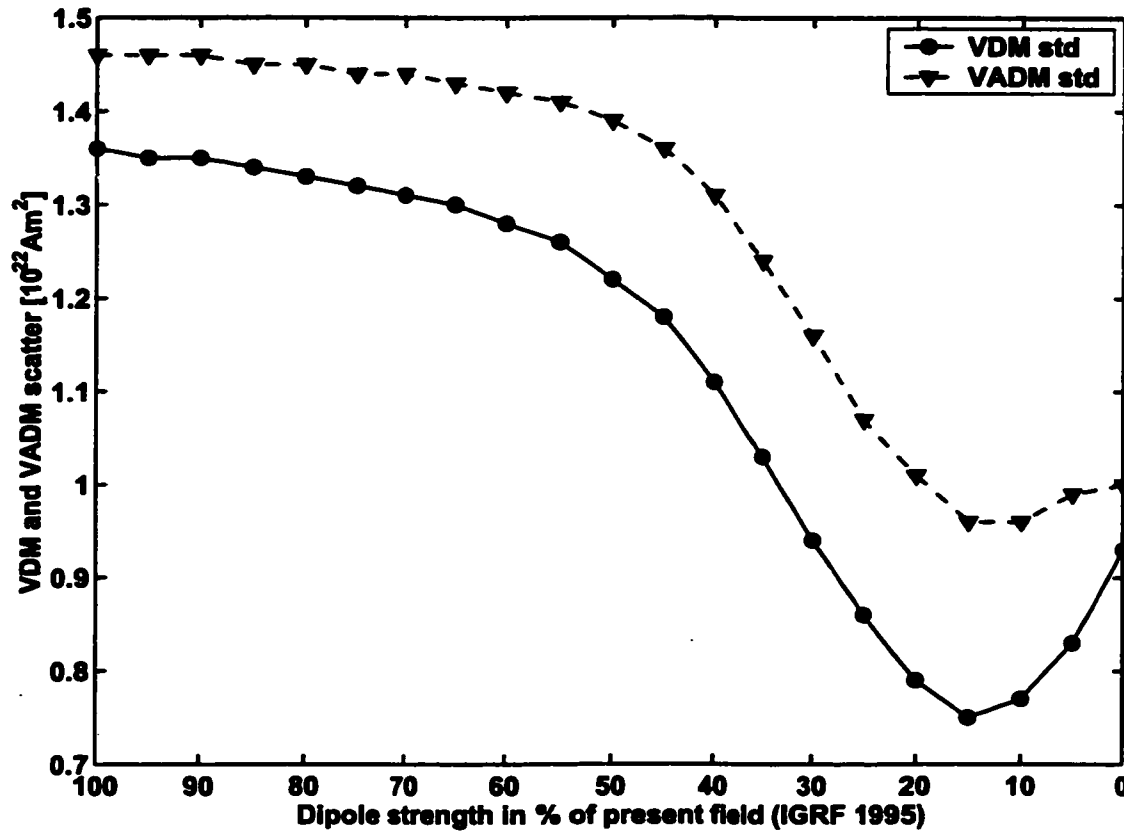


Figure 2.6: VDM and VADM scatter (σ_{VDM} and σ_{VADM}) for a decreasing dipole and constant non-dipole field, based on the IGRF 1995. σ_{VDM} are shown by circles and a solid line, σ_{VADM} by triangles and a dashed line.

reality, on the average the non-dipole field increased when the dipole field was lower or there were much larger equatorial dipole terms relative to the axial dipole field than at present. The analyses shown in the bottom of Figure 2.4 illustrate that it might be very difficult in practice to distinguish between reversal events and excursions.

As expected, VGP scatter increases with decrease in dipole field intensity. This need not be the case for VDM scatter. Indeed, the spatial variation of VDM scatter decreases with a decrease in the present dipole field until a minimum value is reached. Although one needs additional assumptions (such as westward drift of the non-dipole field) to translate this result to the temporal domain, this counterintuitive result

illustrates that the VDM scatter can actually, and easily, decrease with decrease in dipole moment, unlike that for VGP.

Chapter 3

THE VARIATION OF INTENSITY OF EARTH'S MAGNETIC FIELD WITH TIME

3.1 *Summary*

A new and larger database is established to assess the variation of paleointensity with time. It is shown that submarine basaltic glass contains a grain growth chemical remanent magnetization in magnetite. Intensity estimates from these samples are used to establish a lower bound estimate on intensities. Statistical tests on various subsets of the database are used to establish a more reliable database for finding long-term trends of the paleointensity. We can obtain a reasonable estimate for intensity versus time for the Cenozoic but not for the Mesozoic or Late Paleozoic. The distributions of data as a function of time also provide valuable information. In particular, the two well-documented superchrons exhibit different intensity properties, which suggests that there is not a simple correlation between reversal rate and intensity.

3.2 *Introduction*

There are several reasons one wants to obtain the absolute intensity of Earth's magnetic field as a function of time including: to provide data for dynamo modeling, to determine if changing core-mantle boundary conditions occurring over tens of millions of years are manifested in paleointensity data, to determine if superchrons, which are thought to represent different dynamo states (*Merrill and McFadden, 1994*), have intensities that are different from other times as was first proposed by *Pal and Roberts (1988)* and to determine if the growth of the inner core over time has affected the

intensity (*Stevenson, 1983*).

It is well appreciated that it is far more difficult to obtain reliable paleointensity information than paleodirectional information. One of most highly regarded method to obtain absolute paleointensity information was developed over two decades by the Thelliers (*Thellier and Thellier, 1959*) and is commonly referred to as the full Thellier method. In this method thermal demagnetization and acquisition of thermal remanent magnetization, TRM, over a range of temperature intervals are used to provide consistency checks for estimated intensities. Samples that exhibit acceptable consistency checks using the Thellier method are said to exhibit ideal Thellier behavior as opposed to non-ideal Thellier behavior (Section 1.2). *Coe (1967a,b)* gives an excellent discussion of this. Finally, the Thelliers advocated the judicial use of a partial TRM, pTRM, to determine if irreversible changes occurred during the laboratory experiment. Several variations of the Thellier method have also been developed, hereafter collectively referred to as modified Thellier methods. Two of the most widely used modified versions of the Thellier method are those developed by *Coe (1967a,b)* and *Kono and Ueno (1977)*. There also is a class of methods that uses alternating field (AF) demagnetization properties of a sample to obtain consistency checks. The most highly regarded of these is the Shaw method (*Shaw, 1974*), and modifications thereof (*Kono, 1978; Rolph and Shaw, 1985*). Although there are many other methods in addition to the above, they are generally believed to be less reliable and will not be considered in this chapter. A review of these methods can be found in chapter 1 as well as in *Merrill and McElhinny (1983)* and *Dunlop and Özdemir (1997)*.

To compare intensities obtained at different locations, paleomagnetists assume a geocentric dipole field and calculate the intensity at the pole to obtain a virtual dipole moment, VDM, when the sample is oriented (the paleohorizontal can be obtained). Alternatively, when the sample is unoriented, an axial geocentric dipole field is assumed and a virtual axial dipole moment, VADM, is used. The average VADM and the average VDM are not expected to be very different; in chapter 2 we find that the

mean VDM and VADM for the present field are $8.0 \times 10^{22} \text{Am}^2$ and $8.1 \times 10^{22} \text{Am}^2$, respectively. However, the intensity of the present non-dipole field at Earth's surface is 20 to 25% of the total field and it was 17 to 18% of the total field a century ago (chapter 2). Consequently, one must have numerous VDM or VADM to obtain a good estimate of the paleomagnetic dipole moment. This has been further discussed in *McElhinny and Senanayake* (1982), who also find the paleomagnetic dipole moment was approximately 30% higher 2000 years ago and 30% lower 6500 years ago.

All evidence suggests that the paleointensity of Earth's magnetic field varies from the century time scale (e.g., the dipole decreased by approximately 5% during the twentieth century) to the billion year time scale (e.g., associated with changes in the size of the inner core). Indeed, the intensity problem is a difficult one because of such variation and because of the difficulty in obtaining reliable data. Although it is difficult to determine characteristic time scales for the geodynamo because of the non-linearities involved, it is reasonable to assume that intensity changes over less than about a million years are primarily reflecting dynamo processes, while changes over times longer than about 20 Myr are primarily reflecting changes in the boundary conditions (*Merrill et al.*, 1996). Thus, we will refer to changes in intensity on time scales less than a million years as 'short-term changes' and changes that require twenty million years or longer as 'long-term changes'. We will not attempt to analyze changes with characteristic time scales greater than 1 Myr and less than 20 Myr. Furthermore, in this chapter we will be primarily interested in the long-term changes.

Three different views of the long-term paleointensity variation have emerged during the past decade and are illustrated schematically in Figure 3.1. *Prévot et al.* (1990; see also *Prévot and Perrin*, 1992; *Kosterov et al.*, 1997; *Perrin and Shcherbakov*, 1997) advocate a Mesozoic low based on VDM data, as illustrated by model 1 in Figure 3.1. *Juarez et al.* (1998; see also *Pick and Tauze*, 1993a,b, 1994; *Selkin and Tauze*, 2000; *Juarez and Tauze*, 2000) use VADM, many of which come from submarine basaltic glass, SBG, to produce model 2. In this model the intensity has been significantly

higher since about 0.3 Ma (but still lower than the present intensity) with lower intensities prior to that. Note that in particular this model suggests a lower intensity during the Cretaceous Normal Superchron, KNS. *Tarduno et al.* (2001; see also *Cottrell and Tarduno, 2000*) suggest that the intensity was higher during superchrons (model 3: indicated by a star in Figure 3.1) and provide VDM data supporting this for the KNS. This suggestion was made earlier by *Pal and Roberts* (1988) who used unreliable data.

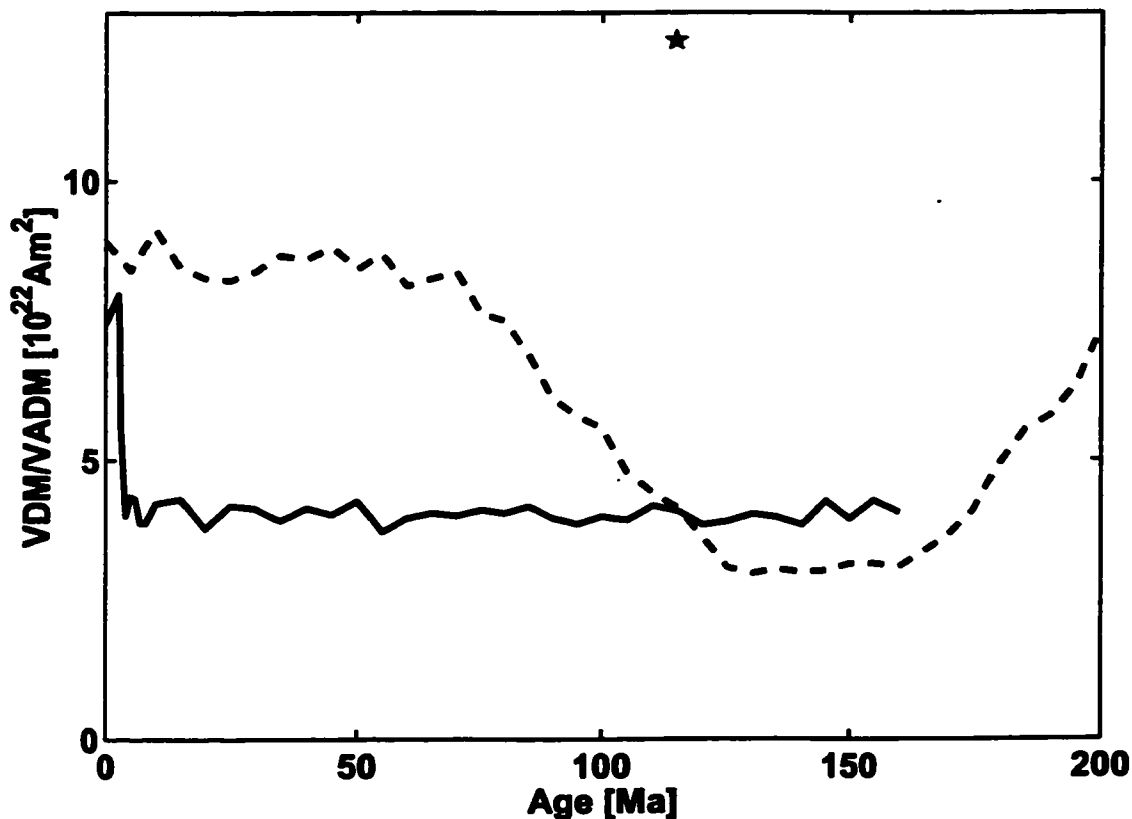


Figure 3.1: Schematic diagram depicting various models for the mean paleointensity. Model 1 (dashed line), has a mean intensity during part of the Mesozoic that is significantly lower than during the Cenozoic (e.g., *Prévot et al., 1990*), model 2 (solid line), shows a mean intensity during the most recent 300 kyr that is about twice as large as during the preceding 160 Myr (e.g., *Selkin and Tauxe, 2000*), and model 3 (star), suggests a high mean intensity throughout the Cretaceous Normal Superchron (e.g., *Tarduno et al., 2001*)

In this chapter we develop a new database, from which several data subsets can be extracted, in an attempt to make some sense of the mutually incompatible models shown in Figure 3.1. In the next section we report on a serious rock magnetic problem that has previously been unnoticed, but which has a major impact on the interpretation of intensity data. In subsequent sections we discuss our data selection criteria and analyze certain subsets of our database to evaluate long-term trends in the intensity. We conclude that long-term trends in paleointensities are at best only weakly defined because of data inadequacies. Nevertheless, we introduce a new approach to extract valuable information from paleointensity data.

3.3 Rock Magnetism: a Lesson from Mineralogy

One common approach to using paleointensity data is to analyze data obtained from different methods and from different rock samples. If rocks of similar age and different mineralogies produce similar paleointensity estimates, this increases one's confidence in the final result. *Juarez and Tauxe (2000)* point out that the same principle does not necessarily apply to the use of different intensity methods because certain methods might introduce systematic errors. They argue that the intensity appears to be lower when more stringent criteria are applied. This appears to be particularly true of SBG samples. These samples have been shown to contain single domain magnetite (*Pick and Tauxe, 1993a,b, 1994*), which is the grain size and composition that is widely preferred by paleomagnetists for use in paleointensity studies. For example, *Levi (1975)* studied magnetite samples that acquired a TRM in known laboratory fields. He showed that non-ideal Thellier behavior was common for multidomain magnetite, but ideal Thellier behavior was commonly exhibited by SD magnetite. More importantly, the estimate of paleointensity for the SD magnetite samples gave the correct laboratory field. There are straight line Arai plots (i.e., they exhibit ideal Thellier behavior) up to 400°C or so in the best SBG samples (referred to as 'class

A samples' by *Juarez and Tauze* (2000). These samples all pass pTRM checks. In short, the SBG samples appear to exhibit qualities that should put them among the best samples for paleointensity studies.

An unresolved puzzle concerning SBG is why do they contain SD magnetite? *Buddington and Lindsley* (1964) determined the equilibrium phases for the iron-titanium oxides as a function of oxygen fugacity and temperature. In particular, this allowed for a determination of oxygen fugacity and temperatures in magmas by examining the coexisting titanomagnetite and titanohematite phases. This work was confirmed by direct measurements in a Hawaiian lava lake (*Sato and Wright*, 1966; *Grommé et al.*, 1969). A sample that is quenched from a basaltic composition at 1100°C should have more than 70 mol% ulvöspinel, Fe_2TiO_4 , in solid solution with magnetite, Fe_3O_4 . Such a composition would have a Néel temperature slightly below room temperature (Néel temperature versus composition is shown in Figure 3.2) and thus such minerals would not contribute to the magnetic record. "Fresh" submarine basalts are predicted from this work, and are found, to contain approximately $.5\text{Fe}_2\text{TiO}_4.5\text{Fe}_3\text{O}_4$ because sub-solidus high temperature oxidation occurred. These titanomagnetites have Néel temperatures near 150°C and are not commonly used in paleointensity studies. It would seem from this that the quenched SBG titanomagnetites should have more Fe_2TiO_4 than the bulk of the oceanic basalt, but they do not.

A solution of this puzzle can be found once one recognizes that there is a solvus in the titanomagnetite system. Although *Lindsley* (1973) made one of the first attempts to resolve this solvus, it was poorly determined because the kinetics are such that measurable exsolution does not occur in this system on a laboratory time scale. *Ghiorso* (1997) used thermodynamic modeling to overcome this kinetic obstacle and his best estimate of the titanomagnetite solvus is shown in Figure 3.2. The explanation of the magnetite in SBG is now apparent. We expect that the glass cooled rapidly to around 0°C in the oceanic environment and initially contained slightly more than 70 mol% ulvöspinel in solid solution with magnetite. Exsolution subsequently

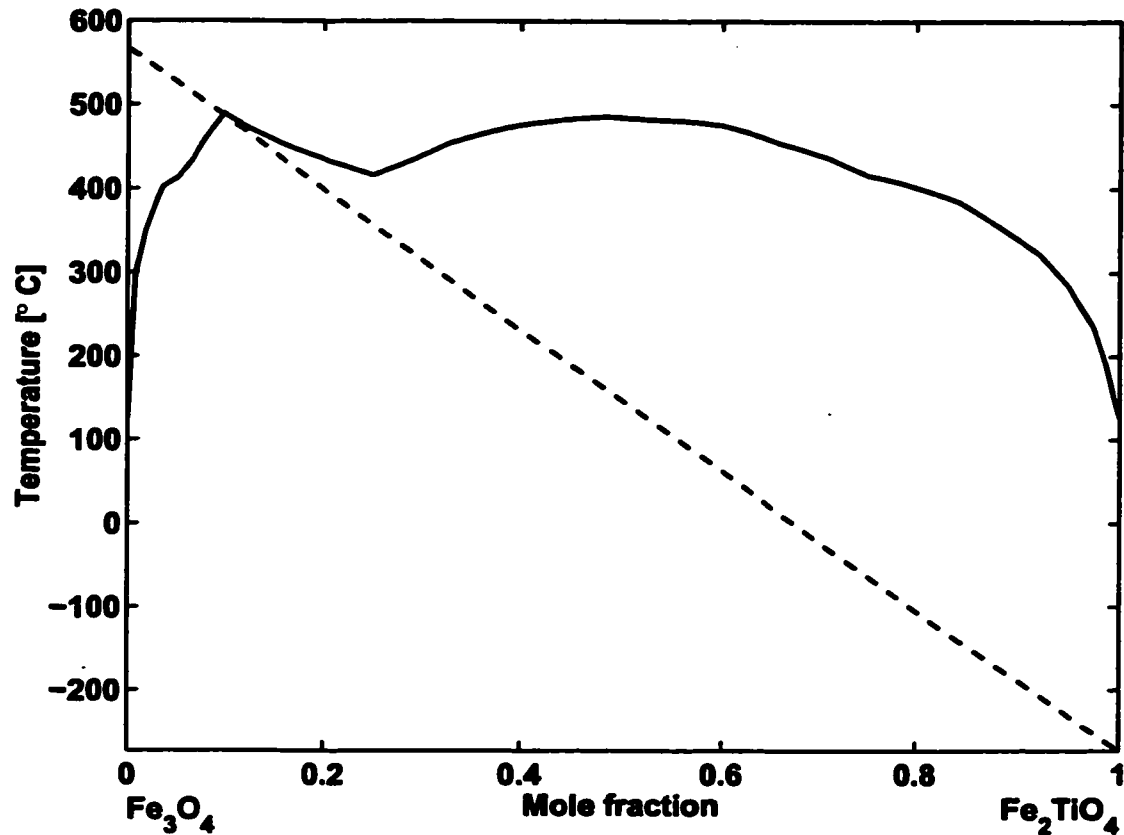


Figure 3.2: Solvus (solid line) and Néel temperature (dashed line) for the magnetite-ulvöspinel system. (After *Ghiorso* (1997))

occurred, forming nearly pure magnetite and ulvöspinel phases. It should be pointed out that *Pick and Tauxe* (1993b) find Néel temperatures in the range 490°C to 550°C, indicating that the SBG titanomagnetites contain up to 10 mole percent ulvöspinel. This suggests that the solvus shown in Figure 3.2 needs slight modification. Indeed *Ghiorso* (1997) discusses the errors in the solvus and these are such that 10 mol% ulvöspinel in magnetite is easily accommodated. We conclude that we are dealing with a low temperature phenomenon in which a low titanium magnetite is essentially growing at ambient conditions on the sea floor.

The above indicates that the remanence in SBG should be a grain growth CRM

(chemical remanent magnetization) rather than a TRM which is required for absolute paleointensity estimates. But why should such a remanence exhibit ideal Thellier behavior out to 400°C or so? *McClelland* (1996) has provided the most recent extension of the theory of grain growth CRM. She was interested in the case in which the grain growth occurred in the laboratory and would be detected by pTRM checks. However, pTRM checks would not detect the grain growth in the SBG case for the kinetic reasons already mentioned. She finds that ideal Thellier behavior is observed out to temperatures of 400°C, or higher, for grain growth in SD magnetite. Although the precise temperature above which the onset of non-ideal Thellier behavior occurs may not be well determined because of the simplified version of SD theory that she uses, the general concepts appear sound and we are not aware of a more reliable theory. Moreover, the theory provides a natural interpretation of the SBG results. In particular, at the blocking volume the estimated intensity would be lower than if the sample had acquired a pure TRM. There is no reason that the grains would stop growing once the blocking volume is reached and further growth would lead to still lower paleointensity estimates. Eventually all growth would end because all the titanomagnetite material (which is at most only a few percent of the basalt) had been exsolved. Therefore, the estimated intensity for the most recent samples (less than 0.3 Ma) would exhibit an intensity that would be somewhat lower than the actual inducing field but still higher than that exhibited by older samples. If the actual intensity of the field had been invariant throughout the past 65 Myr, the intensity of the most recent time would be lower than the present field. Going back further in time there would be a decrease over an interval of time that depends on the kinetics of the system (which remain poorly defined) until nearly constant intensity estimates were obtained for all older rocks. Of course, if the intensity of the field were varying, as it surely must have, this would also affect the intensity recorded in the grain growth CRM. We conclude that there is a rock magnetic explanation for the data used to construct model 2 in Figure 3.1. A confounding factor is whether viscous effects accompany the CRM as

suggested by *McClelland* (1996). When viscous effects are important the SBG data would not necessarily provide a lower bound.

There are several lessons that can be learned from the SBG example. The first is that essentially all existing paleointensity methods can, and probably do, fail in some cases. In the SBG case the hidden variable problem is evident in that neither the solvus (*Ghiorso*, 1997) nor the theory (*McClelland*, 1996) was available when *Pick and Tauxe* (1993a,b, 1994) pioneered the SBG work. The second lesson is that paleomagnetists primarily test their intensity methods using rocks that formed in known fields, which restricts them to approximately the most recent 150 years. They seem particularly concerned with changes that occur on laboratory time scales and can be detected using such tools as pTRM checks. In contrast, many changes, including exsolution, order-disorder and low temperature oxidation, that are known to affect some iron titanium oxides occur on substantially longer time scales. It is typically assumed that such changes will be manifested in non-ideal Thellier behavior. Unfortunately, this manifestation may not occur until very high temperatures are reached, as is evidenced in the SBG example. The third lesson is that one does not want to base intensity interpretation on one method that uses samples with a restrictive origin and composition. Finally, the SBG data may still represent a valuable contribution to intensity interpretations if their intensities are due to a pure CRM and viscous effects are negligible. In this case they provide a lower limit for the actual intensity. Based on the increase in apparent intensity around 300 ka, the lag time between the rock and magnetic ages appears to be less than about 0.3 million years.

3.4 The Database

The database PInt97 was originally compiled by *Tanaka et al.* (1995) and is currently maintained by *Perrin et al.* (1998). It contains only absolute paleointensity determinations obtained from normal, reverse, and transitional directions. We restricted our

analysis to rocks with ages less than 320 Ma. This age was chosen to include both the KNS and the long reverse late Paleozoic (Kiaman) Superchron which lasted from 317 Ma to 262 Ma (e.g., *Opdyke et al.*, 2000). At the time of this study there were 1692 data points in the Pint97 database that were obtained from a host of methods. These data were augmented by about 250 VDM data from studies that were either not included in Pint97 or that have been published more recently. Studies that were explicitly investigating excursions or reversal transitions were not included in our additions (e.g., *Goguitchaichvili et al.*, 1999; *Quidelleur et al.*, 1999; *Riisager and Abrahamsen*, 2000). *Laj and Kissel* (1999) add an impressive 425 paleointensity estimates obtained from a drill hole on the island of Hawaii. Because these are all of Brunhes age (less than 790 ka), they would not affect the results of this study, which focuses on the long-term changes in intensity. Their results were not included because of this and to avoid biasing the data toward one location and study. It should be noted that in several studies there were inconsistencies; for example, between paleodirections and the corresponding VGP locations (e.g., *Thomas et al.*, 1997; *Solodovnikov*, 1998, 1999a,b). We used our recalculated dipole moments when possible or excluded the data if we could not resolve the inconsistencies. We also use the paleointensity data of *Selkin and Tauxe* (2000), a total of 290 VADM obtained from SBG but plot these separately for reasons given in the preceding section.

Our approach was to use statistical tests to determine if subsets of this database could be considered as coming from a common distribution. If not, we would then use other criteria, primarily rock magnetic considerations, to choose between apparently incompatible data sets. For example, the SBG data often had different statistical properties from other data sets, as will be discussed further in the next section, and that led to the rock magnetic analysis of the preceding section. Two non-parametric statistical tests that we use in this chapter are referred to as the KS1 and KS2 tests, after Kolmogorov and Smirnov; these are introduced in Appendix A. *Sachs* (1984) and *Clarke and Cooke* (1998) give a good introduction and discuss the strengths and

weaknesses of these two tests. The KS1 test is used to assess whether a sample could reasonably have been drawn from a specified distribution, whereas the KS2 test is used to assess whether two independent samples could reasonably have been drawn from the same (unknown) distribution.

As an example, we compare data between 5 and 320 Ma obtained by the Shaw method to those obtained from Thellier methods. Many paleomagnetists argue that the Thellier method works better than the Shaw method (e.g., *Prévot and Perrin, 1992; Goguitchaichvili et al., 1999*), although several studies have reported similar intensities from Shaw and Thellier methods (e.g., *Senanayake et al., 1982; Tanaka et al., 1997*). By applying the KS2 test we found that the Shaw and Thellier data do not come from the same distribution at the 95% confidence level. However, one should be careful in considering the implications of this. For example, if there is a long-term change in intensity, then there also is a long-term drift in the distribution. It seems preferable to consider the data in the 320 Ma–present interval as being contained in an envelope of several nested distributions. Thus, if there is an inadequate and different sampling of this interval by the Thellier methods and the Shaw method, one might reject the null hypothesis that the two data sets come from the same distribution even if all the involved data were perfectly reliable. In particular, approximately 95% of the Shaw data come from three 20–Myr intervals whereas the other data are much more evenly distributed. Considering all of the above we decided to act conservatively and exclude the Shaw data. A more detailed description of our analyses is given in Appendix C. There are some data listed in the PInt97 database as Shaw and Thellier. Based on a sampling of original papers, it appears that this usually means that the Shaw method and the Thellier method were both employed on different samples, sometimes from the same rock unit and sometimes from different units. There are only 65 such data and we made the decision to include them in our database.

There are several other criteria that we also used but will not be extensively discussed here. Perhaps most importantly, we excluded all data that were not obtained

by a Thellier method. There were 32 data points older than 5 Ma for which site latitude and intensity, but no inclination were given. For these data a VADM could be calculated. However, we decided to exclude these because one also would need to reconstruct the locations of the tectonic plates for the appropriate ages for each data point. We adopt the conservative approach by excluding outliers, defined as data points more than three standard deviations away from the mean (but see *McFadden*, 1982). Ages as given by the authors were used. However, different interval lengths were used to evaluate the stability of our results as well as the signal on different time scales. There were changes in some of the details of the long-term trends from this but no changes in the general conclusions occur, as will be discussed further later. We also required there to be a minimum of ten points in any time interval that was used and VDM data that exhibited internal scatter ($dF/F \cdot 100$ in PInt97) greater than 25% were excluded.

Figure 3.3 shows the spatial and temporal distribution of both accepted (Figures 3.3a and c) and rejected (Figures 3.3b and d) data. The total number of accepted data used in database 1 is 969. The data are very inhomogeneously distributed in both space and time. For instance, roughly 90% of the data come from sites in the Northern Hemisphere and slightly more than 75% are from sites in lower and mid-latitudes. There is a strong bias toward the most recent 5 Myr which contain about 50% of the data. Moreover, while some ages are almost devoid of data there tend to be clusters around others (partly due to the fact that some ages were based on stratigraphic determinations).

3.5 Data Analyses and Results

To detect long-term trends of the intensity that are most likely due to changes in the core-mantle boundary, CMB, conditions we averaged over several tens of millions of years. The results for age interval lengths of 20 and 40 Myr are shown in Figure 3.4.

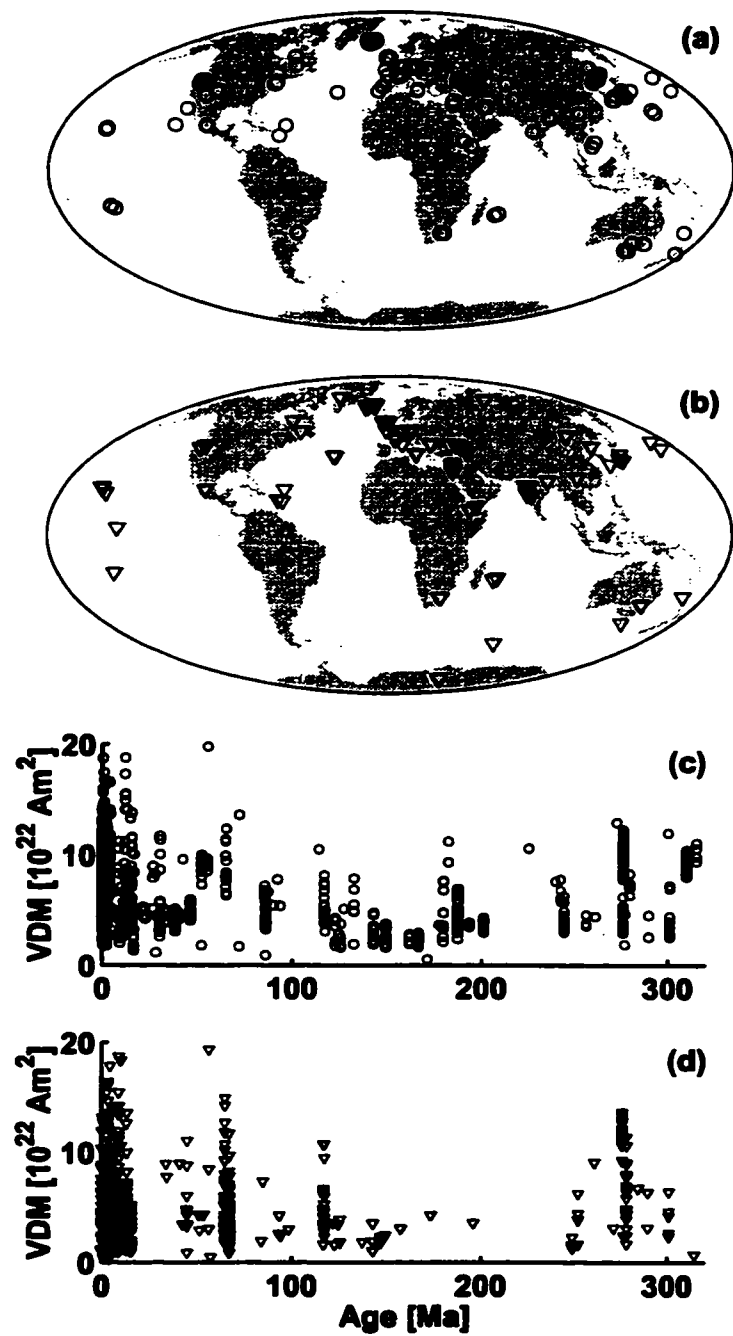


Figure 3.3: Spatial and temporal distribution of VDM data considered in this study. (a) Global distribution of sampling sites for VDM data accepted in database 1. (b) Same as (a) for rejected data. (c) Temporal distribution of VDM data accepted in database 1. (d) Same as (c) for rejected data. In (c) and (d) the data are truncated at $20 \times 10^{22} \text{ Am}^{-2}$ for illustration purposes only.

The averages for the SBG samples (database 2) are shown as open circles and they lie below the estimates for the mean intensity (database 1 consisting of Thellier-obtained VDM) throughout the Cenozoic. Because the data used in database 1 are clearly independent from those in database 2 and because they provide different types of information, it appears that the first order long-term intensity for the Cenozoic may be accurately portrayed in Figure 3.4. This is not evident for the Mesozoic, during which the means for the SBG sometimes exceed the intensity estimates.

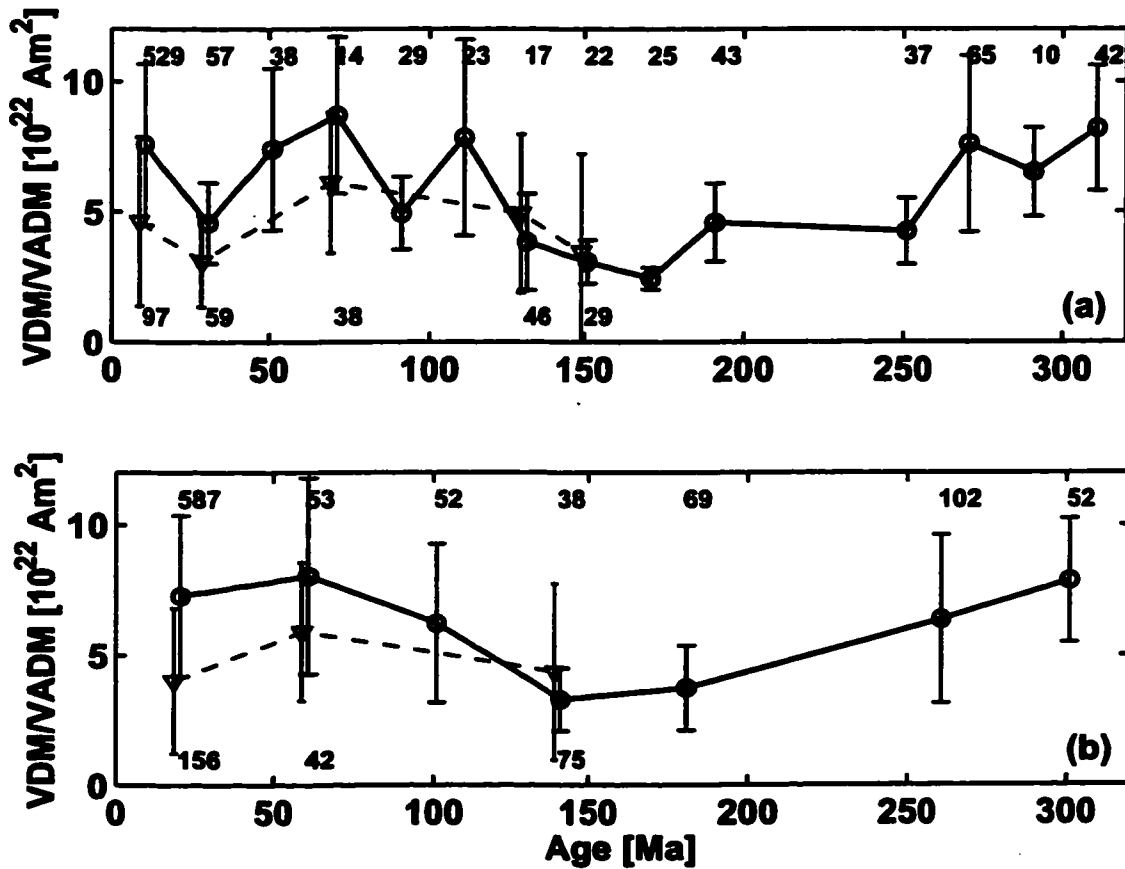


Figure 3.4: Long-term mean dipole moment for database 1 (solid line and circles) and database 2 (SBG data, dashed line and triangles), for VDM/VADM data averaged over (a) 20 Myr and (b) 40 Myr intervals. The number of VDM data in a given age interval are shown at the top (database 1) and bottom (database 2) of each figure.

Figure 3.5 shows histograms of the paleointensity data for database 1 with ages less than 5 Ma and for data with ages greater than 5 Ma. These two age intervals were analyzed separately because roughly half the data have ages less than 5 Ma. The data for the most recent 5 Myr can be reasonably well fit with a normal distribution. Fitting a number of unimodal and bimodal distributions to the data and assessing the goodness-of-fit with the KS1 test we found that we could not reject a normal distribution for the most recent 5 Myr at the 63% (1σ) or the 95% (2σ) confidence level (Figure 3.5a). However, this is not the case for the data with ages between 5 and 320 Ma, which instead appear to be bimodally distributed (Figure 3.5b). Using the KS1 test to assess the goodness-of-fit we found that none of the unimodal distributions considered (normal, lognormal, gamma) adequately fits the data. The data are tested against distributions whose parameters are estimated from the data. In each case the level of confidence for rejecting the null hypothesis that the data follow a particular distribution was close to 1. A reasonable fit can be achieved with a bimodal normal distribution. We will discuss the significance of these results in the following section.

The SBG data exhibit different distributions from those of database 1. We performed a number of KS2 tests on various subsets of databases 1 and 2 and found that for every age interval chosen (0–5 Ma, 5–320 Ma, 0–160 Ma, and 5–160 Ma) the null hypothesis that database 1 and 2 had the same underlying distribution could be rejected at a level of confidence greater than 99%. Figure 3.6a illustrates that a unimodal distribution is not a good fit to the SBG data with ages less than 5 Ma. However, we did find that a unimodal lognormal distribution cannot be rejected for SBG data with ages greater than 5 Ma (Figure 3.6b). The differences in the distributions reflect that the SBG data are different and record a CRM component. The need for a bimodal distribution to fit the data in Figure 3.6 probably reflects the kinetic aspects of the problem: grain growth of magnetite probably ceases several hundred thousand years after the rock formed. Thus, younger rocks will tend to have higher intensities than older ones in the 0–5 Ma interval, as has been found (*Juarez and*

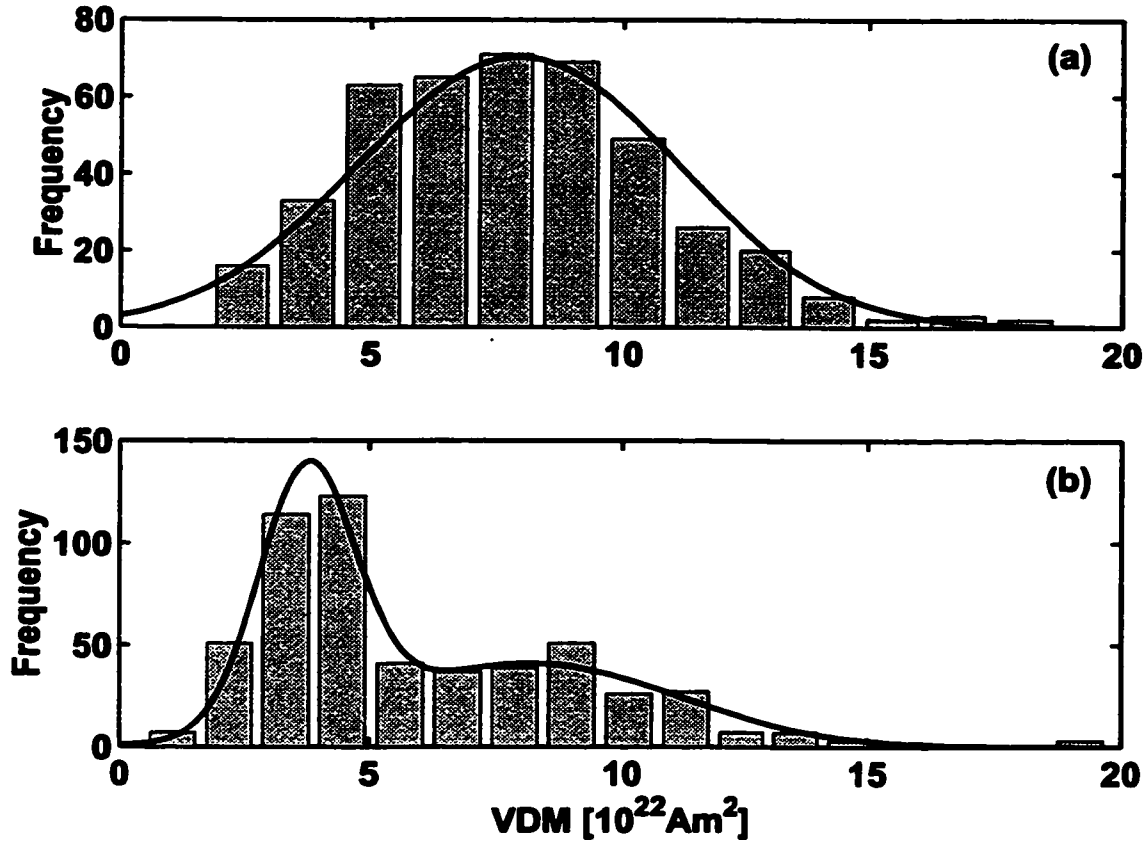


Figure 3.5: VDM data distribution for database 1; (a) VDM $< 5 \text{ Ma}$ with normal fit and (b) VDM $5\text{--}320 \text{ Ma}$ with bimodal normal fit. The histograms are truncated at $20 \times 10^{22} \text{Am}^2$ for illustration purposes only.

Tauxe, 2000).

3.6 Discussion

The intensity was 30% higher and 30% lower during the past 10^4 years than the present intensity. A similar variation is seen when one compares the variation of the mean intensity for 10^4 year intervals over the past 10^5 years, due to the Laschamp excursion (e.g., *McElhinny and Senanayake, 1982; Guyodo and Valet, 1999*). One also expects there to be changes associated with the evolution of CMB conditions on a

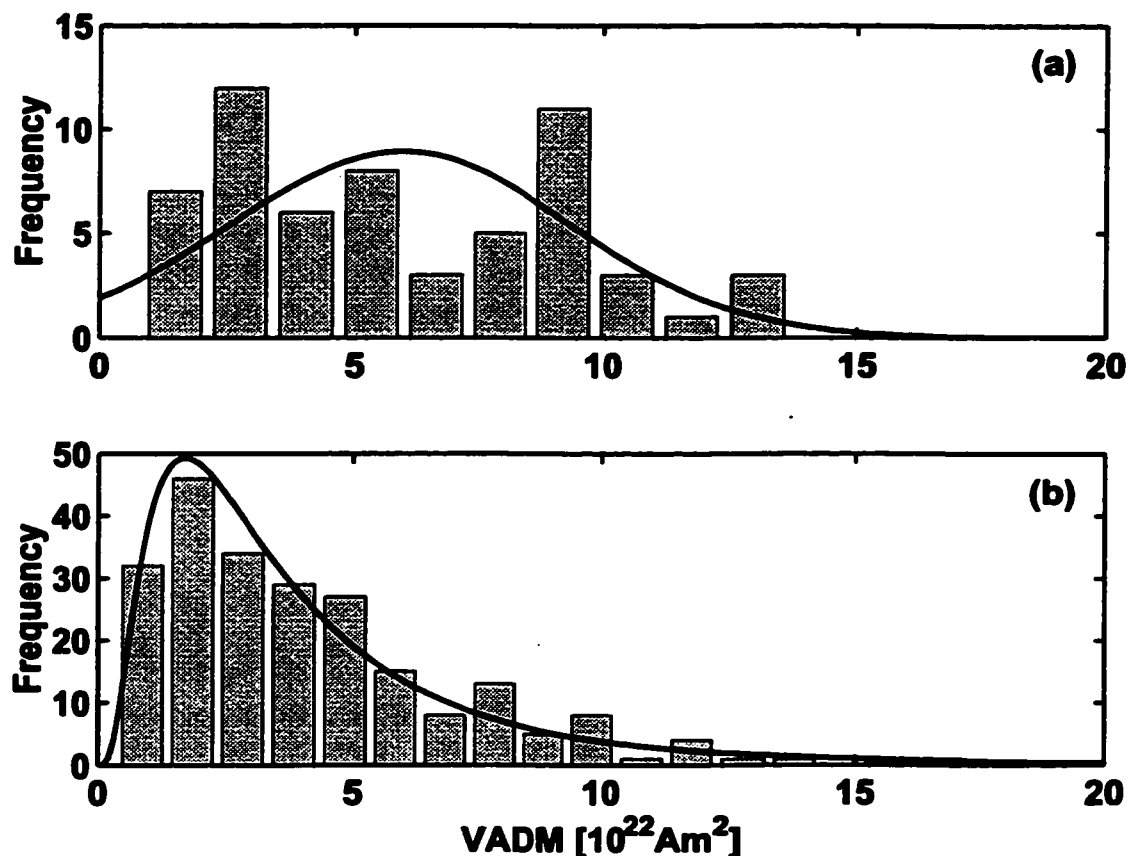


Figure 3.6: VADM data distribution for database 2; (a) VADM < 5Ma with an inadequate normal fit and (b) VADM data with ages 5–320 Ma with an acceptable lognormal fit. The histograms are truncated at $20 \times 10^{22} \text{Am}^2$ for illustration purposes only.

10^7 year or longer time scale. Such variations make it difficult to interpret accurately the intensity data and to assess models such as shown in Figure 3.1.

Nevertheless, we have shown that model 2 in Figure 3.1 can probably be discarded because the SBG samples do not provide an unbiased estimate of the paleointensity. We find this an intuitively appealing result because it is difficult to imagine the mechanism that would have produced a sudden large increase in the mean intensity in the Late Pleistocene above that for the previous 150 Myr. As an aside, it should be pointed out that the direction and intensity of remanence are recorded differently in

CRM. In particular, the direction of remanence for a grain growth CRM is locked in when the grain passes the blocking volume rather than the entire span over which grain growth occurs. In contrast, the intensity of a grain growth CRM depends on the final grain volume and on the distribution of magnetic directions in a grain ensemble at the blocking volume. The theory is only well developed for an ensemble of identical uniformly magnetized grains. Some additional support for our interpretation is provided by the experimental work of *Gogitchaichvili et al.* (1999) who have demonstrated that some forms of CRM associated with palagonization can produce Arai plots similar to those found for the SBG. *Merrill* (1975) presents an overview of CRM and explains why CRM should ultimately be manifested in non-ideal Thellier behavior. Thus any full Thellier experiment that exhibits ideal Thellier behavior up to the Néel temperature should be trusted to provide a reliable paleointensity estimate, except for very unusual circumstances. This then provides a way to test our interpretation. In addition, controlled laboratory experiments on grain growth CRM are encouraged to examine this problem further.

Model 3 in Figure 3.1 is that the intensity is significantly higher during superchrons, such as the KNS. To test this we conservatively define high intensity as that associated with a dipole moment of $8 \times 10^{22} \text{Am}^2$ or higher. This is substantially lower than the high intensity advocated by *Tarduno et al.* (2001) who argue that the intensity during the KNS is more than twice the mean intensity of $5.2 \times 10^{22} \text{Am}^2$ we find for the KNS when the data from *Tarduno et al.* (2001) are excluded. Model 3 is tested by assuming that all the data used in Figure 3.4 are accurate (including those of *Tarduno et al.*) and that they have a normal distribution. We find that the probability of a high mean intensity for the KNS is negligibly small. This test is not particularly sensitive to the distribution assumed (providing it is a reasonable one) but naturally it does depend on the assumption that the data used are reliable and independent. *Tarduno et al.* (2001) use only 8 data points with ages that are restricted to within 116 Ma and 113 Ma. This data coverage of the KNS is too poor

to obtain a mean for the entire KNS, which has an age span of about 35 Myr. It is also possible that there is an undetected bias (presumably of rock magnetic origin) in the data of *Tarduno et al.* (2001) data or in the whole rock VDM data. In any case we conclude that there is little support at this time for model 3. It is interesting that one cannot eliminate the possibility that the Kiaman Superchron (Late Paleozoic Reverse Superchron, extending from 317 Ma to 262 Ma) has a high mean intensity since the mean intensity for 117 Kiaman samples is $7.7 \times 10^{22} \text{Am}^2$. Because *Tarduno et al.* (2001) report estimates so much higher than the others for the KNS, a bimodal distribution is required to fit the KNS data. However, if the data from *Tarduno et al.* (2001), which are based on a method so far only used by them, are excluded, a unimodal distribution provides an adequate fit to the KNS data. In contrast, a bimodal distribution is required to fit the Kiaman data. A KS2 test was used to show that the null hypothesis that the intensities for the Kiaman and KNS Superchrons (with or without Tarduno's data) come from the same distribution can be rejected at the 95% confidence level (see Appendix C).

Model 1 cannot be dismissed. Nevertheless, no model can be strongly supported at this time because of poor temporal coverage. Figure 3.7 shows the VDM data distribution for the Cenozoic; to avoid a bias toward the most recent 5 Myr only data with ages between 65 Ma and 5 Ma were included. As appears to be typical for data from database 1 when a time interval of several tens of millions of years is used, the VDM data in Figure 3.7 have a bimodal distribution. It is possible that this reflects multiple intensity states for the geodynamo or, alternatively, that one of the distributions is a manifestation of an undetected rock magnetic artifact. However, the simplest interpretation is that this is a manifestation of non-uniform sampling of a signal (intensity) that exhibits significant long-term time variation. If the latter interpretation proves correct, even the variation in intensity for the Cenozoic shown in Figure 3.4 has only been crudely determined.

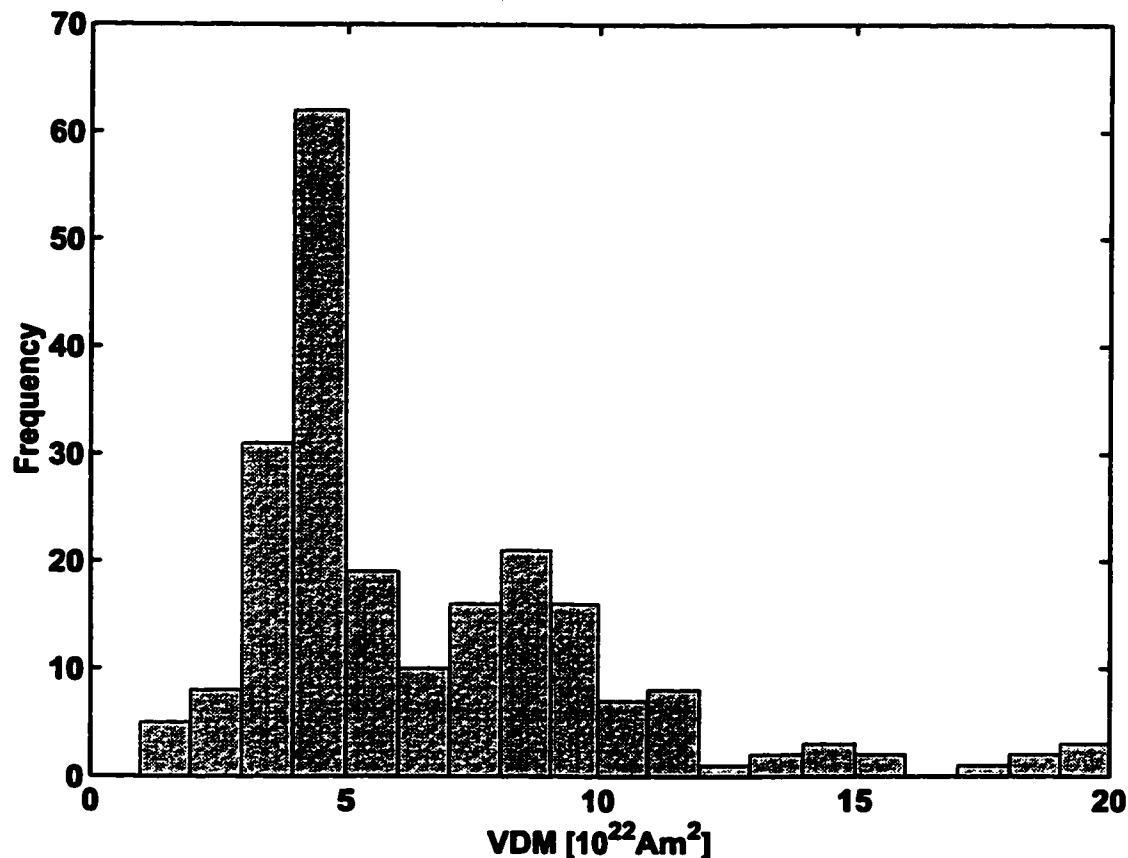


Figure 3.7: Distribution of VDM data with ages between 5 and 65 Ma from database 1. The histogram is truncated at $20 \times 10^{22} \text{Am}^2$ for illustration purposes only.

3.7 Conclusions

Rock magnetic factors are more serious in paleointensity studies than appears to be generally recognized, especially those that are associated with chemical changes that occur in nature but not in the laboratory. However, we have illustrated how some forms of CRM might be used to one's advantage. This is illustrated by considering the SBG samples in which the remanence has been shown to probably be a grain growth CRM. The intensity obtained from these samples can be used to obtain a lower bound on the actual intensity when long-term averages are used and when viscous

magnetization effects can be ignored. Although the intensity data are inadequately distributed in space and time, a first order variation appears to have been obtained for the Cenozoic and it is exhibited in Figure 3.4. There are likely additional second order variations during the Cenozoic that have not been discerned. Trends prior to the Cenozoic are also shown in Figure 3.4, but they are of questionable validity because of inadequacies in the data. The Cretaceous and Kiaman Superchrons appear to exhibit different intensity properties. This suggests that there is not a simple correlation between reversal rate and intensity. Finally, the data do not support a high mean intensity interpretation for the Cretaceous Superchron.

Chapter 4

SHORT-TERM AND LONG-TERM VARIATION OF THE INTENSITY OF EARTH'S MAGNETIC FIELD

4.1 *Summary*

The intensity of Earth's magnetic field and its variability over the past 320 Myr are investigated. The scatter of virtual dipole moments, VDM, is used as a proxy for the short-term variation of intensity. Long-term variation of intensity is defined in terms of the drift of VDM means; each mean is averaged over a minimum length time interval of 20 million years. An investigation of the distributions of VDM data for different time intervals indicates that there are two sources underlying paleointensity data. One source has a mean VDM around 4 to $5 \times 10^{22} \text{Am}^2$ and the second source has a mean about twice that. These means vary little with time. Two alternative interpretations of these sources are given. The first is that there are multiple geodynamo states. The second is that one source is associated with an unidentified rock magnetic artifact. The short-term variation of intensity is correlated with the mean intensity. This correlation does not appear to be a statistical artifact. Instead it appears to be due to either a rock magnetic bias or a property of the paleofield.

4.2 *Introduction*

In theory a magnetic field is uniquely determined in a volume in which Laplace's equation for the scalar potential of that field holds when just the radial component of the magnetic field is specified over the closed surface of that volume. Thus, at first glance, it might seem that it would be simple task to use paleomagnetic data to

determine the history and evolution of the field in time and to provide essential data to theorists to constrain dynamo models. Unfortunately, in practice, directional data are found to be much easier to obtain than intensity data and there are large spatial and temporal gaps in which there are no reliable data and probably never will be.

Paleomagnetists typically describe the directional properties of Earth's magnetic field in terms of virtual geomagnetic poles, VGP, which average over time to paleomagnetic poles under the assumption that the time average geomagnetic field is a geocentric axial dipole field. The scatter of VGP about Earth's rotation axis is commonly used as a proxy for paleomagnetic secular variation (e.g., *McFadden et al.*, 1991). Analogously, virtual dipole moments, VDM, for oriented samples, or virtual axial dipole moments, VADM, for unoriented samples, are used to describe the paleointensity. The time average magnetic field intensity is obtained from averages of VDM or VADM and is referred to as the paleomagnetic dipole moment, PDM. The time required over which one must average VDM or VADM to obtain a PDM is not known. Moreover, this time interval need not be the same as that required for obtaining a paleomagnetic pole from VGP. This follows because in directional studies one needs to average out both the non-dipole field and the equatorial dipole field to obtain the best estimate of the geocentric axial dipole field. In contrast, in VDM intensity studies one only needs to average out the non-dipole field to obtain an estimate for the geocentric dipole field (which need not be along the rotation axis). It has been suggested that only a few hundred years is required to average out the non-dipole field (*Hulot and LeMouél*, 1994), while thousands of years are required to average Earth's magnetic field to a geocentric axial dipole field.

The paleointensity is expected to vary significantly on time scales that range from 10^2 to 10^9 years. The short-term variation, defined as less than a million years, is primarily due to processes acting within Earth's outer core, while the long-term variation, defined as greater than twenty million years, is primarily attributed to changes in boundary conditions (*Merrill et al.*, 1996, see also Chapter 3).

The scatter of VDM is used in this chapter as a proxy for the short-term variation of intensity. The long-term variation of this scatter is referred to as the paleosecular variation of intensity, PSVI. Estimates of PSVI include errors associated with inadequacies in spatial and temporal averaging, measurement errors and rock magnetic errors. In spite of the challenges this poses to determine the PSVI, there are many potential rewards. First, the PSVI provides direct information on the properties and evolution of Earth's magnetic field. A second motivation comes from the common assertion that as the mean intensity decreases the paleosecular variation increases (e.g., *Love, 2000*). Although intuitively appealing, this assertion has never been properly evaluated. Thirdly, the PSVI data should be valuable to dynamo modelers, as is evidenced in *Glatzmaier et al. (1999)* who show that spatial variability in core-mantle heat flux leads to changes in reversal rate, to changes in directional PSV, to changes in mean paleointensity and to changes in PSVI. The first three of those have been determined before, while, here, we make the first attempt to determine the PSVI. Finally, the investigation of PSVI leads to some unexpected results on the interpretation of the long-term changes in Earth's paleointensity.

A variety of different theoretical distributions have been found to describe paleointensity data in the past. For example, *Constable et al. (1998)* use a gamma distribution for relative paleointensity data from the past 11 Myr. *Kono (1971)* reports a normal distribution for 78 VDM data covering the past 10 Myr. In contrast, *McFadden and McElhinny (1982)*, using about twice as many data with ages between 0 and 5 Ma, show that their distribution is truncated by a small value and is skewed toward larger values, and propose a model in which the observed distribution is the superposition of normal distributions (nested distribution). *Tanaka et al. (1995)*, analyzing absolute paleointensity data older than 0.03 Ma and obtained by Thellier or Shaw methods, reject a normal, but not a lognormal distribution for data in 5 Myr intervals between 20 Ma and the present. *Perrin and Shcherbakov (1997)* use Shaw and Thellier data covering the past 400 Myr and find that these are also consistent

with a lognormal distribution. However, when applying a set of 'mild' selection criteria the distribution becomes clearly bimodal. The major emphasis of this chapter is placed on showing that the evolution of the VDM distribution as a function of time provides valuable information for the interpretation of intensity data.

4.3 Paleomagnetic Proxies for Secular Variation

Geomagnetic secular variation is commonly defined as the temporal variation of \mathbf{H} , Earth's magnetic field of internal origin. Hence both the intensity and direction for the field must be known. There are more than an order of magnitude more VGP than VDM for rocks with ages less than 5 Ma and the situation is even worse for older rocks. Therefore, paleomagnetists typically analyze the directional and intensity components of secular variation separately. Paleomagnetists use the scatter of VGP as a proxy for secular variation of igneous rocks. Analogously, a proxy for intensity variation is the scatter of VDM. It should be noted that separately neither the intensity nor the direction, even if specified everywhere on Earth's surface, can uniquely reproduce the field. Thus these proxies cannot be completely acceptable, although they do provide us with valuable information. In this section we apply the ergodic hypothesis of statistical mechanics and use the present field to gain insight into these proxies. In essence, by applying this hypothesis we are saying that the temporal variation of Earth's magnetic field at one location can be characterized by the instantaneous spatial variation over the surface of Earth. Of course, in practice the character of secular variation changes over time and so the hypothesis is not strictly applicable. It will not be used elsewhere in this chapter. However, its use here helps us to illustrate some of the benefits and deficits of these proxies.

The particular geomagnetic field model we choose for the analyses is not crucial and we use the 1995 IGRF for which the present field dipole is tilted with respect to the axis of rotation by 10.5° . To avoid introducing a bias due to this tilted dipole we

rotated all Gauss coefficients so that dipole and axis of rotation are aligned. Intensities F , declinations D , inclinations I , VGP, and VDM were then calculated for 10,000 sites each representing the same amount of surface area for a latitude/longitude grid with a spacing of 2° . This procedure was performed for a series of calculations in which the dipole field was reduced in strength in 5% steps from the present value to zero while the non-dipole Gauss coefficients were held constant.

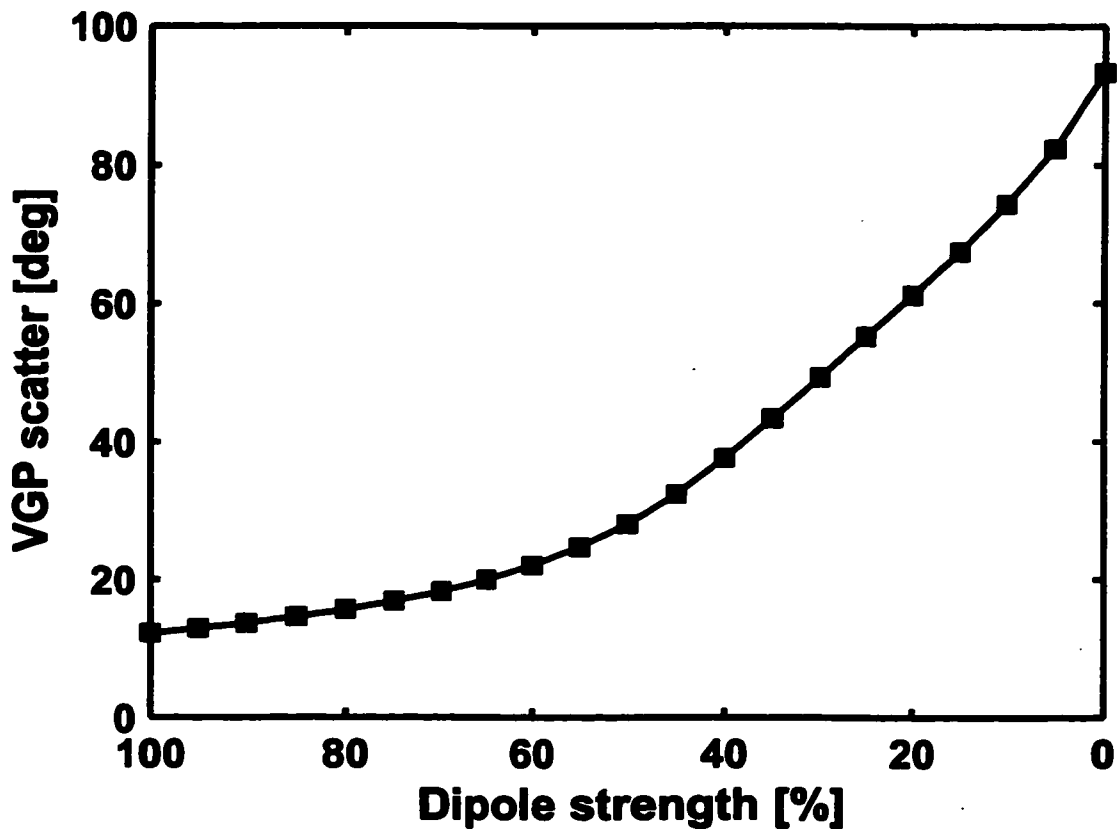


Figure 4.1: Global VGP scatter σ_{VGP} for a decreasing dipole and constant non-dipole field, based on the IGRF 1995.

The angular standard deviation of the VGP distribution is shown in Figure 4.1. As expected, it increases with decreasing dipole strength. The mean VGP in all cases lies well within one angular standard deviation of the geomagnetic pole. Note that

σ_{VGP} has small values initially ($\sim 10^\circ$) but can become fairly large when the dipole is weak.

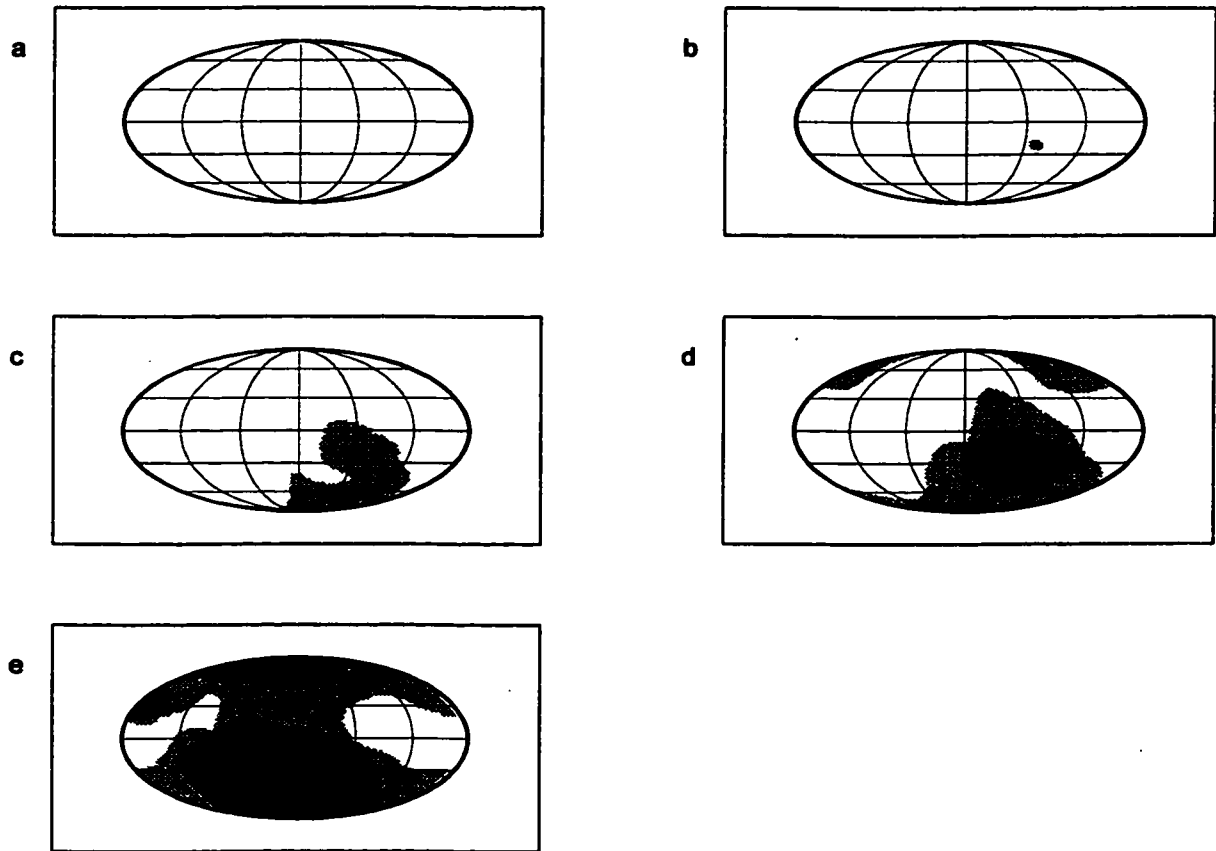


Figure 4.2: Global distribution of VGP for constant non-dipole field and dipole strength a) 100%, b) 75%, c) 50%, d) 25%, and e) zero. The VGP data were separated into normal (white, VGP latitude $\lambda_{VGP} > 45^\circ$), normal transitional (light gray, $0^\circ < \lambda_{VGP} < 45^\circ$), reverse transitional (dark gray, $-45^\circ < \lambda_{VGP} < 0^\circ$), and reverse (black, $\lambda_{VGP} < -45^\circ$).

Figure 4.2 shows how the field polarity, as determined from VGP, varies on the surface of Earth for various dipole strengths. The VGP data were separated into normal, normal transitional, reverse transitional, and reverse. The present geomagnetic field has no transitional VGP. The first transitional VGP in our calculations appear when the dipole has been reduced by roughly 25%. The area with transitional VGP

grows gradually as the dipole is reduced in size. Both absolute and relative intensity data indicate that excursions occurred during the Brunhes when the dipole intensity was 40 to 50% of its usual value (e.g., *Merrill et al.*, 1996; *Guyodo and Valet*, 1999). Figure 4.2d shows both transitional regions and regions of local reversals (as determined from VGP). The phenomenon of producing local reversals from the non-dipole field was first suggested by *Whitney et al.* (1971) and is now well recognized. Our results suggest that major excursions (showing reverse directions) require that either the non-dipole field intensity increases while the dipole intensity decreases or that the dipole deviates substantially from a geocentric axial dipole during an excursion. This follows because the dipole intensity had to be reduced by more than 60% to produce any reverse directions. During geomagnetic reversals the dipole intensity decreases to a minimum near 25% of its previous state (e.g., *Tanaka et al.*, 1995; *Merrill and McFadden*, 1999). For this strength about 40% of the area has transitional or reverse polarity.

Finally, the VDM data from our model were generated following the same procedure as for the VGP analyses above, i.e. each point represents the same surface area, to allow for a straightforward statistical treatment. The mean and standard deviation of global VDM distributions were then determined as a function of dipole strength. As expected, the mean VDM decreases as the dipole is reduced. The slope is almost constant until the dipole is reduced to about 2/3 of its initial value, the percentage reduction in mean VDM in that part of the curve is close to that in dipole strength. The curve gradually levels off as non-dipole fields become more significant.

The VDM scatter as a function of dipole strength is shown in Figure 4.3. Note that unlike the standard deviation of the VGP distribution, the VDM standard deviation decreases initially until it reaches a minimum (for dipole strength $\sim 15\%$) and then increases again. So, while VGP scatter increases with decreasing dipole strength that is not the case for the VDM scatter in this model. This result indicates that the decrease in dipole field strength does not imply that the scatter in VDM will increase.

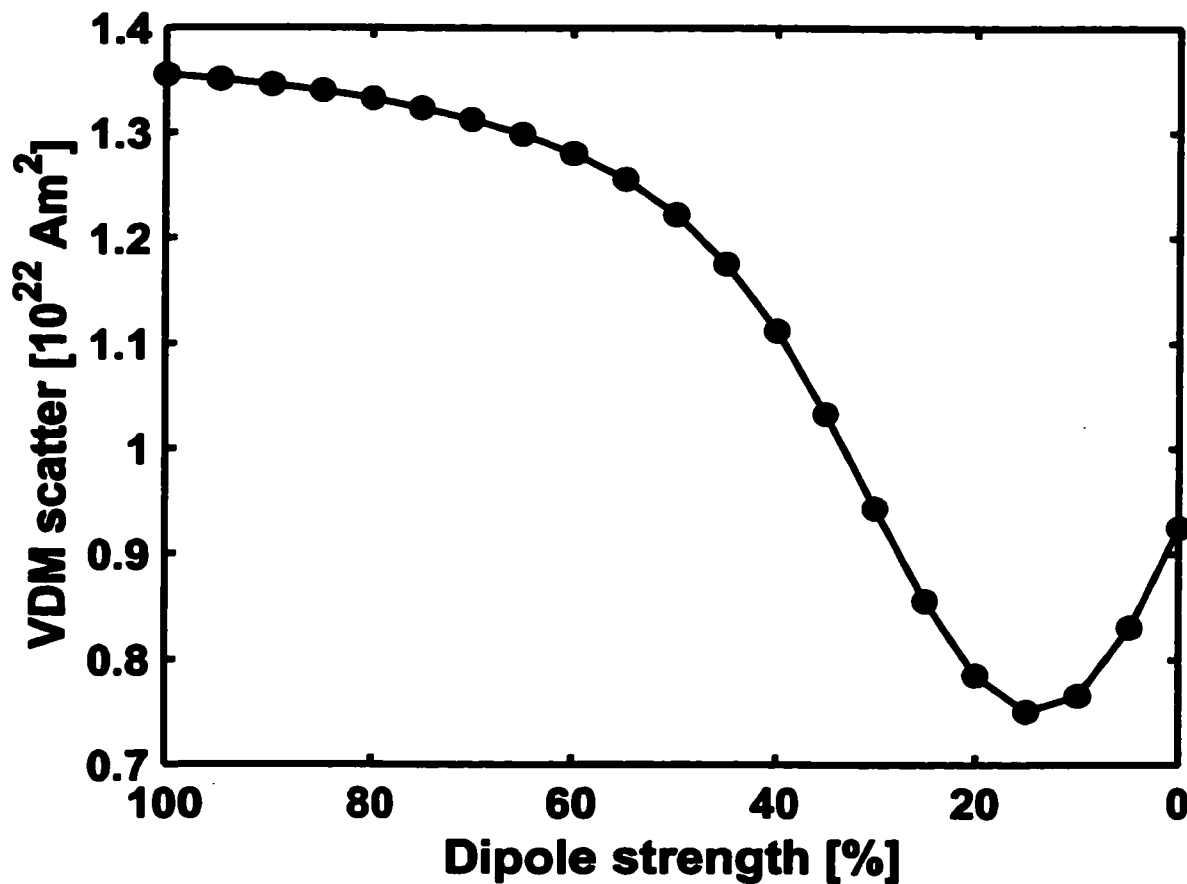


Figure 4.3: VDM scatter σ_{VDM} for a decreasing dipole and constant non-dipole field, based on the IGRF 1995.

Although it may increase or decrease depending on the properties of the non-dipole field, it would decrease if the paleofield resembles that of the present field.

4.4 Data Analyses

The data used in this chapter are the same as database 1 used in Chapter 3. These data are 969 Thellier derived VDM from rocks younger than 320 Ma, an age selected to include the well-documented superchrons, the Late Paleozoic Reverse Superchron (Kiaman) and the Cretaceous Normal Superchron (KNS). The data are unevenly

distributed in space and time. For example, approximately 50% have ages less than 5 Ma and 90% come from the Northern Hemisphere. Previous analyses also used VADM intensities from submarine basaltic glass, SBG, samples to establish a lower bound (Chapter 3). The SBG samples were shown to carry a grain growth chemical remanent magnetization, CRM, from which linear Thellier curves could be used to obtain a lower limit on the actual intensity. Our analyses suggested that the variation of intensity was reasonably well obtained for the Cenozoic. Older trends in intensity were less well determined.

Figure 4.4 shows the temporal dependence of the mean intensity obtained from database 1 as well as the VDM scatter. One notes that the mean VDM and the VDM scatter are correlated; a decrease in intensity is accompanied by a decrease in scatter. At first this may seem counterintuitive, but this is precisely what was found in the previous section that used the present field as a model. Nevertheless, it is wise to determine if there are other explanations for this correlation, including that it is an artifact that has nothing to do with field behavior.

4.5 Potential Statistical Artifacts

Perrin and Shcherbakov (1997) note both a correlation between the mean and the standard deviation of VDM and a correlation between the VDM standard deviation and the number of cooling units involved in calculating this scatter. They speculate that the two correlations might be connected suggesting that the complete spectrum of secular variation has not been sampled sufficiently. This is discussed further in Section 4.7.

The most serious potential artifact from the brute force application of statistics concerns the fact that any intensity distribution must be zero-bound: there are no negative intensities. Intuition into this zero-bound effect can be gained by considering a normal distribution. Such a distribution would have to be truncated at zero since

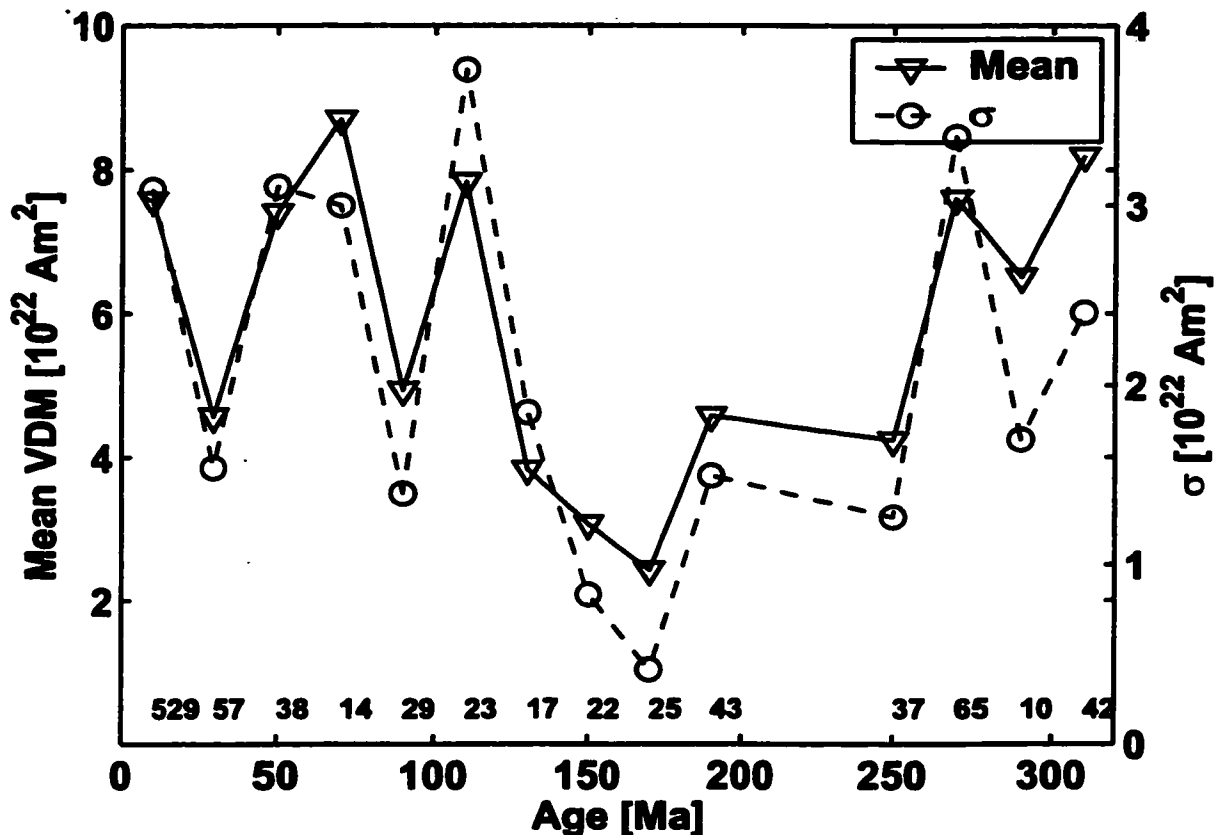


Figure 4.4: Means (triangles and solid line) and standard deviations (circles and dashed line) of VDM data as a function of time for 0-320 Ma. The data were binned in age intervals of length 20 Myr, the number of data points in each interval is given at the bottom of the figure.

negative values are not allowed. If the intensity mean is decreased, the truncation occurs closer to the mean and the variance is decreased. The zero-bound effect acts to squeeze the distribution such that there is a correlation between intensity and variance.

For a zero-bound distribution the variance σ^2 is typically scaled roughly by the mean or expectation μ^2 . For example, for a gamma distribution

$$\sigma^2 = \frac{\mu^2}{k} \quad (4.1)$$

For a lognormal distribution based on a normal distribution with mean M and variance S^2 , we have that

$$\mu = e^{M + \frac{1}{2}S^2} \quad (4.2)$$

and the variance is

$$\begin{aligned} \sigma^2 &= e^{2M + S^2} (e^{S^2} - 1) \\ &= \mu^2 (e^{S^2} - 1) \end{aligned} \quad (4.3)$$

So the gamma (and therefore Poisson) distribution scales exactly with σ^2 and the lognormal distribution scales approximately with σ^2 .

Most real distributions constrained by the origin can be roughly approximated by the triangular distribution shown in Figure 4.5. For this distribution

$$\mu = \frac{a + b}{3} = \frac{2a + d}{3} = \frac{a(2 + f)}{3}; \quad f = \frac{d}{a} \quad (4.4)$$

and

$$\begin{aligned} \sigma^2 &= \frac{\mu^2 (1 + f + f^2)}{2 (2 + f)^2} \\ &= \frac{\mu^2 (1 + g + g^2)}{2 (1 + 2g)^2}; \quad g = \frac{1}{f} \end{aligned} \quad (4.5)$$

So it is clear that in general distributions constrained by the origin will have their variance scale roughly according to their mean. By changing the relative values of a and b (or d) the shape of the distribution can be changed to approximate most real distributions.

To investigate whether the correlation between VDM mean and variance is indeed due to the zero-bound effect we use a Monte Carlo test to assess the probability that generated data produced by distributions following $\mu^2 = k\sigma^2$ could produce the

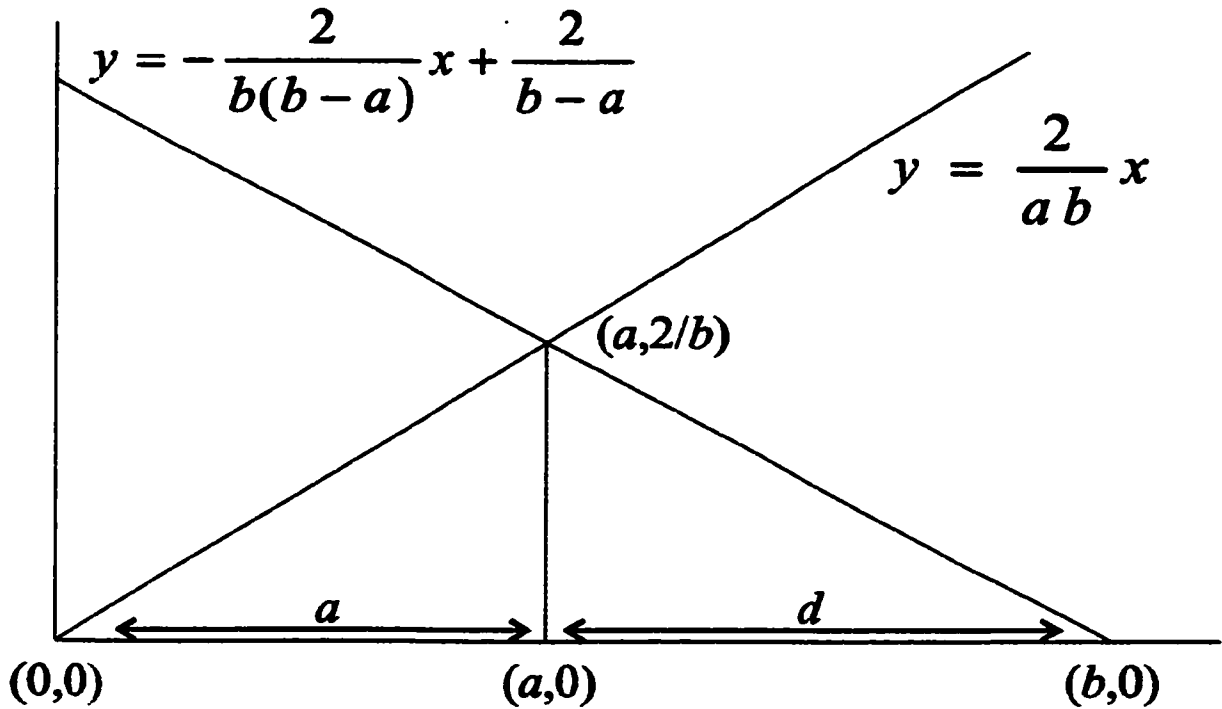


Figure 4.5: Triangular distribution with end points $(0,0)$, $(b,0)$ and $(a, 2/b)$, can be used to approximate most real distributions that are constrained by the origin. Keeping the area of the triangle constant and the distribution fixed to the origin, a decrease in the mean will result in a decrease in the standard deviation.

observed data. In this test, an assumption has to be made about the distribution underlying the VDM data. Both lognormal and gamma distributions have been used to model paleointensity data (e.g., *Tanaka et al.*, 1995; *Constable et al.*, 1998) and are used here for illustration sake. The null hypothesis H_0 is that the VDM data were drawn from distributions where μ^2 scales with σ^2 , i.e. $H_0: \mu^2 = k\sigma^2$. The constant k must be estimated from the observed data. For the observed means and standard deviations, $\mu_{\text{VDM},i}$ and $\sigma_{\text{VDM},i}$. Figure 4.6 shows μ^2/σ^2 as well as the best fitting value for k . To reduce the effect of outliers we estimate k by minimizing the total absolute distance of the observed points from the horizontal line representing k .

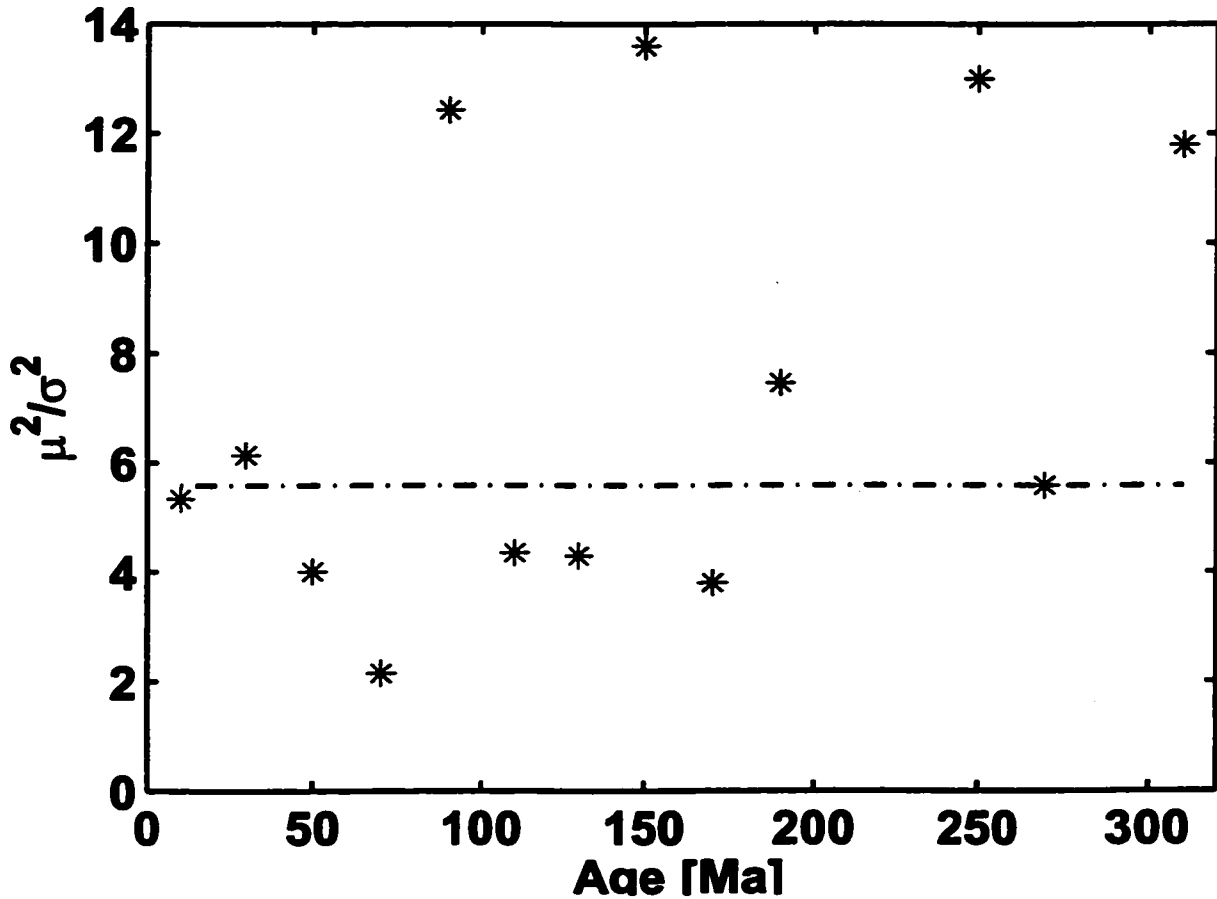


Figure 4.6: Monte Carlo procedure to test whether the correlation between the VDM data means and variances are due to distributions constrained by the origin. Shown are the ratios μ^2/σ^2 for VDM data between 0 and 320 Ma in age intervals of 20 Myr length as well as the best estimate of $k = \mu^2/\sigma^2$. For random data generation in the Monte Carlo process the data points were projected onto the horizontal line k .

The test statistic D_{obs} is given by:

$$D_{\text{obs}} = \sum_i \left| \frac{\mu_i^2}{\sigma_i^2} - k \right| \quad (4.6)$$

The theoretical distribution of D can be obtained as follows: first the empirical points $(\mu_{\text{VDM},i}/\sigma_{\text{VDM},i})^2$ are projected onto the horizontal line k by taking the observed means, $\mu_{\text{VDM},i}$, and adjusting the standard deviation so that $\mu_{\text{VDM},i}^2/\sigma_{\text{mc},i}^2 = k$,

i.e. the parameters for Monte Carlo random number generation are $\mu_{mc,i} = \mu_{VDM,i}$ and $\sigma_{mc,i}^2 = \mu_{VDM,i}^2/k$. Assuming either a lognormal or gamma distribution, N_i random VDM data are then generated for parameters $\mu_{mc,i}$ and $\sigma_{mc,i}$, where N_i is the number of data points in the i^{th} age interval. For these random data means $\mu_{rnd,i}$ and standard deviations $\sigma_{rnd,i}$ are determined and used to calculate one value of D (Equation 4.6). Repetition of this process yields the distribution of D . Finally, the observed value D_{obs} is compared to the theoretical distribution to assess the probability $p(D > D_{obs})$. A small value for p suggests rejection of the null hypothesis.

For our preferred data selection we can reject H_0 at a level of confidence of well over 95%, for both lognormal and gamma distributions and for all bin widths.

It is important to note that the Monte Carlo test used here tests for a linear relationship between mean and scatter. Therefore, any linear relationship between mean and scatter that is caused by the paleofield and not due to the zero-bound effect, would be in the test's null space. This means that the above test is a very conservative one that is based on the use of the non-linear part of the correlation between long-term mean intensity and intensity PSV to reject the null hypothesis. We conclude that the observed correlation between long-term mean intensity and PSVI is not due to the zero-bound effect.

4.6 Paleointensity Variation

The distributions of intensity data for all 20 million year intervals was determined in an attempt to determine the reason for the correlation of PSVI with long-term paleointensity variation. However, this was not completely satisfactory because some intervals contained too few data. A second problem was that the data were often clumped around certain ages and using the mean of the age for a given interval produced misleading graphs. These problems were solved by using overlapping intervals of variable length. Each interval was required to contain a minimum of 50 points.

A subsequent interval was determined by increasing the youngest age until at least 20 points were removed (more than 20 points were removed when a large number of data had the same age). This meant that the oldest age of the interval also had to be increased to maintain a minimum of 50 data points in the interval. A minimum length of an interval of 20 or 40 Myr is used, depending on the degree of smoothing desired. Although the age of the interval is still represented by its mean, large clumping of ages is manifested by the close proximity of successive points. We find this provides a good visual picture of the evolution of the intensity, but at the cost that successive points are not independent.

An example of the above procedure is shown in the histograms of Figure 4.7, where a minimum length of 40 Myr was employed. Note that in these analyses the most recent 5 Myr, which contain roughly half the data, were excluded. The data from 5 Ma to present were unimodally distributed as discussed in Chapter 3 and will not be discussed extensively in this chapter. The change in histograms with age in Figure 4.7 illustrates that the procedure of using overlapping intervals provides a good way to depict the evolution of the intensity distribution with time.

Figure 4.7 shows that the distributions in most intervals are bimodal. The data were fit with bimodal normal distributions, using non-linear least squares fitting by the Gauss-Newton method. The model parameters determined by this fit are the means (μ_{high} and μ_{low}) and the standard deviations (σ_{high} and σ_{low}) as well as the percentage of high and low distributions. A Kolmogorov-Smirnov goodness-of-fit test (see Appendix A, also *Sachs* (1984) and *Press et al.* (1992)) was then used to assess the fit statistically. Unfortunately, this test was not always satisfactory due to instabilities that (infrequently) occurred with minor shifts in some of the data. A consequence is that some subjectivity was used when making decisions whether a unimodal fit was adequate. The reader can refer back to the histograms in Figure 4.7 to decide whether to agree with our choices in the few marginal cases.

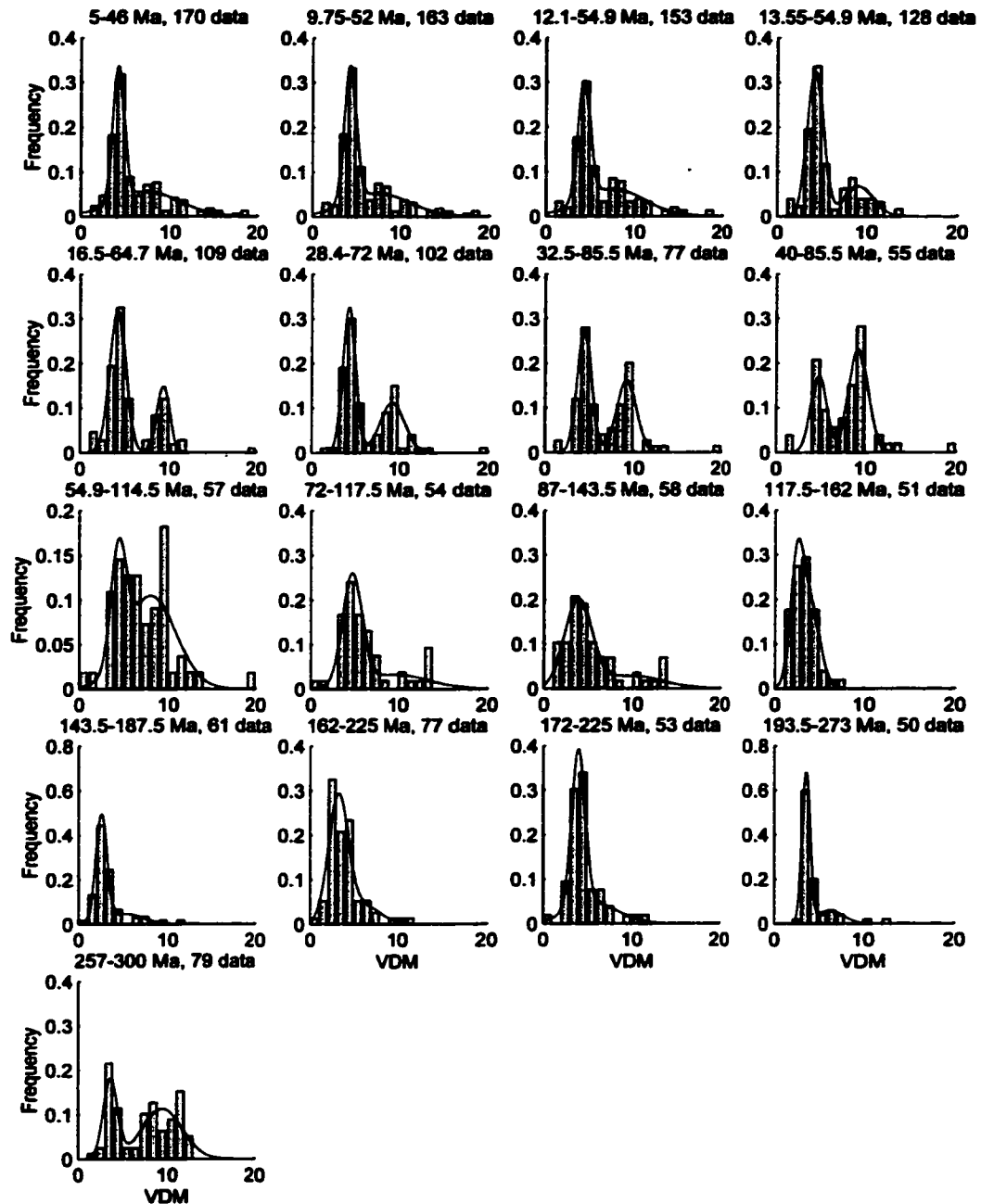


Figure 4.7: Evolution of VDM data distribution for ages 5–320 Ma. Each histogram spans at least 40 Myr and has a minimum of 50 VDM data. The data window is shifted by at least 20 data points between groups. Minimum and maximum ages as well as the number of data are given at the top of each histogram. All histograms include the best bimodal normal fit (as described in the text) with the exception of the last histogram in row 3 where a unimodal normal fit was preferred. Only VDM less than $20 \times 10^{22} \text{Am}^2$ are plotted.

Figure 4.8 shows the results of bimodal and unimodal normal distribution fits for the Cenozoic for a minimum time interval of 20 Myr. In addition to μ_{high} and μ_{low} the mean value of the intensity for a unimodal normal distribution, μ , and the mean VADM from SBG data are given. One sees that the SBG results fall below μ_{low} for the Cenozoic. This is not the case for the Mesozoic for which the SBG not only

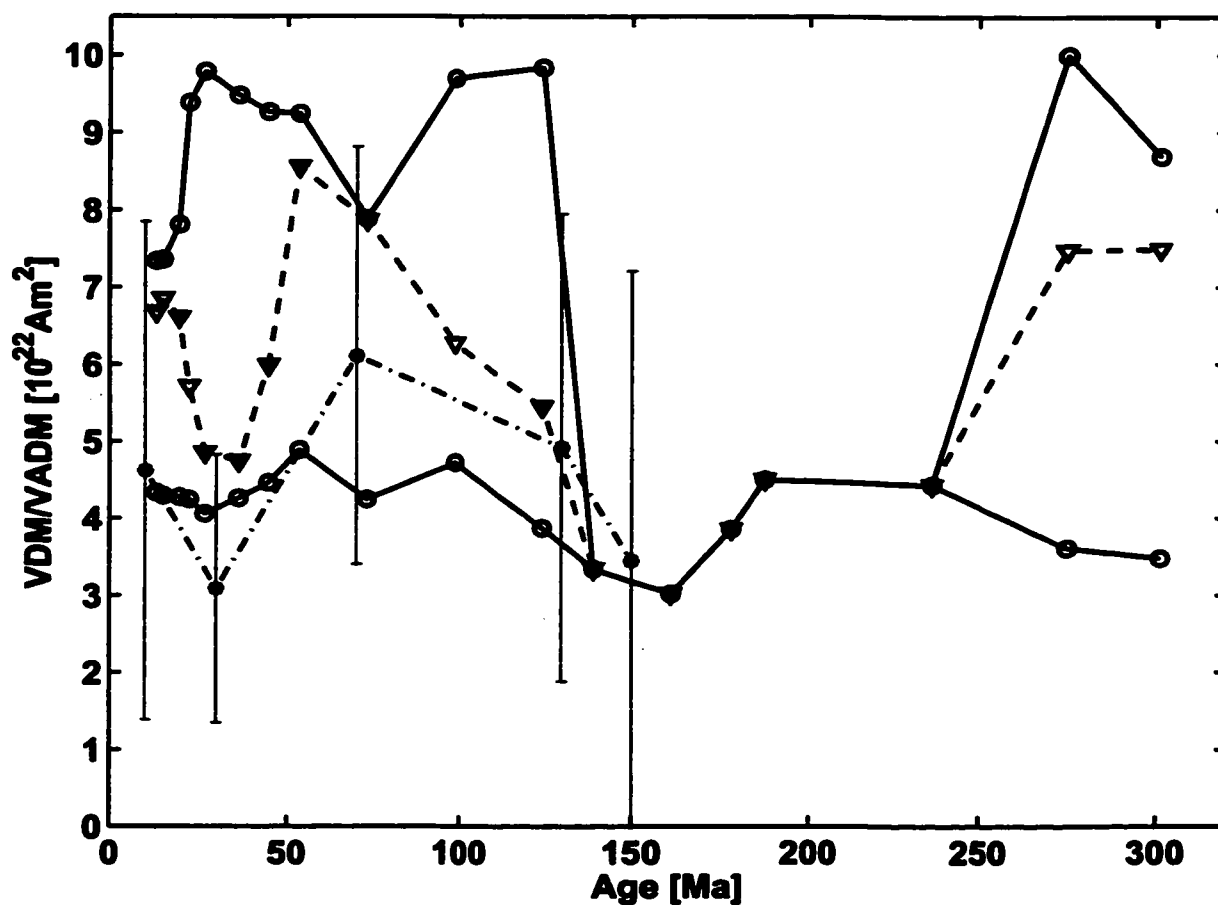


Figure 4.8: Mean paleointensity as a function of time for 0–320 Ma. The means from bimodal normal fits to VDM data in our database, μ_{high} and μ_{low} , are represented by circles and solid and dotted black lines. Also shown are means from unimodal normal fits (triangles and dark grey, dashed line) and SBG means (stars and light grey, dashdot line). Error bars (1σ) are shown only for SBG data, for error bars of bimodal normal fits, see Figure 4.9b).

sometimes rise above μ but also above μ_{high} . However, the error bars are so large for the Mesozoic SBG data that we place no significance on this. Note also that μ varies significantly during the Cenozoic while μ_{high} and μ_{low} do not. This reflects the variable contributions of high and low distributions to the total distribution (see Figure 4.7).

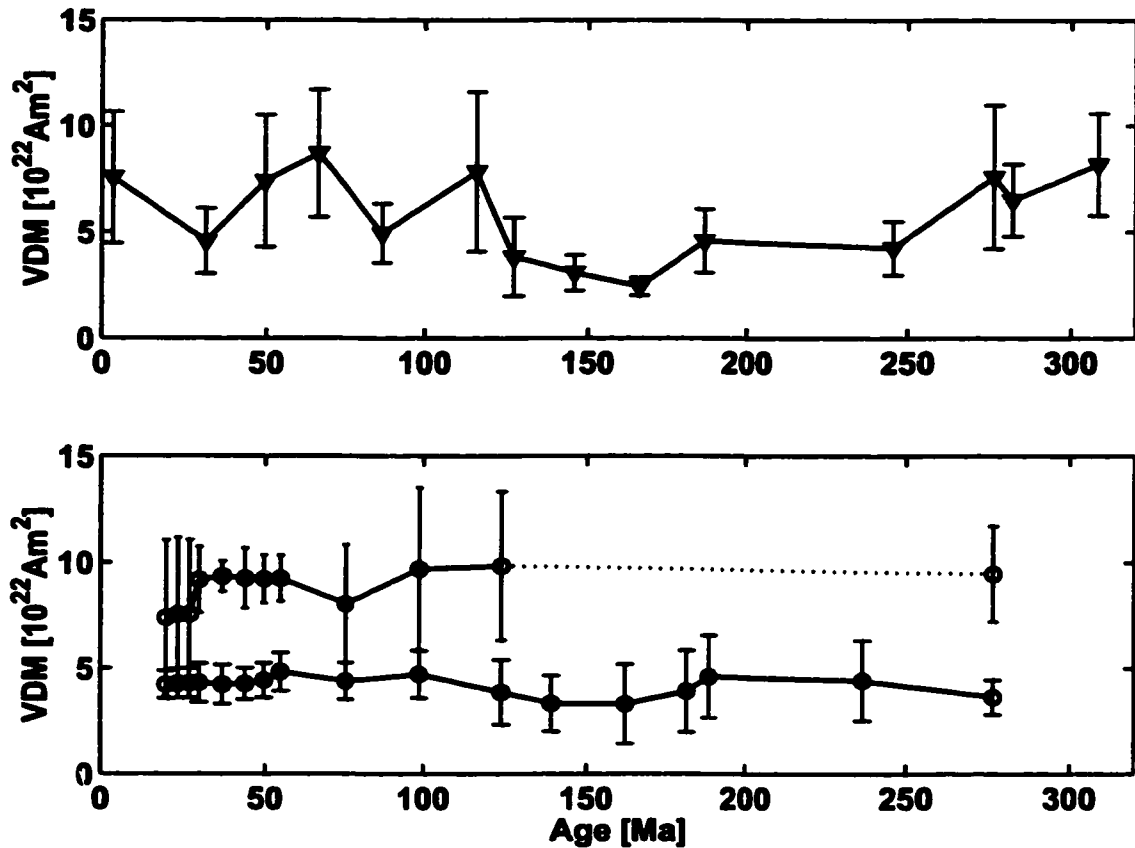


Figure 4.9: Mean paleointensity and scatter (1σ) as a function of time (a) for unimodal normal distributions of VDM data grouped in age intervals of length 20 Myr, and (b) for unimodal and bimodal distributions from groups containing a minimum of 50 data points and spanning at least 40 Myr.

Figure 4.9a shows the mean intensity since 320 Ma in the format used in studies on the paleointensity prior to this one. There are many variations in intensity, including a Mesozoic low that has often been reported from the use of similar, but smaller,

data sets (e.g., *Prévot et al.*, 1990; *Tanaka et al.*, 1995; *Perrin and Shcherbakov*, 1997). Figure 4.9b shows the curves for μ_{high} and μ_{low} for the past 320 Myr for a minimum age interval length of 40 Myr. Only during the first half of the Mesozoic was a unimodal distribution acceptable. This curve illustrates that there appear to be two different mechanisms contributing to intensity estimates. The first mechanism, hereafter referred to as source 1, gives rise to mean values usually in the range of 4 to $5 \times 10^{22} \text{Am}^2$ and the second (source 2) to mean values almost twice this. Surprisingly, the values are almost constant. This is also reflected in the data in Figure 4.7. Note in particular that values in the neighborhood of $6 \times 10^{22} \text{Am}^2$ for μ_{high} or μ_{low} are absent, in contrast with the intensity estimates shown in Figure 4.9a.

4.7 Interpretations

In Chapter 3 we point out that a simple explanation for a bimodal distribution of intensities in an interval is inadequate temporal sampling of a nonstationary intensity signal. However, this is probably not the explanation for the bimodal distributions discussed in the previous section. Bimodal distributions are sometimes seen in the data from time intervals that are just 20 Myr in duration. It is difficult to perceive a mechanism controlled by CMB processes that could account for this bimodality. These data exhibit a similar range of intensities as do those from substantially longer intervals. Even more startling is the lack of a peak of one of the distributions ever having an intermediate value near $6 \times 10^{22} \text{Am}^2$. Moreover, the nearly constant mean values for the source 1 and source 2 distributions are hard to explain by inadequate temporal, but random sampling, of a nonstationary signal. Therefore we conclude that there are two different sources contributing to the intensity estimates.

There are several possible interpretations for these sources. The first is that both distributions in the bimodal distribution provide unbiased estimates of Earth's paleointensities; that is, there are two quasi-equilibrium states with different mean inten-

sities. Of course there are multiple solutions to the dynamo equations, as illustrated by the fact that if the magnetic field \mathbf{H} is a solution, then so is $-\mathbf{H}$. It is also possible that there are two solutions for any given polarity: one with a higher mean intensity and one with a lower mean intensity. Such multiple solutions to a set of coupled partial differential equations are common in many areas of research, including in rock magnetism, where LEM (local energy minimum) states have strong theoretical and experimental verification (e.g., *Dunlop and Özdemir, 1997*). There is also some suggestion that they exist in dynamo theory. In particular, *Zhang and Gubbins (2000)* point out that the geodynamo could fluctuate between the strong and weak field regimes and thereby exhibit different intensities. (*Glatzmaier et al., 1999*) showed diagrams in which the intensity and secular variation change character after a magnetic field reversal. This again implies multiple states since the average reverse and normal polarity states should be identical except for sign. However, it should be added that some input parameters in all dynamo models are orders of magnitude off those appropriate for Earth. For example, the Ekman number is many orders of magnitude too small (e.g., *Busse, 2000; Glatzmaier and Roberts, 2000*). A consequence of this is that it is premature to use dynamo theories to constrain actual intensities or to assess whether there are multiple intensity states assessable to Earth's dynamo. Indeed some dynamo theorists turn the problem around and adjust their models to try and obtain a good fit to Earth's dipole intensity.

One needs to also contend with the possibility that one of the sources is an artifact, probably of rock magnetic origin. We think it is unlikely that both sources are artifacts resulting from, say, two different types of alteration that led to estimates that were either high or low. However, the possibility that one of the sources is biased due to unidentified rock magnetic problems is significant. First let us assume that it is the source of high intensities, source 2, that is in error and hence the majority of estimates (source 1) provide unbiased estimates of the paleointensity. This would mean that that the intensity was significantly lower, almost by a factor of 2, than the present intensity

for the vast majority of the past 320 Myr. For unknown reasons the intensity increased significantly during the most recent few million years, an intuitively unappealing result. The alternative is that the lower intensities associated with source 1 are biased. This means the majority of VDM estimates obtained by versions of the Thellier method are in error, a suggestion previously made by *Tarduno et al.* (2001) in a milder form. As an aside, we point out that the lack of adequate rock magnetic information (for example, information on mineralogy and grain size) in present databases makes it impossible to determine if there are systematic differences in the rock magnetic properties of samples that lead to the two sources of intensities.

Without being able to determine uniquely the sources of intensity, it is not possible to determine the source of the PSVI. Nevertheless, one can eliminate some possibilities for the origin of the estimates of PSVI. It appears that almost all the variation in intensity shown in Figure 4.9a can be accounted for by adding in more of source 1. It depends little on the magnitude of the intensity associated with source 1 and 2, each of which nearly remains constant. If this interpretation is accepted, then the discussion of the artifact sources arising from inadequate statistical analyses, considered in Section 4.5, becomes moot. In light of this the correlation between the number of cooling units and VDM scatter as reported by *Perrin and Shcherbakov* (1997) (see Section 4.5) might occur because more cooling units would increase the probability of sampling both sources 1 and 2. We find a good correlation between $\mu_{\text{high}} - \mu_{\text{low}}$ and the PSVI estimates. That is, the PSVI variation predominantly depends on the amount of source 2 present and only in a minor way does it depend on the scatter associated with each of the separate distributions that comprise the bimodal distribution. Therefore the correlation between long-term intensity and VDM scatter shown in Figure 4.4 reflects true field behavior only if the interpretation that there are multiple acceptable states for the dynamo is valid. The alternative is the correlation is due to a rock magnetic artifact.

4.8 Conclusions

A paleomagnetic database of nearly a thousand VDM obtained with the Thellier method has been used to examine the short and long-term variation of paleointensity. The mean of this database for different time windows is positively correlated with the variance. This correlation is not due to a statistical artifact and can occur if the paleofield is similar to the present day field. Analyses of the evolution of the data distributions of VDM indicate that there are two sources contributing to the intensity estimates. One source has a mean dipole moment around 4 to $5 \times 10^{22} \text{Am}^2$ and the second source has a mean about twice that. These means vary little with time. However, the relative contribution of the individual sources in a given interval is highly variable. The data are inadequate to determine if this variation reflects time variations of the sources or is due to inadequate sampling. The origins of the two sources are also unknown, but at least one probably reflects a reasonably unbiased estimate of the intensity of Earth's paleofield. If both sources represent reliable field estimates, then the geodynamo has multiple states it accesses during most time intervals. The relative occupancy of these states probably would vary with time reflecting the evolution in the core-mantle boundary conditions. It is also possible that one of the sources represents an estimate of the paleofield that is systematically biased by an undetermined rock magnetic factor. The difference in the means of these two sources is correlated with the long-term intensity variance. Therefore the interpretation for this correlation appears to be directly tied to the origins of the VDM sources.

Chapter 5

CONCLUSIONS

Earth's magnetic field \mathbf{H} is a vector field and, hence, for a fuller understanding of the geodynamo's evolution with time and its mechanics one needs to know the full vector information, i.e. the paleomagnetic field's direction as well as its intensity. While the main focus of this thesis is on paleointensities we also investigated some of the fundamental concepts used in paleomagnetism, namely VGP and VDM. Virtual geomagnetic poles are used commonly in paleomagnetism to describe the paleomagnetic field in times of constant polarity and for magnetic reversal transitions. While for times of constant polarity one can expect the dipole part of the field to be vastly dominant this may not be the case during reversal transitions. For example, using a new method for determining what percentage of the field is due to its dipole and non-dipole components, respectively, we find that for the present field (Chapter 2) the non-dipole contribution accounts for approximately 20–25%, a value slightly larger than a century ago when it was about 17–18%. However, there is evidence that during a reversal transition the total intensity of the field is reduced to approximately 25% of its pretransitional value (e.g., *Tanaka et al.*, 1995). In addition, transitional VGP data show erratic behavior during reversal transitions (e.g., *Tric et al.*, 1991; *Prévot and Camps*, 1993; *Channell and Lehman*, 1997). Does this erratic behavior reflect high variability in the dipole field or is it simply due to a relatively larger contribution of the non-dipole field? We investigate this question in Chapters 2 and 4 using a simple model based on the present field and find that not only does the VGP behavior become highly erratic even when the dipole still has 50% of its strength, the field also apparently reverses in different places at different times. The non-dipole

field in our model is held constant which is unlikely to reflect real field behavior. A highly fluctuating transitional non-dipole field would make VGP paths observed at one location even more erratic. We conclude that the concept of VGP, in order to be meaningful, requires a highly dominant dipole field and that, therefore, extreme caution should be exercised when using VGP to describe the paleofield's behavior during times when the magnetic field reverses.

Reliable estimates of the paleomagnetic field's absolute intensity are among the most difficult paleomagnetic quantities to obtain. The data available to us today vary greatly in character and quality for a number of reasons. The techniques for determining paleointensities have been evolving greatly as have the purposes of paleointensity studies. More data abundance and reliability allowed addressing questions regarding the strength of the field and even the field's paleosecular variation. The two most reliable methods for determining absolute paleointensities from igneous rocks are the Thellier and the Shaw method (see Section 1.2). However, there is some controversy over which method is more reliable, with some studies finding similar paleointensity results with both methods (e.g., *Senanayake et al.*, 1982; *Tanaka et al.*, 1997) while others find discrepancies (e.g., *Prévot and Perrin*, 1992; *Goguitchaichvili et al.*, 1999). We attempted to distinguish between the Thellier and Shaw data using the KS2 test (see Appendix A), however, the results are not conclusive as it is difficult to find a time interval in which the data from both methods have comparable age distributions (see Appendix C). Age determinations as well vary greatly in character and quality, from radiometric to stratigraphic, again reflecting differences in the kinds of rocks used and the purpose of particular studies. Generally, this is of minor concern for the questions investigated in this thesis; uncertainties of even a few million years can be expected to have little impact as the timescales considered here are an order of magnitude larger. However, there are studies using stratigraphic age methods that have uncertainties that make the data inadequate for inclusion in our analyses, for example, *Sakai and Funaki* (1988) report ages between 144 and 208 Ma for their

data. Matters are further complicated by the fact that there is a large variability of rock magnetic factors (such as composition, as well as grain size and shape distributions) between rocks used in paleointensity studies. Obtaining similar paleointensity estimates from different mineralogies can give more confidence in the results. On the other hand, as shown in Section 3.3, a specific mineralogy may yield a systematic bias which, in the case of SBG data, has been detected but which might also be present for other mineralogies and undetected in the totality of VDM data. In addition to uncertainties associated with individual paleointensity data the interpretation in terms of long-term trends in the data is complicated by the inhomogeneous temporal and spatial distribution of the data as well as the overall sparsity of data (see Section 3.4).

Despite all the difficulties associated with the data the long-term paleointensity record may contain important clues about the history of the geodynamo and its interaction with the core-mantle boundary. Figure 5.1 contains a summary of some of the findings obtained in this thesis as well as long-term trends of the reversal rate and paleosecular variation from directions (*McFadden et al.*, 1991; *Merrill et al.*, 1996). Previously, to find long-term trends in the paleointensity record, VDM data were simply plotted as a function of time or averaged in age intervals of several tens of millions of years. An example is given in Figure 5.1a where means and standard deviations of Thellier data from our database 1 (see Chapter 3) are plotted for age intervals of length 20 Myr. We provide the first attempt to obtain the long-term trend of PSVI, paleosecular variation from intensities, and find a correlation between the mean VDM and its standard deviation (Figure 5.1c) which does not appear to be a statistical artifact (Chapter 4). Displaying trends in the long-term mean paleointensity as in Figure 5.1a may be misleading as the VDM data exhibit a bimodal distribution, not only if all of the Thellier data are considered but also within many individual age intervals. Therefore, our new way of displaying VDM data involves a combination of unimodal and bimodal fits, as shown in Figure 5.1b. Surprisingly, the two peaks of the bimodal distributions appear to be almost constant as a function of time.

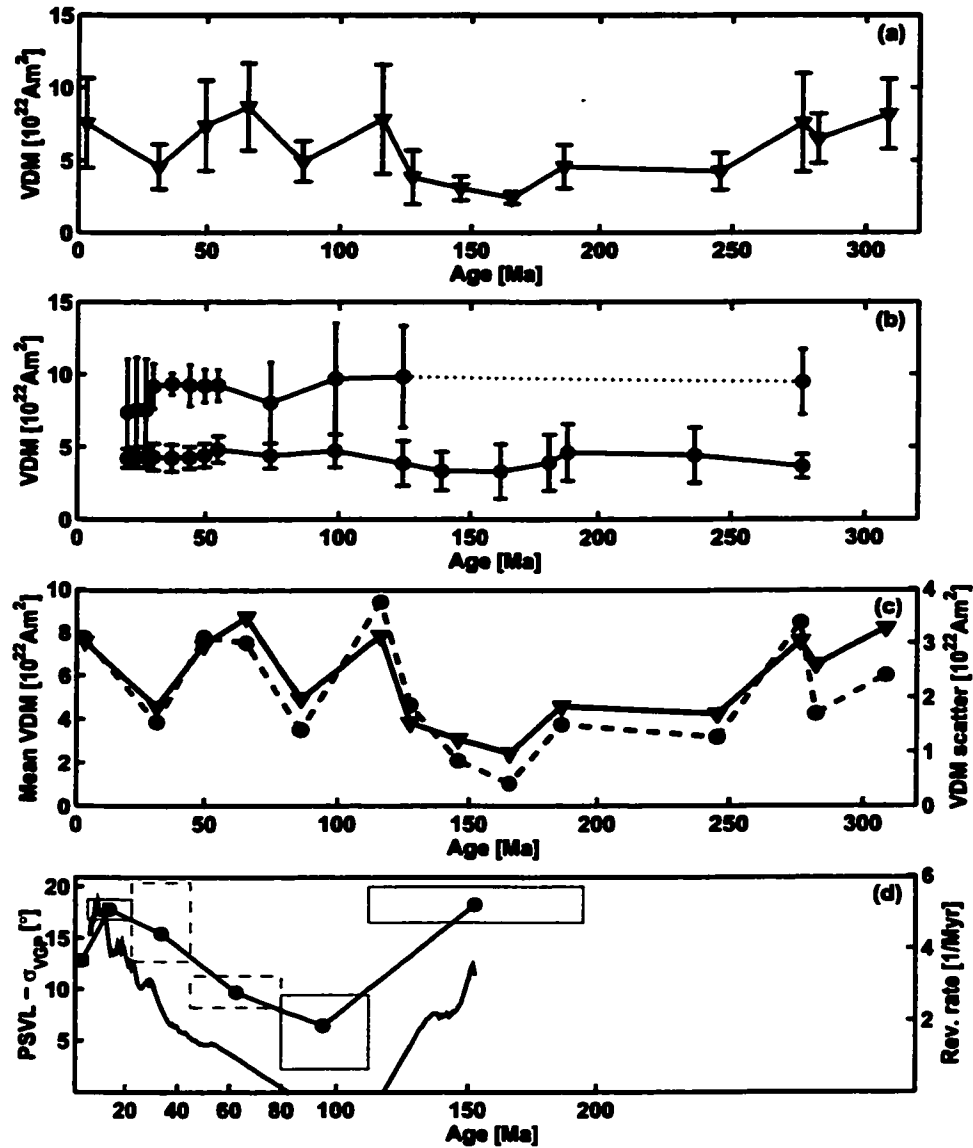


Figure 5.1: Long-term mean paleointensity, PSVI, reversal rate and directional PSV. (a) Old way of displaying trends of the mean paleointensity using unimodal distributions only, for details, see Figure 3.4a. (b) New way of displaying paleointensity trends that incorporates the bimodality in many of the distributions; shown are the high and low means and standard deviations, for details, see Figure 4.9. (c) Correlation between VDM mean (triangles, solid line) and its standard deviation (circles, dashed line), for details, see Figure 4.4. (d) Reversal rate (lower, solid line) and proxy of directional PSV (circles and solid line); boxes indicate the range of ages and the 95% confidence limits on the estimates, a solid (dashed) box indicates a good (poor) fit. After *McFadden et al. (1991)* and *Merrill et al. (1996)*.

Figures 5.1a – c allow to address a number of questions regarding the long-term paleointensity and PSVI during the past 320 Myr. However, in interpreting the VDM data we need to consider a number of different scenarios. The first question to address is whether we believe that the bimodality in the paleointensity distribution does or does not reflect true paleofield behavior. Depending on the answer to this question our interpretations of the data in terms of trends in the long-term mean paleointensity (Figure 5.1b) and PSVI (Figure 5.1c) will vary.

Was the paleointensity bimodal or are some of the data systematically biased? At present, based on the data and on theoretical considerations, we cannot uniquely distinguish between these two possibilities and therefore, need to consider each of them in turn. We can try to gain some insight by comparing the results to other paleointensity information, i.e. relative paleointensity data as well as absolute paleointensity data from the most recent five million years. For example, *Constable et al.* (1998) analyzed relative paleointensity data covering the past 11 Myr and did not find bimodality; instead they found that a gamma distribution provides the best fit. Their data, however, are based on one sedimentary core only, and, thus, have all the uncertainties associated with relative paleointensities (see, for example *Tauxe*, 1993). Relative paleointensity estimates, in general, do not have consistency checks as in the Thellier and Shaw methods, but instead are obtained by normalizing the NRM by some sediment property, such as ARM, SIRM, or susceptibility χ (e.g., *Merrill et al.*, 1996; *Tauxe*, 1993). Attempts to gain more confidence in the relative paleointensity estimates by correlating a number of cores have so far produced results for only the most recent 800 kyr (*Guyodo and Valet*, 1999), a length of time too short to be comparable to the time scales under investigation here. Similarly, absolute paleointensity data covering the most recent five million years, also do not show bimodal paleointensities. However, the contributions of high and low paleointensities in our analyses vary greatly and it is possible that the present field is one with a dominant high field contribution. We conclude that, even though the most recent several million years

suggest a unimodal paleointensity distribution this does not rule out the possibility of bimodality during the preceding 300 Myr.

Let us first consider the possibility that both peaks in the bimodal distributions are unbiased estimates of the paleointensity, i.e. both upper and lower curves in Figure 5.1b are taken to reflect true paleofield behavior. There are two (almost constant) means, with a hiatus of the high mean during part of the Mesozoic and Paleozoic, suggesting the presence of LEM states in the geodynamo. This would not be inconsistent with dynamo theory, as multiple solutions to a set of coupled partial differential equations are quite common. There is also some suggestion that they exist in dynamo theory. In particular, *Zhang and Gubbins (2000)* point out that the geodynamo could fluctuate between the strong and weak field regimes and thereby exhibit different intensities. The bimodality in the paleointensity data also provides an explanation for the correlation between the mean paleointensity and the PSVI in Figure 5.1c. The estimate of PSVI, in this scenario, would reflect the high/low intensity content. The long-term trends of reversal rate and paleosecular variation from directions (Figure 5.1d) have been shown to be correlated (*McFadden et al., 1991*); however, they do not appear to be correlated with either the long-term trends of the bimodal and unimodal mean intensity (Figure 5.1b) or PSVI (Figure 5.1c), suggesting that different CMB mechanisms control these paleomagnetic observables.

The second explanation for bimodality in the paleointensity distribution is the presence of one or more mechanisms that lead to a systematic bias in some of the paleointensity results. It should be noted that this does not require all of the high (or low) paleointensity results to be biased, as some would be expected from a unimodal distribution. However, it means that either some of the high paleointensity estimates are erroneously high or, alternatively, that some rocks yield a systematically low paleointensity. Of these two cases the latter seems more likely; if the high paleointensity estimates were biased the true paleointensity would have been significantly lower than (about half of) the present field, requiring a sudden increase in intensity around five

million years ago and a low intensity prior to that. If, on the other hand, the lower peaks in the VDM distributions contain biased estimates of the paleointensity and the upper curve in Figure 5.1b is taken to represent the paleointensity this means that the paleointensity has not changed significantly at least since the middle of the Mesozoic, and possibly not since the Kiaman Reverse Superchron (see dashed line in Figure 5.1c). In the presence of biased high or low intensities the correlation between the mean paleointensity and PSVI is most likely an artifact (caused by the data bias) and would be meaningless in terms of field behavior. However, this would not invalidate the procedure for estimating PSVI that was introduced in Section 4.4 as it should still work for an appropriate data selection. If only the upper curve in Figure 5.1b reflects the long-term paleointensity we conclude that Earth's magnetic field had a nearly constant mean intensity and does not appear to vary significantly if the CMB conditions change. This model is the least complex in terms of dynamo theory and intuitively the most appealing. For example, suppose that the overall heat flux through the CMB changes significantly on a time scale of $\sim 10^9$ Myr and further that this determines the vigor of convection in the outer core as well as, in turn, the average intensity of the geomagnetic field. This means that the changes in CMB conditions due to the change in total heat flux have an insignificant effect on paleointensity data. The reversal rate as well as the paleosecular variation from directions, on the other hand, might be more sensitive to lateral changes in heat flux which could change on shorter time scales ($\sim 10^8$ Myr) in response to changing patterns of subduction zones.

Chapter 6

FUTURE RESEARCH

The most enigmatic puzzle coming out of this thesis is the bimodality in the VDM distributions. The question of whether it is due to some artifact or to paleofield behavior needs to be addressed in order to gain confidence in any long-term paleointensity model. Does the geodynamo have LEM states that might be controlled by changes in CMB conditions? Was the paleointensity variable or constant during the last 300 Myr? Was it high and similar to the present field or significantly lower than the present field intensity? The answer to these questions should prove extremely useful to geodynamo modelers as well as our understanding of changing boundary conditions at the CMB. Unfortunately, the paleointensity database that was used for and extended in this work lacks reliable information that would be useful to address this issue at present, for example, on certain rock magnetic properties, on some experimental procedures as well as, in numerous instances, on magnetic polarity. The reason for this is that some information on experimental procedures is not routinely published and therefore difficult to collect in a database. Furthermore, the original database was established by *Tanaka et al. (1995)* to address questions different from those arising from this thesis. For example, many studies do not explicitly report the magnetic polarity (transitional, reverse or normal) of their samples which is denoted by an 'O' in the database. This is most likely not crucial; the total time spent by the field in reversal transitions can be estimated from an estimated reversal transition duration (1–10 kyr, (e.g., *Merrill and McFadden, 1999*)) and the reversal rate. Using $\Delta t = 10000$ yr and a reversal rate of 5/Ma, a conservative estimate of the time spent in reversal transitions would be approximately 5%. Thus, one can safely assume that

most of the data with unspecified magnetic polarity were non-transitional and should therefore be included in data analyses. However, magnetic polarity transitions are of particular interest to paleomagnetism and there may be a relative bias towards transitional data in the database. Since the paleointensity has been shown to be significantly lower during times of reversal transitions this is not expected to account for but might contribute to a bias and therefore the bimodality in the data. Furthermore, the database information on the magnetic mineralogy is, at present, inadequate to identify rocks with reasonably similar properties and history to investigate whether there might be a bias similar to the one affecting SBG data (Section 3.3).

One promising mechanism that might produce a systematic bias toward low paleointensity estimates involves the use of short and high temperature intervals in Thellier intensity determinations. Ideal Thellier behavior, as discussed in Section 1.2, is manifested by a straight line in the Arai plot. Unfortunately, most real samples do not show ideal Thellier behavior; instead, one often obtains a concave-up curve, an extreme case of which is shown in Figure 6.1. Usually, the low temperature segment is interpreted as being due to a magnetization acquired by the sample subsequent to formation (secondary remanent magnetization, see Section 1.1) while the high temperature segment, often taken to represent the primary remanent magnetization, is used to determine the paleointensity. The actual length of the temperature interval, ΔT , used for paleointensity determination varies greatly from sample to sample. Generally, the longer ΔT the higher the confidence one has in the result. Unfortunately, occasionally ΔT only slightly exceeds 100°C. If the temperature interval becomes too short it might be possible that a CRM affecting the respective measurements remains undetected while the linearity requirements are still fulfilled. In these cases the low temperature interval might actually represent the primary remanent magnetization (dashed line in Figure 6.1) or, more likely, the sample should have been rejected altogether.

There is some suggestion that the above might be significant; Johnson, Kissel and

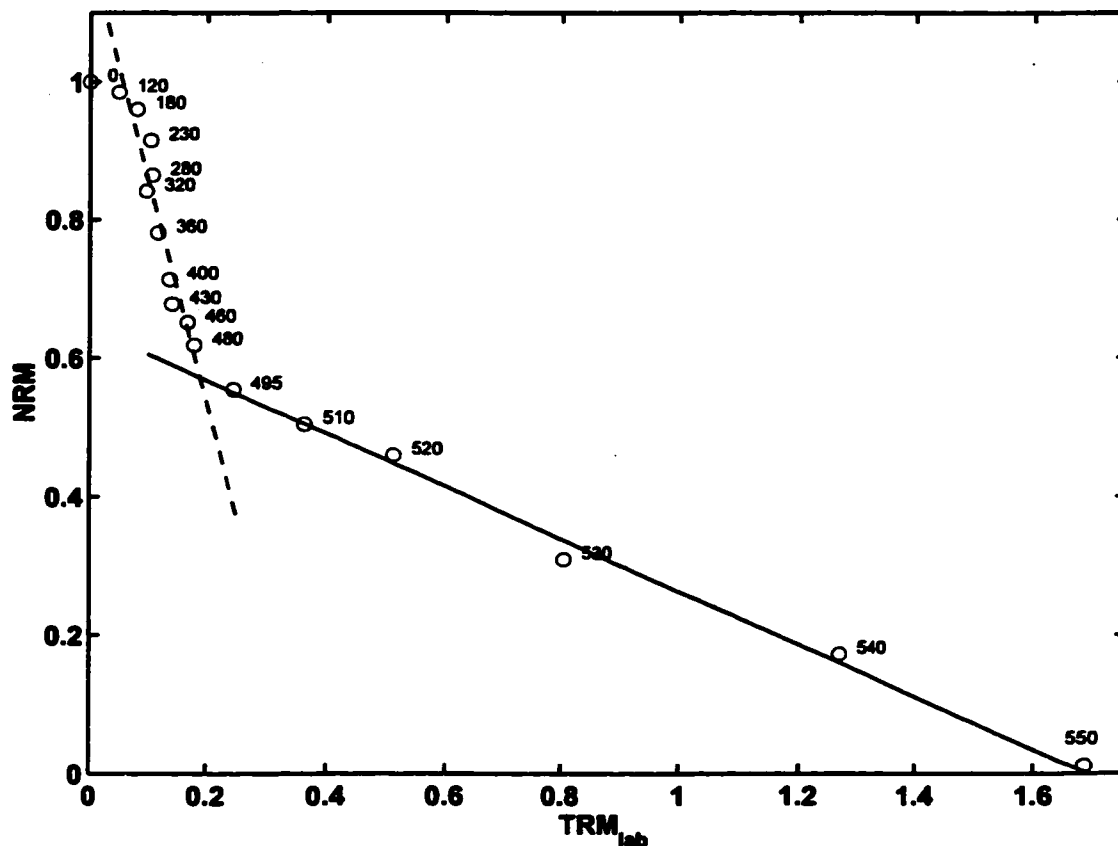


Figure 6.1: Arai plot with 'concave-up' NRM-TRM curve. The data are fit with straight lines in the low (dashed line) and high (solid line) temperature segments. Temperatures are given next to points. Data from Johnson, Kissel and Laj (unpublished; Johnson, personal communication)

Laj (unpublished data; Johnson, personal communication) found bimodally distributed paleointensities which suggest that the use of short, high temperature intervals might yield significantly low results. Figure 6.2 shows histograms of the intensity data as well as the temperature intervals used for paleointensity determinations. The distribution of all of the intensity data looks somewhat bimodal. However, when plotting the distributions of intensities obtained from short (and high) and long temperature intervals separately (Figures 6.2c and d) it becomes apparent that the paleointensities with short and high ΔT are systematically low.

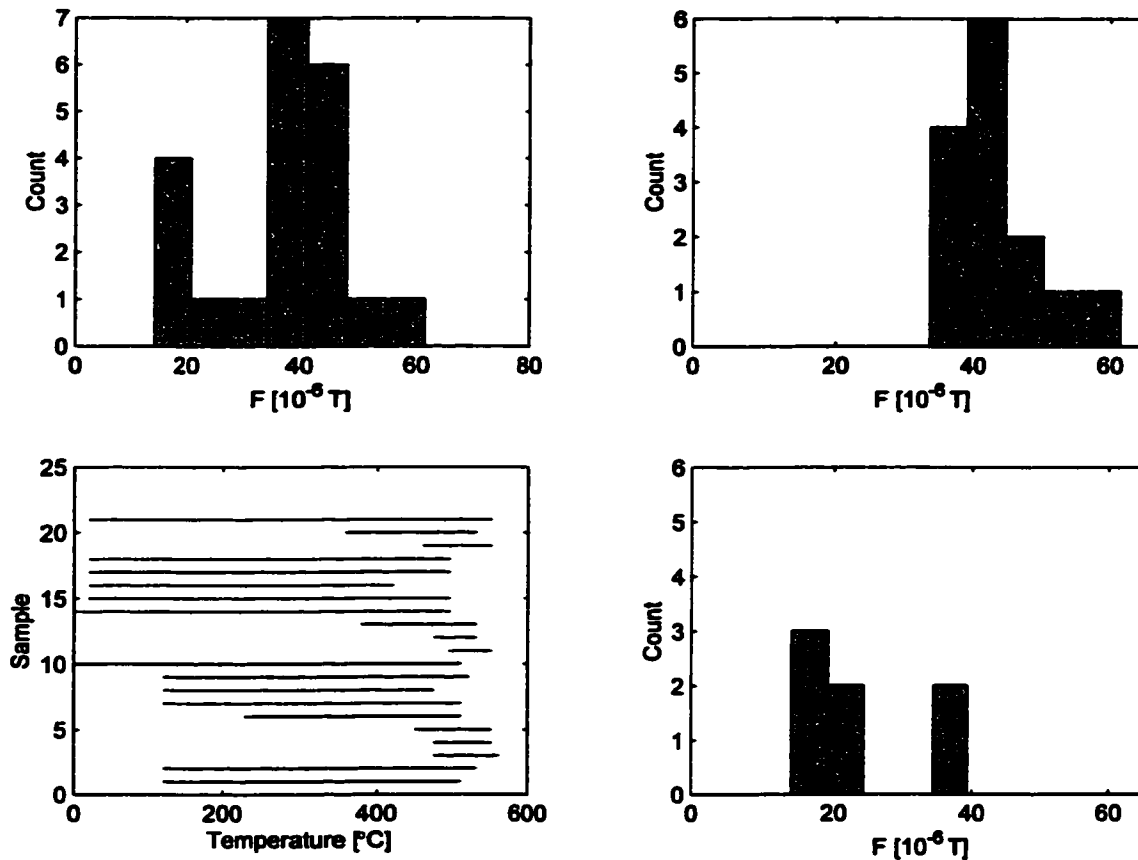


Figure 6.2: Spences Bridge intensity data. Shown are (a) the histogram of all intensities, (b) temperature intervals used for paleointensity determination, and the histograms of intensity data obtained from long (c) and short and high (d) temperature intervals, 360°C was used as a cut-off temperature. (With permission from Paul Johnson)

Unfortunately, the current paleointensity database does not contain information on the temperature intervals used. Matters are further complicated by two factors; most often the temperature intervals are not given and often only site-mean data, but not necessarily details on the complete set of samples are published. Therefore, an investigation of whether the usage of short, high temperature intervals produces a bias in the data similar to the data in Figure 6.2 should first be done for publications with complete information. Ultimately, however, it would be very useful to establish a

database that includes full information on individual samples, mineralogy, magnetic polarity etc. This is particularly important for paleointensity data because of the exceptionally high degree of inhomogeneity in the data and techniques.

Because of the bimodality in the data we could not completely resolve the question of PSVI. The technique for obtaining a proxy for PSVI (Section 4.3) remains valid; however, if the contribution to the total VDM scatter of rock magnetic and experimental errors becomes large (as would be the case if the bimodal distributions are the result of a bias in the data) in comparison with the contribution from the actual PSV, the VDM scatter ceases to be useful. Hence, once the cause for the bimodality is understood, one should repeat the PSVI analysis with an adequate data selection.

Finally, if trends in PSVI can be resolved one might attempt to combine this information with directional PSV. Paleosecular variation consists of both variability of field directions as well as intensities, and the separation into PSVL and PSVI is somewhat arbitrary. This would be difficult at present; there are more than an order of magnitude more directional than intensity data and, overall, paleointensity data are much more problematic than paleodirections. Nevertheless, to provide the full vector information, both are needed.

BIBLIOGRAPHY

- Allredge, L. R., A discussion of impulses and jerks in the geomagnetic field, *J. Geophys. Res.*, 89, 4403–4412, 1984.
- Backus, G. E., Current meters in the core of the Earth, in *Fluid mechanics and related matters*, edited by R. Salmon, and D. Betts, p. 97, Scripps Inst. Ocean. Ref. Ser., 91-24, 1991.
- Backus, G. E., R. H. Estes, D. Chinn, and R. A. Langel, Comparing the jerk with other global models of the geomagnetic field from 1960 to 1978, *J. Geophys. Res.*, 92, 3615–3622, 1987.
- Barton, C. E., Geomagnetic secular variation: Directions and intensity, in *Encyclopedia of Solid Earth Geophysics*, edited by D. E. James, pp. 560–577, Van Nostrand-Reinhold, New York, 1989.
- Bloxham, J., and D. Gubbins, The secular variation of the Earth's magnetic field, *Nature*, 317, 777–781, 1985.
- Bloxham, J., and D. Gubbins, Geomagnetic field analysis, iv. Testing the frozen-flux hypothesis, *Geophys. J. Roy. Astron. Soc.*, 84, 139–152, 1986.
- Buddington, A. F., and A. F. Lindsley, Iron-titanium oxide minerals and synthetic equivalents, *J. Petrol.*, 5, 310–357, 1964.
- Bullard, E. C., C. Freedman, H. Gellman, and J. Nixon, The westward drift of the earth's magnetic field, *Phil. Trans. Roy. Astron. Soc. London*, A243, 67–92, 1950.

- Busse, F. H., Homogeneous dynamos in planetary cores and in the laboratory, *Annu. Rev. Fluid Mech.*, *32*, 383–408, 2000.
- Butler, R. F., *Paleomagnetism*, Blackwell Scientific Publications, Boston, 1992.
- Champion, D., M. Lanphere, and M. Kuntz, Evidence for a new geomagnetic reversal from lava flows in Idaho: Discussion of short polarity reversals in the Brunhes and late Matuyama polarity chrons, *J. Geophys. Res.*, *93*, 11667–11680, 1988.
- Channell, J., and B. Lehman, The last two geomagnetic polarity reversals recorded in high-deposition-rate sediment drifts, *Nature*, *389*, 712–715, 1997.
- Clarke, G. M., and D. Cooke, *A basic course in statistics*, Arnold, New York, 4th edn., 1998.
- Coe, R. S., Paleo-intensities of the Earth's magnetic field determined from Tertiary and Quaternary rocks, *J. Geophys. Res.*, *72*, 3247–3262, 1967a.
- Coe, R. S., The determination of paleointensities of the earth's magnetic field with emphasis on mechanisms which could cause non-ideal behaviour in Thelliers method, *J. Geomag. Geoelect.*, *19*, 157–179, 1967b.
- Constable, C. G., L. Tauxe, and R. L. Parker, Analysis of 11 Myr of geomagnetic intensity variation, *J. Geophys. Res.*, *103*, 17735–17748, 1998.
- Cottrell, R. D., and J. A. Tarduno, In search of high-fidelity geomagnetic paleointensities: A comparison of single plagioclase crystal and whole rock Thellier-Thellier analyses, *J. Geophys. Res.*, *105*, 23579–23594, 2000.
- Courtilot, V., and J.-L. LeMouél, Geomagnetic secular variation impulses: A review of observational evidence and geophysical consequences, *Nature*, *311*, 709–716, 1984.

- Courtilot, V., J. Ducruix, and J.-L. LeMouël, Sur une accélération récente de la variation séculaire du champ magnétique terrestre, *C. R. Acad. Sci. Paris, D287*, 1095–1098, 1978.
- Cox, A., Analysis of the present geomagnetic field for comparison with paleomagnetic results, *J. Geomag. Geoelect.*, *13*, 101–112, 1962.
- Ducruix, J., V. Courtilot, and J.-L. LeMouël, The late 1960s secular variation impulse, the eleven year magnetic variation and the electrical conductivity of the deep mantle, *Geophys. J. Roy. Astron. Soc.*, *61*, 73–94, 1980.
- Dunlop, D. J., and Ö. Özdemir, *Rock magnetism: fundamentals and frontiers*, Cambridge University Press, New York, 1997.
- Ghiorso, M. S., Thermodynamic analysis of the effect of magnetic ordering on miscibility gaps in the FeTi cubic and rhombohedral oxide minerals and the FeTi oxide geothermometer, *Phys. Chem. Minerals*, *25*, 28–38, 1997.
- Glatzmaier, G. A., and P. H. Roberts, Geodynamo theory and simulations, *Rev. Mod. Phys.*, *72*(4), 1081–1123, 2000.
- Glatzmaier, G. A., R. S. Coe, L. Hongré, and P. H. Roberts, The role of the Earth's mantle in controlling the frequency of geomagnetic reversals, *Nature*, *401*, 885–890, 1999.
- Goguitchaichvili, A., M. Prévot, J. Thompson, and N. Roberts, An attempt to determine the absolute geomagnetic field intensity in Southwestern Iceland during the Gauss-Matuyama reversal, *Phys. Earth Planet. Int.*, *115*, 53–66, 1999.
- Grommé, C. S., T. L. Wright, and D. L. Peck, Magnetic properties and oxidation of iron-titanium oxide minerals in Alae and Makaopuhi lava lakes, Hawaii, *J. Geophys. Res.*, *74*, 5277–5293, 1969.

- Guyodo, Y., and J.-P. Valet, Global changes in intensity of the Earth's magnetic field during the past 800 kyr, *Nature*, 399, 249–252, 1999.
- Hulot, G., and J.-L. LeMouél, A statistical approach to the Earth's main magnetic field, *Phys. Earth Planet. Int.*, 82, 167–183, 1994.
- Irving, E., *Paleomagnetism and Its Application to Geological and Geophysical Problems*, Wiley, New York, 1964.
- Juarez, M. T., and L. Tauxe, The intensity of the time-averaged geomagnetic field: the last 5 Myr, *Earth Planet. Sci. Lett.*, 175, 169–180, 2000.
- Juarez, M. T., L. Tauxe, J. S. Gee, and T. Pick, The intensity of the Earth's magnetic field over the past 160 millions years, *Nature*, 394, 878–881, 1998.
- Koenigsberger, J. G., Natural residual magnetism of eruptive rocks, 1, *Terrest. Magnetism Atmospheric Elec.*, 43, 119–127, 1938a.
- Koenigsberger, J. G., Natural residual magnetism of eruptive rocks, 2, *Terrest. Magnetism Atmospheric Elec.*, 43, 299–320, 1938b.
- Kono, M., Intensity of the earth's magnetic field during the Pliocene and Pleistocene in relation to the amplitude of mid-ocean ridge magnetic anomalies, *Earth Planet. Sci. Lett.*, 11, 10–17, 1971.
- Kono, M., Reliability of palaeointensity methods using alternating field demagnetization and anhysteretic remanence, *Geophys. J. Roy. Astron. Soc.*, 54, 241–261, 1978.
- Kono, M., and N. Ueno, Paleointensity determination by a modified Thellier method, *Phys. Earth Planet. Int.*, 13, 305–314, 1977.

- Kosterov, A. A., M. Prévot, M. Perrin, and V. A. Shashkanov, Paleointensity of the Earth's magnetic field in the Jurassic; new results from a Thellier study of the Lesotho Basalt, Southern Africa, *J. Geophys. Res.*, *102*, 24859–24872, 1997.
- Laj, C., and C. Kissel, Geomagnetic field intensity at Hawaii for the last 420 kyr from the Hawaii Scientific Drilling Project core, Big Island, Hawaii, *J. Geophys. Res.*, *104*, 15317–15338, 1999.
- Langel, R. A., The main field, in *Geomagnetism Vol. 1*, edited by J. A. Jacobs, pp. 249–512, Academic Press, London, 1987.
- Levi, S., Comparison of two methods of performing the Thellier experiment (or, how the Thellier experiment should not be done), *J. Geomag. Geoelect.*, *27*, 245–255, 1975.
- Lindgren, B. W., *Statistical Theory*, Macmillan, New York, 1962.
- Lindsley, D. H., Delimitation of the hematite-ilmenite miscibility gap, *Geol. Soc. Amer. Bull.*, *84*, 657–661, 1973.
- Love, J. J., Palaeomagnetic secular variation as a function of intensity, *Phil. Trans. Roy. Astron. Soc. London*, *358*, 1191–1223, 2000.
- McClelland, E., Theory of CRM acquired by grain growth, and its implications for TRM discrimination and palaeointensity determination in igneous rocks, *Geophys. J. Int.*, *126*, 271–280, 1996.
- McClelland, E., and J. C. Briden, An improved methodology for Thellier-type paleointensity determination in igneous rocks and its usefulness for verifying primary thermoremanence, *J. Geophys. Res.*, *101*, 21995–22013, 1996.
- McElhinny, M. W., and P. L. McFadden, *Paleomagnetism, Continents and Oceans*, Academic Press, San Diego, 1999.

- McElhinny, M. W., and W. E. Senanayake, Variations in the geomagnetic dipole. 1. The past 50000 years, *J. Geomag. Geoelect.*, *34*, 39–51, 1982.
- McFadden, P. L., Rejection of palaeomagnetic observations, *Earth Planet. Sci. Lett.*, *61*, 392–395, 1982.
- McFadden, P. L., and M. W. McElhinny, Variations in the geomagnetic dipole. 2. Statistical analysis of VDM's for the past 5 million years, *J. Geomag. Geoelect.*, *34*, 163–189, 1982.
- McFadden, P. L., R. T. Merrill, M. W. McElhinny, and S. Lee, Reversals of the Earth's magnetic field and temporal variations of the dynamo families, *J. Geophys. Res.*, *96*, 3923–3933, 1991.
- Merrill, R. T., Magnetic effects associated with chemical changes in igneous rocks, *Geophys. Surv.*, *2*, 277–311, 1975.
- Merrill, R. T., and M. W. McElhinny, *The Earth's Magnetic Field, Its History, Origin and Planetary Perspective*, Academic Press, San Diego, 1983.
- Merrill, R. T., and P. L. McFadden, Geomagnetic field stability: Reversal events and excursions, *Earth Planet. Sci. Lett.*, *121*, 57–69, 1994.
- Merrill, R. T., and P. L. McFadden, Geomagnetic polarity transitions, *Rev. Geophys.*, *37*(2), 201–226, 1999.
- Merrill, R. T., M. W. McElhinny, and P. L. McFadden, *The Magnetic Field of the Earth, Paleomagnetism, the Core, and the Deep Mantle*, Academic Press, San Diego, 1996.
- Merrill, R. T., M. W. McElhinny, and P. L. McFadden, *The Magnetic Field of the Earth, Paleomagnetism, the Core, and the Deep Mantle*, Academic Press, San Diego, 1998.

- Miller, L. H., Table of percentage points of Kolmogorov statistics, *J. Amer. Statist. Assoc.*, *51*, 113–115, 1956.
- Néel, L., Théorie du trainage magnétique des ferromagnétiques aux grains fins avec applications aux terres cuites, *Ann. Geophys.*, *5*, 99–136, 1949.
- Opdyke, N. D., J. Roberts, J. Claoue-Long, E. Irving, and P. J. Jones, Base of the Kiaman; its definition and global stratigraphic significance, *Geol. Soc. Amer. Bull.*, *112*, 1315–1341, 2000.
- Pal, P. C., and P. Roberts, Long-term polarity stability and strength of the geomagnetic dipole, *Nature*, *331*, 702–705, 1988.
- Perrin, M., and V. Shcherbakov, Paleointensity of the Earth's magnetic field for the past 400 Ma: Evidence for a dipole structure during the Mesozoic low, *J. Geomag. Geoelect.*, *49*, 601–614, 1997.
- Perrin, M., E. Schnepp, and V. Shcherbakov, Paleointensity database updated, *EOS*, *79*, 198, 1998.
- Pick, T., and L. Tauxe, Holocene paleointensities; Thellier experiments on submarine basaltic glass from the East Pacific Rise, *J. Geophys. Res.*, *98*, 17949–17964, 1993a.
- Pick, T., and L. Tauxe, Geomagnetic palaeointensities during the Cretaceous normal superchron measured using submarine basaltic glass, *Nature*, *366*, 238–242, 1993b.
- Pick, T., and L. Tauxe, Characteristics of magnetite in submarine basaltic glass, *Geophys. J. Int.*, *119*, 116–128, 1994.
- Press, W., S. Teukolsky, W. Vetterling, and B. Flannery, *Numerical recipes in Fortran, The art of scientific computing*, Cambridge University Press, New York, 1992.
- Prévot, M., and P. Camps, Absence of preferred longitudinal sectors for poles from volcanic records of geomagnetic reversals, *Nature*, *366*, 53–57, 1993.

- Prévot, M., and M. Perrin, Intensity of the Earth's magnetic field since Precambrian time from Thellier-type paleointensity data and inferences on the thermal history of the core, *Geophys. J. Int.*, 108, 613–620, 1992.
- Prévot, M., M. E. Derder, M. O. McWilliams, and J. Thompson, Intensity of the Earth's magnetic field: Evidence for a Mesozoic dipole low, *Earth Planet. Sci. Lett.*, 97, 129–139, 1990.
- Quidelleur, X., P.-Y. Gillot, J. Carlut, and V. Courtillot, Link between excursions and paleointensity inferred from abnormal field directions recorded at La Palma around 600 ka, *Earth Planet. Sci. Lett.*, 168, 233–242, 1999.
- Riisager, P., and N. Abrahamsen, Palaeointensity of West Greenland Palaeocene basalts: asymmetric intensity around the C27n-C26r transition, *Phys. Earth Planet. Int.*, 118, 53–64, 2000.
- Rolph, T., and J. Shaw, A new method of paleofield magnitude correction for thermally altered samples and its application to lower carboniferous lavas, *Geophys. J. Roy. Astron. Soc.*, 80, 773–781, 1985.
- Sachs, L., *Applied statistics: a handbook of techniques*, Springer-Verlag, New York, 2nd edn., 1984.
- Sakai, H., and M. Funaki, Paleomagnetic study of the Beacon Supergroup in Antarctica; remagnetization in the Jurassic time, in *Proceedings of the NIPR Symposium on Antarctic Geosciences. 2*, pp. 46–54, National Institute of Polar Research, Tokyo, Japan, 1988.
- Sato, M., and T. L. Wright, Oxygen fugacities directly measured in volcanic gases, *Science*, 153, 1103–1105, 1966.
- Selkin, P. A., and L. Tauxe, Long-term variations in palaeointensity, *Phil. Trans. Roy. Astron. Soc. London*, 358(A), 1065–1088, 2000.

- Senanayake, W. E., M. W. McElhinny, and P. L. McFadden, Comparison between the Thelliers' and Shaw's palaeointensity methods using basalts less than 5 million years old, *J. Geomag. Geoelect.*, *34*, 141–161, 1982.
- Shaw, J., A new method of determining the magnitude of the palaeomagnetic field, *Geophys. J. Roy. Astron. Soc.*, *39*, 133–141, 1974.
- Siegel, S., *Nonparametric statistics for the behavioral sciences*, McGraw-Hill, New York, 1956.
- Smith, P. J., The intensity of the Tertiary geomagnetic field, *Geophys. J. Roy. Astron. Soc.*, *12*, 239–258, 1967a.
- Solodovnikov, G. M., The intensity in the Eocene geomagnetic field, *Izv., Earth Phys.*, *34*, 865–869, 1998.
- Solodovnikov, G. M., Paleointensity of the geomagnetic field determined from Oligocene and Miocene rocks, *Izv., Earth Phys.*, *35*, 334–339, 1999a.
- Solodovnikov, G. M., Geomagnetic intensity in the Pliocene, *Izv., Earth Phys.*, *35*, 871–875, 1999b.
- Spell, T. L., and I. McDougall, Revisions to the age of the Brunhes-Matuyama boundary and the Pleistocene geomagnetic polarity timescale, *Geophys. Res. Lett.*, *19*, 1181–1184, 1992.
- Stacey, F. D., *Physics of the Earth*, Brookfield Press, Brisbane, 3rd edn., 1992.
- Stevenson, D. J., Planetary magnetic fields, *Rept. Prog. Phys.*, *46*, 555–620, 1983.
- Tanaka, H., M. Kono, and H. Uchimura, Some global features of palaeointensity in geological time, *Geophys. J. Int.*, *120*, 97–102, 1995.

- Tanaka, H., K. Kawamura, K. Nagao, and B. F. Houghton, K-Ar ages and paleosecular variation of direction and intensity from Quaternary lava sequences in the Ruapehu volcano, New Zealand, *J. Geomag. Geoelect.*, *49*, 587–599, 1997.
- Tarduno, J. A., R. D. Cottrell, and A. V. Smirnov, High geomagnetic intensity during the Mid-Cretaceous from Thellier analyses of single plagioclase crystals, *Science*, *291*, 1779–1783, 2001.
- Tauxe, L., Sedimentary records of relative paleointensity of the geomagnetic field; theory and practice, *Rev. Geophys.*, *31*, 319–354, 1993.
- Thellier, E., Sur l'animation des terres cuites et ses applications géophysiques, *Ann. Inst. Phys. Globe*, *16*, 157–302, 1938.
- Thellier, E., and O. Thellier, Sur l'intensité du champ magnétique terrestre dans le passé historique et géologique, *Ann. Geophys.*, *15*, 285–376, 1959.
- Thomas, D. N., T. C. Rolph, and D. F. Friel, Permo-Carboniferous (Kiaman) palaeointensity results from the western Bohemian Massif, Germany, *Geophys. J. Int.*, *130*, 257–265, 1997.
- Tric, E., C. Laj, J.-P. Valet, C. Kissel, A. Mazaud, and S. Iaccarino, High-resolution record of the upper Olduvai transition from Po Valley (Italy sediments; support for dipolar transition geometry?, *Phys. Earth Planet. Int.*, *65*, 319–336, 1991.
- Valet, J.-P., and L. Meynadier, Geomagnetic field intensity and reversals during the past 4 million years, *Nature*, *366*, 234–238, 1993.
- Verosub, K. L., and S. K. Banerjee, Geomagnetic excursions and their paleomagnetic record, *Rev. Geophys. Space Phys.*, *15*, 145–155, 1977.
- Whitney, J., H. P. Johnson, S. Levi, and B. W. Evans, Investigations of some magnetic

and mineralogical properties of the Laschamp and Olby flows, France, *Quat. Res.*, 1, 511–521, 1971.

Zhang, K., and D. Gubbins, Scale disparities and magnetohydrodynamics in the Earth's core, *Proc. R. Soc.*, 358, 899–920, 2000.

Appendix A

KOLMOGOROV-SMIRNOV TESTS

In database analyses, it is often necessary to compare subsets of data either with one another or against some theoretical distribution. For example, in our analyses, we are interested in questions like: are Thellier data significantly different from Shaw data? Does a given set of data more likely have a unimodal or a bimodal distribution? Unfortunately, when investigating paleointensity data, most often it is not clear which distribution underlies a given set of data. Obviously, we cannot expect the most straightforward tests, developed for normal distributions, to work in these cases. For this reason, we had to resort to the non-parametric tests of Kolmogorov and Smirnov (e.g., *Sachs*, 1984; *Press et al.*, 1992). The first of the two, the Kolmogorov-Smirnov goodness-of-fit test (henceforth referred to as KS1 test) is used to assess how well an observed distribution fits a theoretically expected one. The second test, the Kolmogorov-Smirnov two-sample, or KS2 test, on the other hand, allows comparing two independent samples in terms of whether they were drawn from the same (unknown) distribution. Both the KS1 and KS2 test can be applied to continuous and discrete data and are non-parametric, or distribution-free, i.e. no assumption with respect to the distribution underlying the data has to be made, with the drawback of being less powerful than their parametric counterparts. More details on the strengths and weaknesses can be found elsewhere (e.g., *Sachs*, 1984; *Clarke and Cooke*, 1998).

The KS1 test compares the sample's cumulative distribution function (cdf), F_{obs} , to that of the theoretically expected distribution, F_{exp} . The null hypothesis that the sample originated in a population with known distribution function F_{exp} is tested against the alternate hypothesis that the population underlying the sample does not

have F_{exp} as its distribution function. The maximum absolute difference between the two relative cdfs serves as the test statistic:

$$D_{\text{obs}} = \max |F_{\text{obs}} - F_{\text{exp}}| \quad (\text{A.1})$$

D_{obs} is compared to its theoretical distribution which depends on the sample size N . Critical values D_{crit} for various levels of significance, are tabulated in the literature (e.g., *Miller*, 1956). If an observed value D_{obs} equals or exceeds the tabulated value D_{crit} , the null hypothesis H_0 can be rejected at the corresponding significance level.

Similar to the KS1 test, the KS2 test compares the relative cdfs, F_1 and F_2 , of the two samples of size N_1 and N_2 , using the maximum absolute difference between F_1 and F_2 as the test statistic:

$$D_{\text{obs}} = \max |F_1 - F_2| \quad (\text{A.2})$$

Here, the null hypothesis H_0 is that the two samples exhibit the same distribution. As for the KS1 test, critical values D_{crit} , at various levels of significance, are found in the literature (e.g., *Siegel*, 1956; *Lindgren*, 1962), and can be approximated for large sample sizes ($N = N_1 + N_2 > 35$) (*Sachs*, 1984). For our purposes, the latter is the only relevant case. If D_{obs} equals or exceeds D_{crit} , the null hypothesis can be rejected at the corresponding level of significance.

Appendix B

CODE FOR ROTATING A GIVEN MAGNETIC FIELD IN SPHERICAL COORDINATES

In Chapter 2 the VGP and VDM scatter as well as the mean VDM and VADM were determined for a model based on the IGRF 1995 in which the dipole field was successively reduced in strength while the non-dipole field was held constant. The field was sampled such that each sample represented the same surface area. To avoid a bias due to the tilt of the dipole we rotated the field to align the geomagnetic pole with the axis of rotation and then conducted the sampling. As there has been some interest in the method for rotating a field given in a spherical coordinate system the Matlab code is given below. Given are two files, *RotateCoordGauss.m*, and *RotateCoord.m*.

RotateGaussCoord.m

```
function [gauss_2] = RotateCoordGauss(gauss_1, NoE, eulerangle1,...
    eulerangle2,eulerangle3)
%
% [gauss_2] = RotateCoordGauss(gauss_1, NoE, eulerangle1,...
%     eulerangle2,eulerangle3)
% Program to calculate the Gauss coefficients in a rotated coordinate
% system. The new coordinate system is transformed from the old
% system by three Euler rotations about consecutive rotation axes
% x3, x2', and x3'', and angles of rotation as specified in
% eulerangle1, eulerangle2, and eulerangle3 (given in radians).
```

```

% Subscript _1 refers to 'old' (unrotated) and _2 to 'new' (rotated)
%
% gauss_1:
% cell array of cells containing the Gauss coefficients in the
% unrotated coordinate system. At this point I won't worry about
% their time dependence, that'll come later (thus, t=1).
%
% NoE:
% Number of equations used to determine the new Gauss coefficients.
% A minimum of 2l+1 (where l is the degree in question) is required.
% More mean the system is overdetermined which could be used to
% reduce the already negligible error. NoE can be a scalar or a
% vector of length lmax. If it is a scalar there are two
% possibilities:
% a) NoE==1 the program queries this. If it is true then the
% minimum number of equations for each l is calculated and used
% to determine the new Gauss coefficients. This will be the easiest.
% b) NoE~=1 then the program terminates if NoE < 2*lmax+1 (with
% errormessage) or else creates a vector NoE of length lmax with
% identical elements NoE (the value of the scalar).
% If NoE is a vector of length lmax then the l-th element is the
% number of equations used to determine the new Gauss coefficients
% for that particular degree l.
%
% eulerangle1:
% angle of first rotation, in radians, about x3-axis, right hand
% eulerangle2:
% angle of second rotation, in radians, about x2'-axis, right hand

```

```

% eulerangle3:
% angle of third rotation, in radians, about x3"-axis, right hand
%
% gauss_2:
% same format as gauss_1, Gauss coefficients in the rotated
% coordinate system.
%

% FORMAT OF GAUSS_1 AND GAUSS_2:
%
% Gauss coefficients are contained in cell array gauss_1
% gauss_1 has three elements:
% gauss_1{1} -- is itself a cell array with lmax cells. Its first
% cell contains the Gauss coefficient g10 (m=0) as a function
% of time, i.e. gauss_1{1}{1}(1) is the Gauss coefficient
% g10 for the first time value gauss_1{1}{1}(2) that for
% the second time value and so on.
% gauss_1{2} -- as above is a cell array, but with lmax x lmax
% cells. Here the rows count the degree l and the columns the
% order m. gauss_1{2} contains the Gauss coefficients
% glm where m>0 as a function of time. Thus,
% gauss_1{2}{1,1}(1) is the Gauss coefficient g11 for the
% first time value. gauss_1{2} has rows and columns,
% the cells with m>1 are empty, in every row m goes from 1 to l.
% gauss_1{3} -- same as gauss_1{2}, except for hlm.
%
% Functions and m-files:
% RotateCoord.m

```

```
% extract Gauss coefficients:
gl0_1=gauss_1{1};
glm_1=gauss_1{2};
hlm_1=gauss_1{3};

lmax=max([length(gl0_1), size(glm_1,1), size(hlm_1,1)]);

% check whether NoE is a scalar or a vector of length lmax:
dimNoE=size(NoE);
if dimNoE~= [1 lmax] & dimNoE~= [lmax 1] & dimNoE~= [1 1]
    error(['The variable NoE (number of equations) must ' ...
          'have length 1 or 'num2str(lmax)])
end

% if I don't want to think how large NoE must be, just set
% it to 1 and program calculates minimum
if NoE==1
    ll=1:lmax;
    NoE=2*ll+1;
end

% make NoE length lmax if it is scalar
if length(NoE)==1
    NoE=ones(lmax,1)*NoE;
end

% The rotation doesn't change the potential at a fixed point.
% Therefore, if we calculate the potential Psi at location
% (r_1,th_1,phi_1) we must obtain the same value if we
```

```

% calculate Psi in the new coordinate system where the new
% coordinates are (r_2,th_2,phi_2) and the new Gauss
% coefficients are given by gauss_2. Since we need to determine
% the new Gauss coefficients we set up a system of (at least) 2l+1
% equations. We randomly determine as many locations
% (r_1=1, th_1 and phi_1 random) as we want equations (NoE(l)) and
% calculate the corresponding value for Psi. That value must also
% result from the new coordinates and Gauss coefficients. Setting up
% a matrix A from the partially normalized Schmidt functions and the
% phi-dependence in new coordinates we get an equation Ax=b where b
% is Psi for all the chosen locations, x is the vector of new
% Gauss coefficients and A is the matrix described above.
%
% I need to do the calculation separately for every degree l. The
% CHARACTER of a multipole field does not change by rotation, only
% the coefficients. See Jackson and Arfken for details. The functions
% of every degree can be described by functions of
% the same degree in the new coordinate system.

t=1; % don't want to deal with time dependence now, set it to 1
% for now:
for l=1:lmax

    % check that there are enough equations for given degree l:
    if NoE(l) < 2*l+1
        error(['Number of equations for l='num2str(l) ' is ' ...
              num2str(NoE(l)) ' but must be at least ' num2str(2*l+1)])
    end
end

```

% GET RANDOM LOCATIONS

**% set up NoE(1) random locations with (r=1) in OLD coordinate
% system:**

```
r_1 = ones([1,NoE(1)]);
th_1 = pi*rand([1,NoE(1)]); % these are all ROW vectors
phi_1=2*pi*rand([1,NoE(1)]);
```

% ROTATE COORDINATE SYSTEM

% calculate the coordinates in NEW coordinate system:

```
[r_2, th_2, phi_2] = RotateCoord(r_1,th_1,phi_1,'s',...
    eulerangle1,eulerangle2,eulerangle3);
```

% make these row vectors:

```
r_2=(r_2(:))';
th_2=(th_2(:))';
phi_2=(phi_2(:))';
```

% GET POTENTIAL PSI

% Calculate the geomagnetic potential Psi for locations in old

% coord system: set up partially normalized Schmidt functions:

```
Plm_1=legendre(1,cos(th_1),'sch');
```

% The potential Psi is the sum of the axial (m=0) and

% non-axial (m>0) contributions:

% m=0

```
Psi=gl0_1{1}(t)*Plm_1(1,:);
```

```

% m>0
for m=1:l
    Psi=Psi+glm_1{l,m}(t)*Plm_1(m+1,:).*cos(m*phi_1) + ...
        hlm_1{l,m}(t)*Plm_1(m+1,:).*sin(m*phi_1);
end
% Psi is now a row vector, the i-th row containing the potential
% in (r_1(i),th_1(i),phi_1(i))

% SET UP MATRIX A

% do the same as above for the new coord system except set up
% matrix A since we do not know the new Gauss coefficients:
Plm_2=legendre(1,cos(th_2),'sch');

A=zeros(NoE(1),2*l+1);
% Note:  put the stuff for ONE location in the same ROW of A:
% Therefore, put coefficients for ONE new Gauss
%         coefficient in same COLUMN:

% m=0:
A(:,1)=(Plm_2(1,:))'; % first column of A
% m>0:
for m=1:l
    A(:,2*m) =( Plm_2(m+1,:).*cos(m*phi_2) )';
    % second, fourth etc. column of A
    A(:,2*m+1)=( Plm_2(m+1,:).*sin(m*phi_2) )';
    % third, fifth etc. column of A
end

```



```

% now we can solve our matrix equation Ax=Psi where A is known,
% so is Psi, and x is unknown. We can solve this by matrix left
% division (\): A\Psi=x

```

```

% SOLVE FOR NEW GAUSS COEFFICIENTS

```

```

% make sure Psi is column vector:

```

```

Psi=Psi(:);

```

```

x=A\Psi; % new Gauss coefficients in a long vector

```

```

% Round the new Gauss coefficients at, say, fifth position after
% the comma. I do that for the following reason: if the Gauss
% coefficients for the nonaxial dipole are supposed to go to zero
% in a transformation (to geomagnetic pole) then g11 and h11
% will typically be of the order of 10-11 but not exactly zero.
% That might cause problems in later calculations. Therefore,
% since this is irrelevant accuracy anyways,
% I cut off those values.

```

```

x=round(x*106)/106;

```

```

% x contains the new Gauss coefficients. We still need to transfer
% them to our usual cell structure:

```

```

% m=0

```

```

g10_2{1}(t)=x(1);

```

```

% m>0

```

```

for m=1:l

```

```

    glm_2{1,m}(t) = x(2*m);

```

```

        hlm_2{1,m}(t) = x(2*m+1);
    end

end

% FUNCTION OUTPUT GAUSS_2

% collect results in gauss_2 cell array:
gauss_2{1}=gl0_2;
gauss_2{2}=glm_2;
gauss_2{3}=hlm_2;

RotateGauss.m

function [x1_new, x2_new, x3_new]=RotateCoord(x1_old,x2_old,...
    x3_old,coord,eulerangle1,eulerangle2,eulerangle3)
%
% function [x1_new, x2_new, x3_new] = RotateCoord(x1_old,...
% x2_old,x3_old,coord,eulerangle1,eulerangle2,eulerangle3)
% Program to calculate the Gauss coefficients in a rotated coordinat
%
% RotateCoord can rotate a coordinate system by three consecutive
% Euler rotations about axis x3 (eulerangle1 in radians), about axis
% x2' (eulerangle2 in radians), and about axis x3"
% (eulerangle3 in radians). The new coordinates in the rotated
% coordinate system of vectors given by x1_old, x2_old and x3_old
% in spherical or Cartesian coordinates are calculated
% (x1_new, x2_new and x3_new). The resulting new coordinates are

```

```
% again spherical or Cartesian and are the coordinates of the same
% vectors, but in the new coordinate system. The input coordinates
% can be 1xN vectors in which case the calculation is done for all
% N vectors.
%
% x1_old:
% 1xN vector where the m-th element is r_m (x_m) component
% of the m-th vector in old coord system, in spherical (Cart.) coords
% x2_old:
% ditto, except m-th element is th_m (y_m)
% x3_old:
% ditto, except m-th element is phi_m (z_m)
% coord:
% 's' for spherical, or 'c' for Cartesian coordinate system
% eulerangle1:
% angle of first rotation in radians, about x3-axis
% eulerangle2:
% angle of second rotation in radians, about x2'-axis
% eulerangle3:
% angle of third rotation in radians, about x3"-axis
% x1_new:
% vector containing the r (x) components of the vectors in
% rotated coordinate system. m-th element is the
% r-component (x-component) of m-th vector
% in spherical (Cartesian) coordinates
% x2_new:
% ditto, except m-th element is th-component (y-component)
% x3_new:
```

```
% ditto, except m-th element is phi-component (z-component)
%

% Check if input for coord is correct
if and(coord=='s', coord=='c')
    error='Input variable coord has to be c for ' ...
        'Cartesian or s for spherical'
end

% Number of vectors for which new coordinates are to be determined
N=length(x1_old);
% set up matrix in which old vectors will be columns
oldvectors=zeros(3,N);

% make x1_old, x2_old, x3_old column vectors:
x1_old=x1_old(:);
x2_old=x2_old(:);
x3_old=x3_old(:);

% convert spherical to Cartesian if coord=='s'
if coord=='s'
    x_old=x1_old.*sin(x2_old).*cos(x3_old);
    y_old=x1_old.*sin(x2_old).*sin(x3_old);
    z_old=x1_old.*cos(x2_old);
elseif coord=='c'
    x_old=x1_old;
    y_old=x2_old;
    z_old=x3_old;
```

```
end
```

```
% put x_old, y_old, and z_old into 3xN matrix oldvectors:
```

```
oldvectors(1,:)=x_old';
```

```
oldvectors(2,:)=y_old';
```

```
oldvectors(3,:)=z_old';
```

```
% Calculate matrix 'RotationCoord' that transforms coords of
```

```
% vectors in 'oldvectors':
```

```
% Principle: do three coordinate transformations, the final
```

```
% matrix will be the coordinate transformation matrix
```

```
a=eulerangle1;
```

```
b=eulerangle2;
```

```
c=eulerangle3;
```

```
% first rotation: about x3-axis, angle a:
```

```
Ra=[ cos(a) sin(a) 0; ...
```

```
    -sin(a) cos(a) 0; ...
```

```
      0      0      1 ];
```

```
% second rotation: about x2'-axis, angle b:
```

```
Rb=[ cos(b) 0 -sin(b)      ;      ...
```

```
      0      1      0      ;      ...
```

```
    sin(b) 0  cos(b)      ];
```

```
% third rotation: about x3"-axis, angle c:
```

```
Rc=[ cos(c) sin(c) 0 ; ...
```

```

        -sin(c)  cos(c)  0  ; ...
            0    0    1 ]];

% calculate matrix for complete coordinate transformation
R=Rc*Rb*Ra;

RotationCoord=R;

% now calculate the new vectors:
newvectors=RotationCoord*oldvectors;

% new components (in Cartesian coords)
x_new=newvectors(1,:);
y_new=newvectors(2,:);
z_new=newvectors(3,:);

if coord=='s'
    r_new=sqrt(x_new.^2+y_new.^2+z_new.^2);
    h=sqrt(x_new.^2+y_new.^2);
    phi_new=      acos(x_new./(h+(h==0))).*(h>0).*(y_new>=0) + ...
                (2*pi-acos(x_new./(h+(h==0)))).*(h>0).*(y_new<0);
    th_new = acos(z_new./(r_new+(r_new==0))).*(r_new>0);
end

% assign results to output variables x1_new, x2_new and x3_new:
if coord=='c'
    x1_new= x_new(:);
    x2_new= y_new(:);

```

```
    x3_new= z_new(:);  
elseif coord=='s'  
    x1_new= r_new(:);  
    x2_new= th_new(:);  
    x3_new=phi_new(:);  
end
```

Appendix C

KOLMOGOROV-SMIRNOV TWO-SAMPLE TEST RESULTS

In Section 3.4 I use the Kolmogorov-Smirnov two-sample test (see Appendix A) to investigate whether various paleointensity methods yield significantly different results and whether, based on these analyses, data from certain intensity methods should be accepted or rejected. This appendix gives a more detailed description of the procedures and results of these analyses.

The KS2 test can be used to assess the probability that two samples, X_1 and X_2 , were drawn from the same underlying distribution, i.e. in principle, it can be employed to investigate whether, for instance, the Thellier and Shaw methods give the same paleointensity results. If, based on the test outcome, they do not, other information (such as rock magnetic factors) can be used to decide which data are preferable. However, caution should be exercised in interpreting the test results. Suppose the null hypothesis that X_1 and X_2 have the same underlying distribution can be rejected; then the test outcome only indicates that X_1 and X_2 were drawn from different distributions. Whether this is due to differences in the paleointensity techniques or to the fact that different ages were sampled, must be evaluated by using the temporal distributions of X_1 and X_2 . To complicate matters further, even if the temporal distributions of X_1 and X_2 are different, the paleointensity might still have been the same, i.e. in this case a decision cannot be made with confidence. Figures C.1 – C.6 show the cumulative distribution functions of X_1 and X_2 (top) and the temporal distributions of the samples (bottom) for various age intervals and intensity methods.

The KS2 test was not only used to distinguish between different intensity methods but also to analyze data obtained with the same methods but from different age intervals to see whether the distributions were significantly different. In the example of Figure C.7 the paleointensities from the two most recent Superchrons, the Kiaman Reverse and the Cretaceous Normal Superchron, were compared (see Chapter 3), and found to be significantly different at the 95% confidence level.

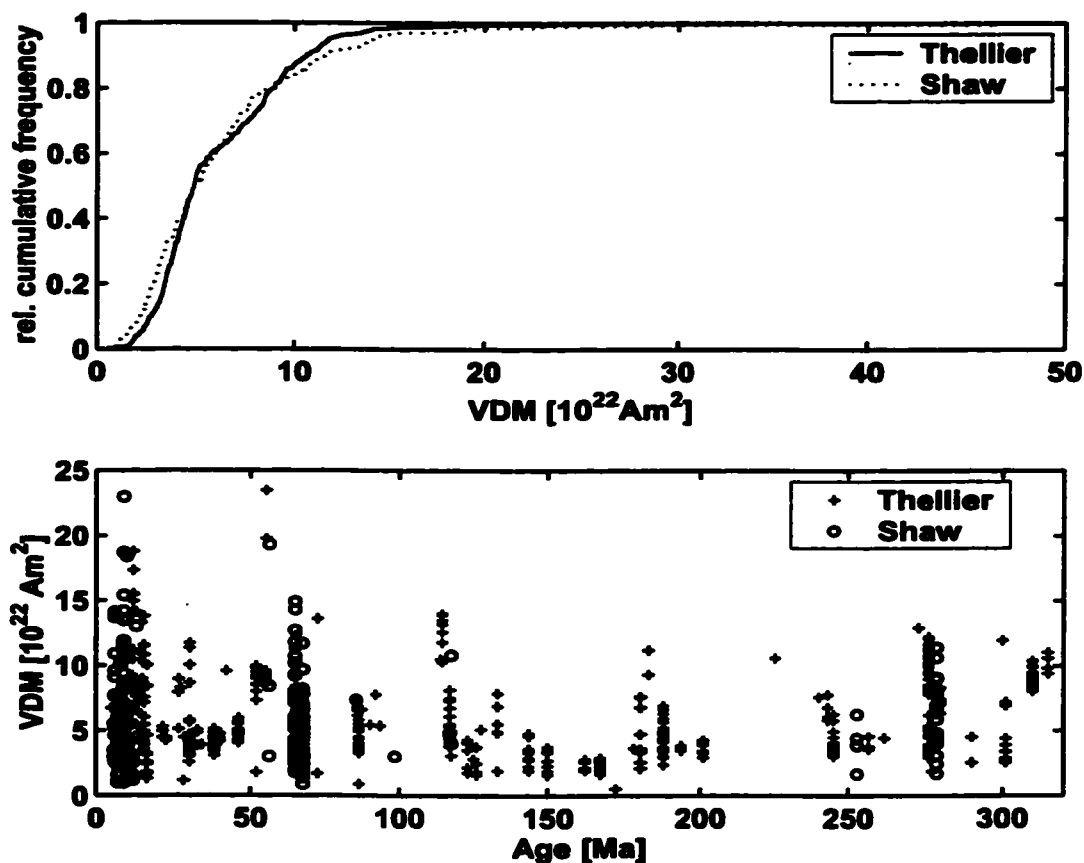


Figure C.1: Kolmogorov-Smirnov two-sample test for Thellier and Shaw data with ages between 5–320 Ma. Top figure: the cumulative distribution functions for Thellier data (solid line) and Shaw data (dotted line); bottom figure: the age distributions (Thellier: +, Shaw: circles)

Figure C.1 shows the results of the KS2 test for Thellier and Shaw data with ages between 5 and 320 Ma. There are 541 Thellier and 205 Shaw data. The null hypothesis that both Thellier and Shaw data were drawn from the same underlying distribution can be rejected at the 98.3% confidence level. However, the age distribution of the data (bottom figure) shows that Thellier and Shaw data most often occupy different age intervals.

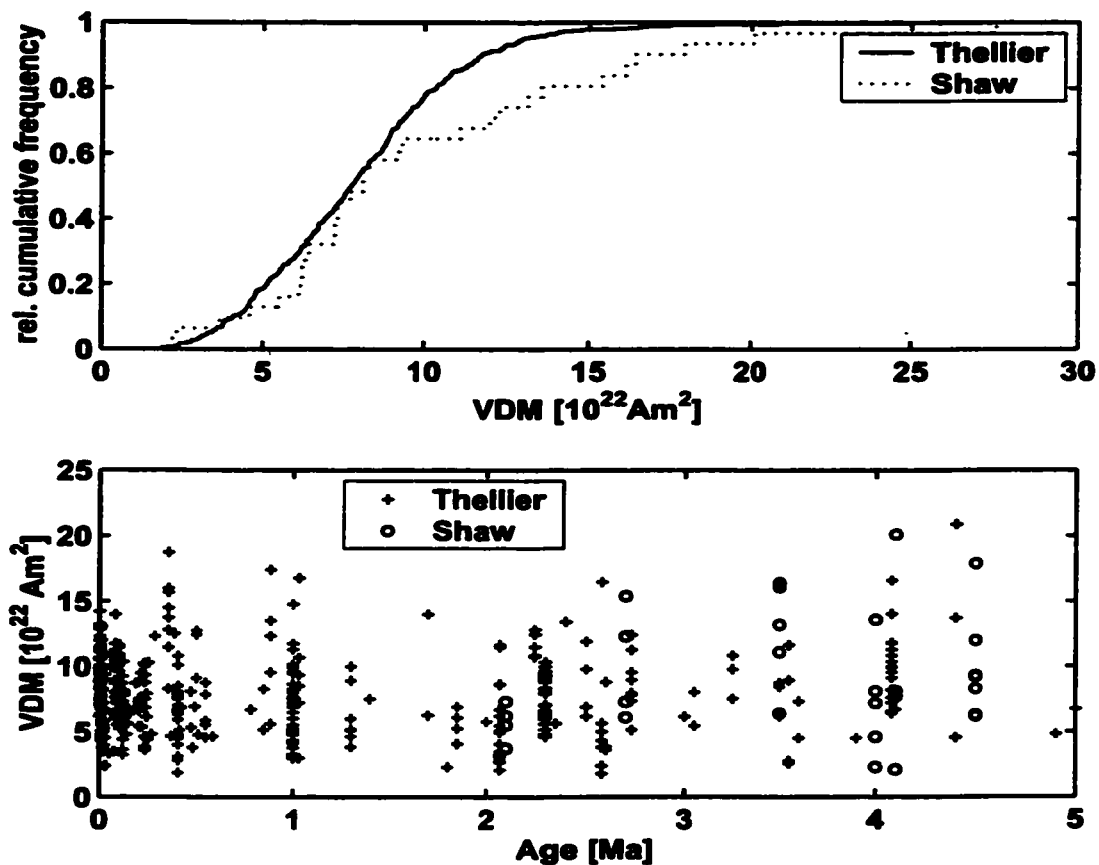


Figure C.2: Kolmogorov-Smirnov two-sample test for Thellier and Shaw data with ages between 0–5 Ma. Top figure: the cumulative distribution functions for Thellier data (solid line) and Shaw data (dotted line); bottom figure: the age distributions (Thellier: +, Shaw: circles)

Figure C.2 shows the results of the KS2 test for Thellier and Shaw data with ages between 0 and 5 Ma. There are 429 Thellier and 31 Shaw data. The null hypothesis that both Thellier and Shaw data were drawn from the same underlying distribution can be rejected at the 92.9% confidence level. However, the age distribution of the data (bottom figure) shows that Thellier and Shaw data most often occupy different age intervals. In addition, there are only 31 Shaw data.

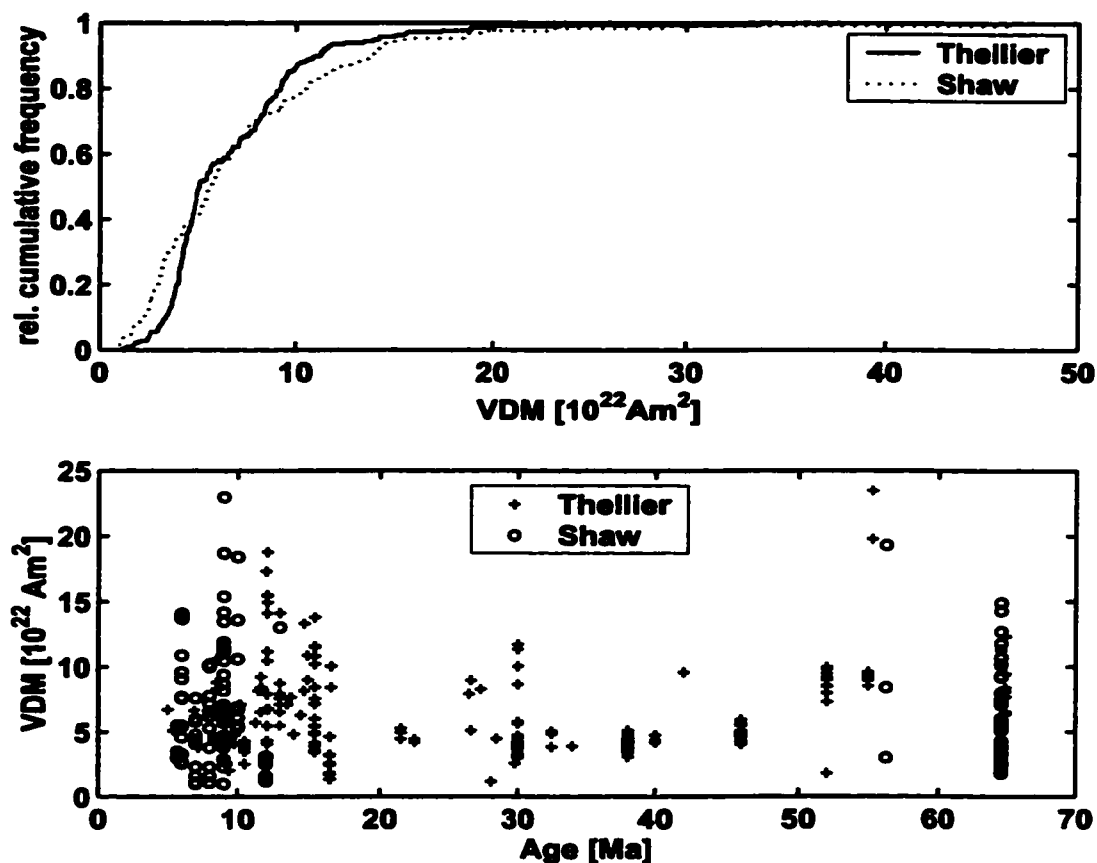


Figure C.3: Kolmogorov-Smirnov two-sample test for Thellier and Shaw data with ages between 5–65 Ma. Top figure: the cumulative distribution functions for Thellier data (solid line) and Shaw data (dotted line); bottom figure: the age distributions (Thellier: +, Shaw: circles)

Figure C.3 shows the results of the KS2 test for Thellier and Shaw data with ages between 5 and 65 Ma. There are 217 Thellier and 127 Shaw data. The null hypothesis that both Thellier and Shaw data were drawn from the same underlying distribution can be rejected at the 99.7% confidence level. However, the age distribution of the data (bottom figure) shows that Thellier and Shaw data most often occupy different age intervals.

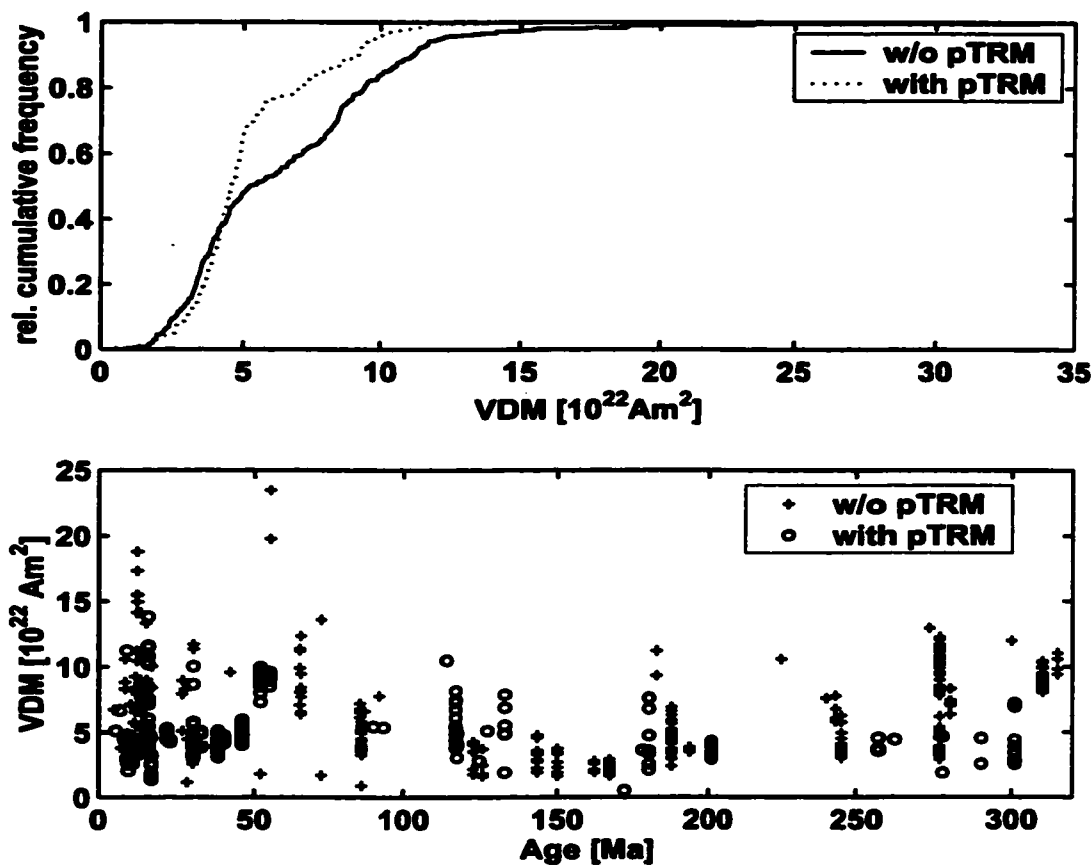


Figure C.4: Kolmogorov-Smirnov two-sample test for Thellier data with and without pTRM checks and ages between 5–320 Ma. Top figure: the cumulative distribution functions for Thellier data without pTRM checks (solid line) and with pTRM checks (dotted line); bottom figure: the age distributions (Thellier without pTRM checks: +, Thellier with pTRM checks: circles)

Figure C.4 shows the results of the KS2 test for Thellier data with and without pTRM checks and ages between 5 and 65 Ma. There are 335 Thellier data with and 199 Thellier data without pTRM checks. The null hypothesis that both Thellier data with and without pTRM checks were drawn from the same underlying distribution can be rejected at the 100% confidence level. However, the age distribution of the data (bottom figure) shows the data most often occupy different age intervals.

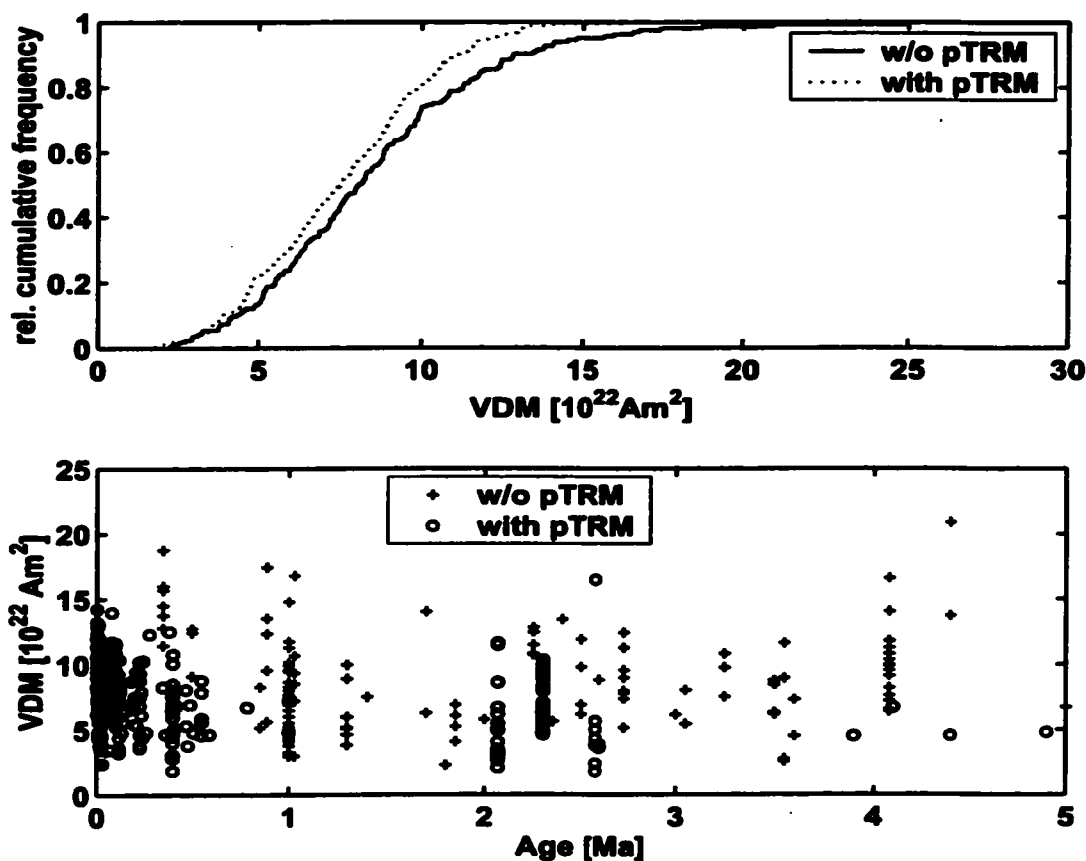


Figure C.5: Kolmogorov-Smirnov two-sample test for Thellier data with and without pTRM checks and ages between 0–5 Ma. Top figure: the cumulative distribution functions for Thellier data without pTRM checks (solid line) and with pTRM checks (dotted line); bottom figure: the age distributions (Thellier without pTRM checks: +, Thellier with pTRM checks: circles)

Figure C.5 shows the results of the KS2 test for Thellier data with and without pTRM checks and ages between 0 and 5 Ma. There are 165 Thellier data with and 264 Thellier data without pTRM checks. The null hypothesis that both Thellier data with and without pTRM checks were drawn from the same underlying distribution can be rejected at the 91.3% confidence level. However, the age distribution of the data (bottom figure) shows the data most often occupy different age intervals.

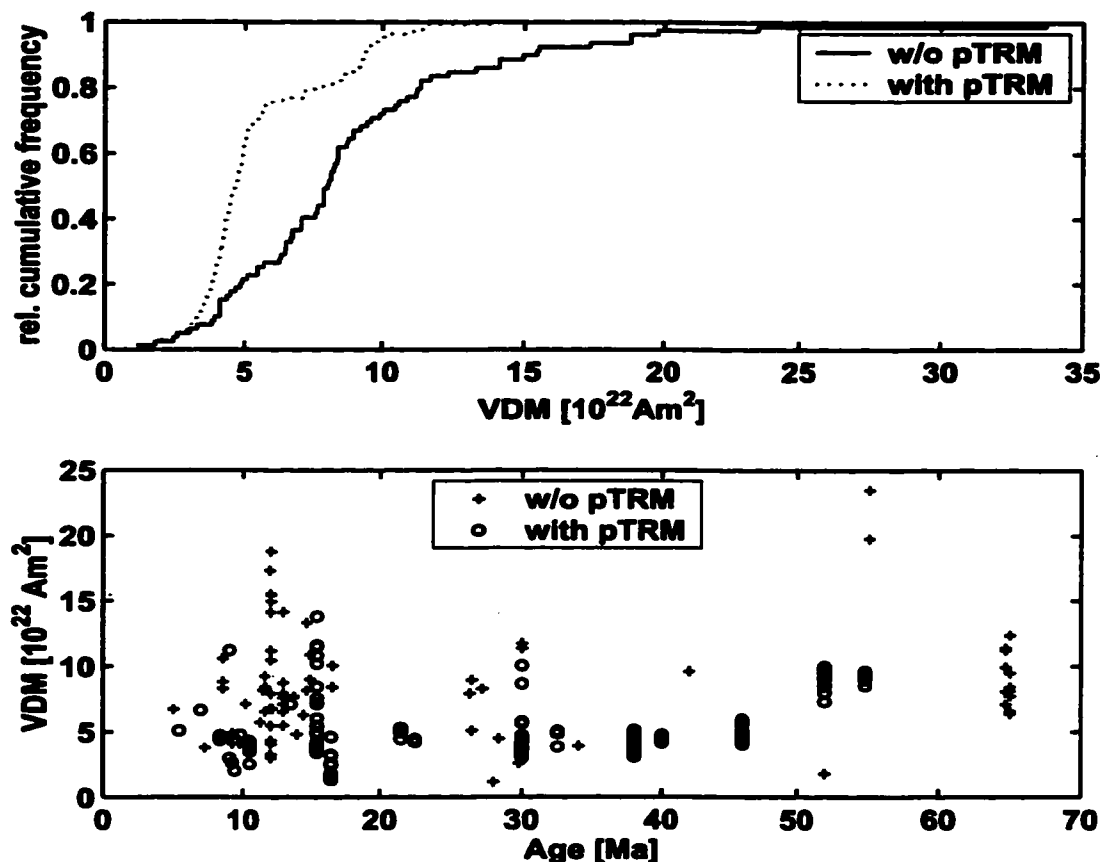


Figure C.6: Kolmogorov-Smirnov two-sample test for Thellier data with and without pTRM checks and ages between 5–65 Ma. Top figure: the cumulative distribution functions for Thellier data without pTRM checks (solid line) and with pTRM checks (dotted line); bottom figure: the age distributions (Thellier without pTRM checks: +, Thellier with pTRM checks: circles)

Figure C.6 shows the results of the KS2 test for Thellier data with and without pTRM checks and ages between 5 and 65 Ma. There are 79 Thellier data with and 138 Thellier data without pTRM checks. The null hypothesis that both Thellier data with and without pTRM checks were drawn from the same underlying distribution can be rejected at the 100% confidence level. However, the age distribution of the data (bottom figure) shows the data most often occupy different age intervals.

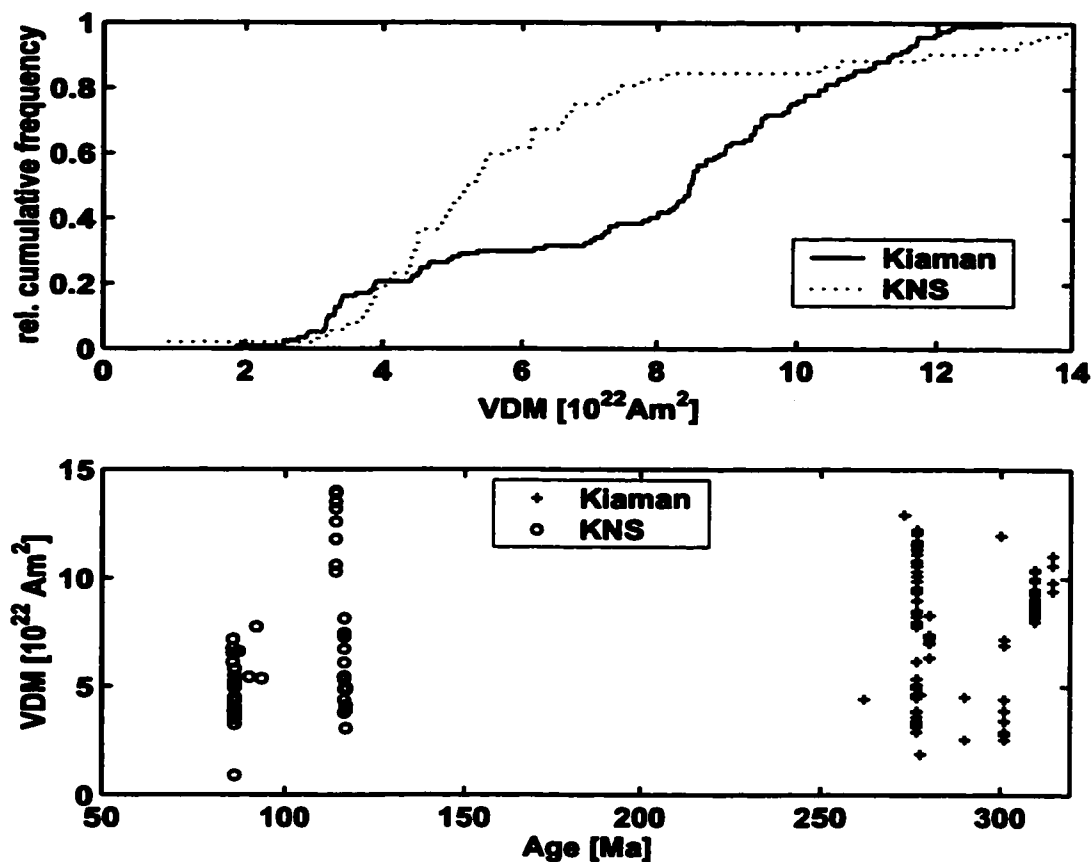


Figure C.7: Kolmogorov-Smirnov two-sample test for VDM data from the Kiaman and the KNS. Top figure: the cumulative distribution functions for Kiaman VDM data (solid line) and KNS VDM data (dotted line); bottom figure: the age distributions (Kiaman: +, KNS: circles)

Figure C.7 shows the results of the KS2 test for Thellier data from the Kiaman Reverse and the Cretaceous Normal Superchron. There are 117 Thellier data for the Kiaman and 52 Thellier data for the KNS. The null hypothesis that both datasets were drawn from the same underlying distribution can be rejected at the 100% confidence level. In this test there was no difference between the intensity methods used to obtain the data; thus, provided that there is no other source of systematic bias in the data, we conclude that the intensities during the Kiaman and the KNS were significantly different.

Appendix D

VDM DISTRIBUTIONS AND BIMODAL AND UNIMODAL MEAN VDM

In Chapter 4 the bimodality of VDM data between 5–320 Ma is investigated with a sliding window analysis where each age interval covers a minimum of $\Delta T_{\min} = 40$ Myr, and has at least $N_{\min} = 50$ data points. The window is shifted by at least $N_{\text{shift},\min} = 20$ data points between steps. This Appendix contains more details of this analysis including the individual VDM histograms with best bimodal and unimodal fits and the corresponding age distributions (Figure D.2 and Figures D.5 – D.9) as well as the VDM histograms for $\Delta T_{\min} = 20$ Myr, $N_{\min} = 50$ and $N_{\text{shift},\min} = 20$ (Figure D.1). Also given are histograms for the ‘non-sliding window’ case: no restrictions are made on the number of data points, the length of the age interval is 20 Myr (Figure D.3) and 40 Myr (Figure D.4).

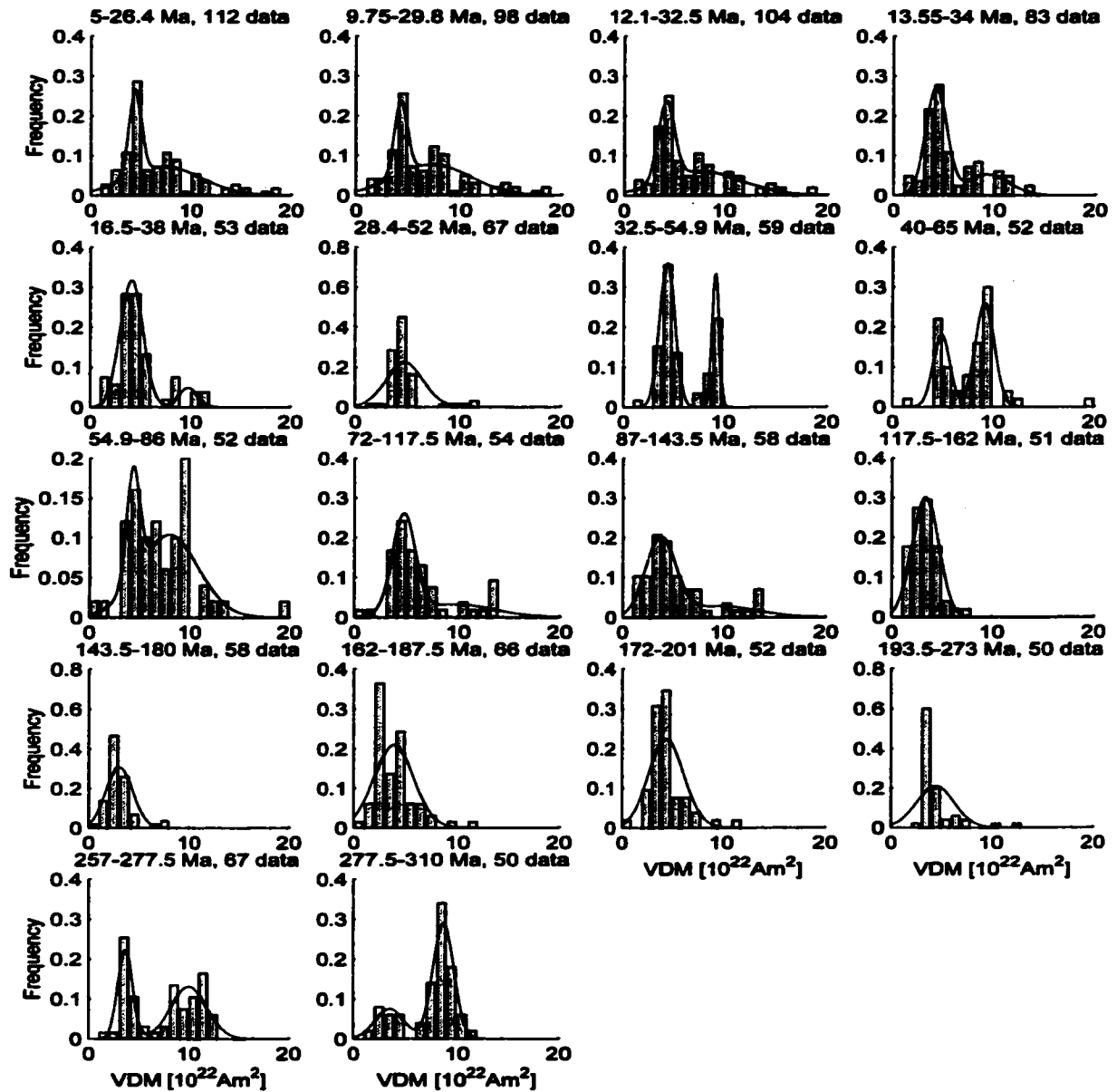


Figure D.1: Evolution of VDM data distribution for ages 5–320 Ma. Each histogram spans at least 20 Myr and has a minimum of 50 VDM data. The data window is shifted by at least 20 data points between groups. Minimum and maximum ages as well as the number of data are given at the top of each histogram. Histograms 6 and 12 through 16 include a unimodal and all others a bimodal normal fit. Only VDM less than $20 \times 10^{22} \text{Am}^2$ are plotted.

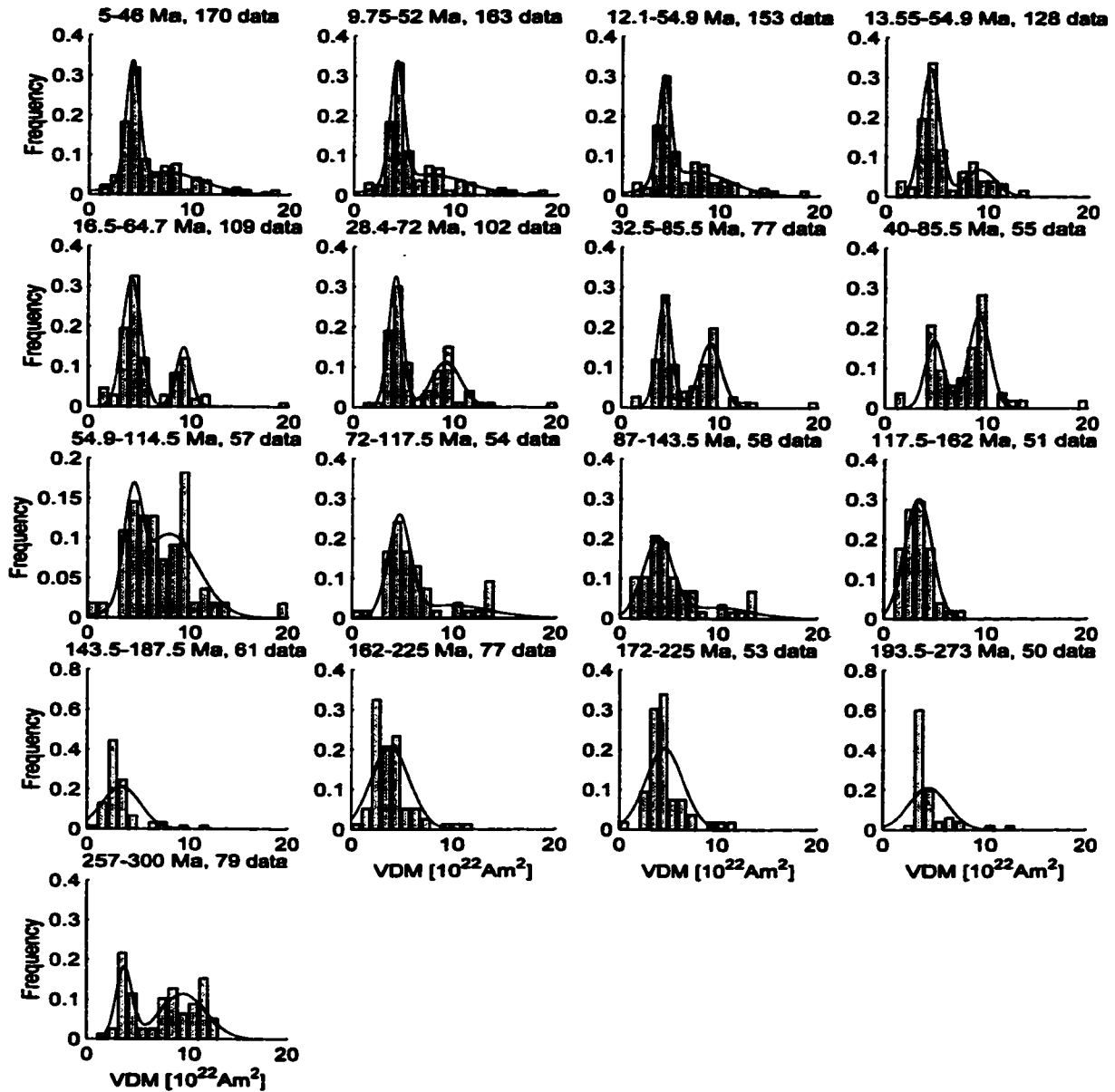


Figure D.2: Evolution of VDM data distribution for ages 5–320 Ma. Each histogram spans at least $\Delta t_{\min} = 40$ Myr and has a minimum of $N_{\min} = 50$ VDM data. The data window is shifted by at least 20 data points between groups. Minimum and maximum ages as well as the number of data are given at the top of each histogram. Histograms 12 through 16 include a unimodal and all others a bimodal normal fit. Only VDM less than $20 \times 10^{22} \text{Am}^2$ are plotted.

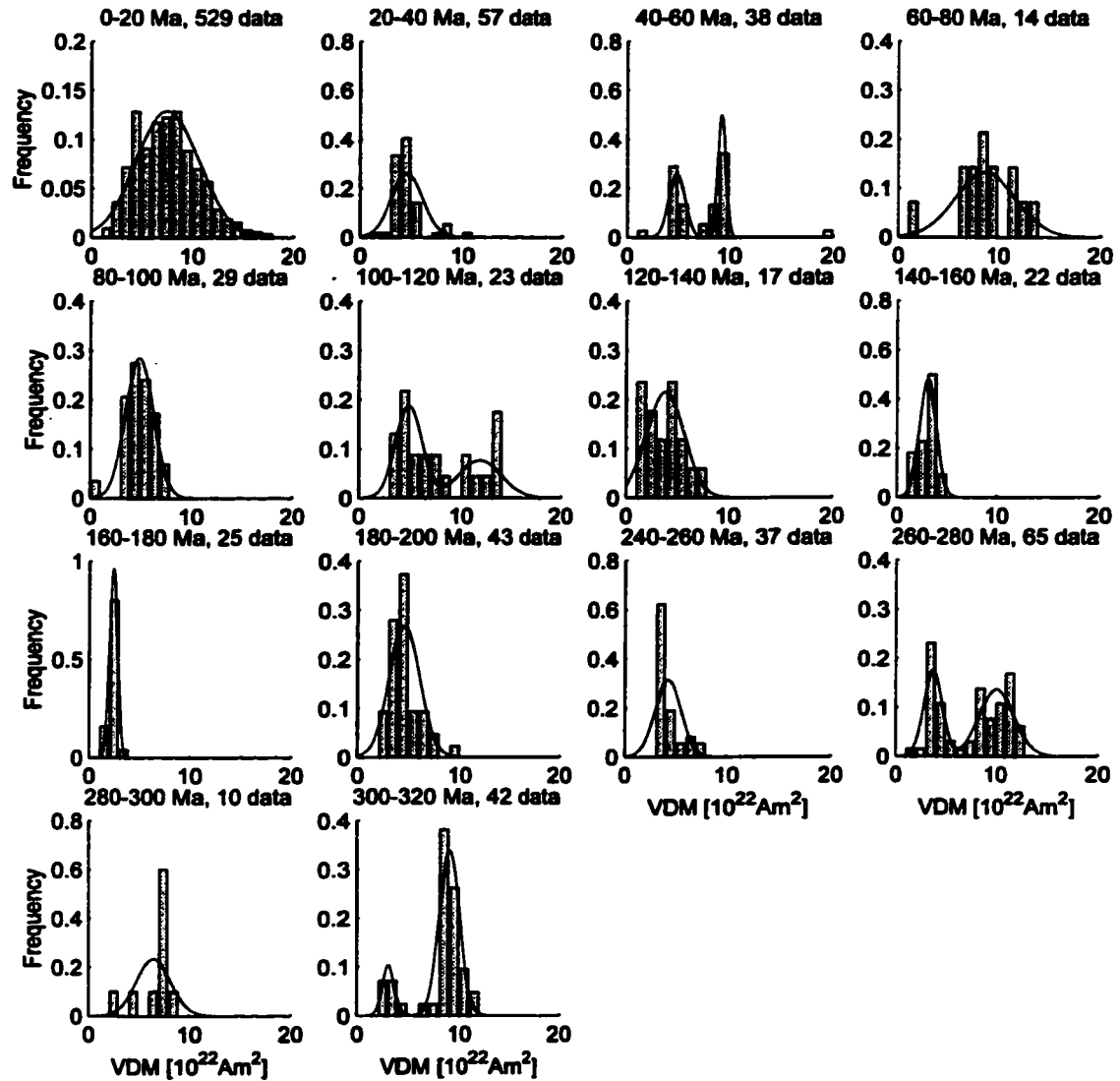


Figure D.3: Evolution of VDM data distribution for ages 0–320 Ma. Each histogram spans $\Delta t = 20$ Myr. Minimum and maximum ages as well as the number of data are given at the top of each histogram. Histograms 1, 2, 4, 5, 7, 8, 9, 10, 11 and 13 include a unimodal and all others a bimodal normal fit. Only VDM less than $20 \times 10^{22} \text{Am}^2$ are plotted.

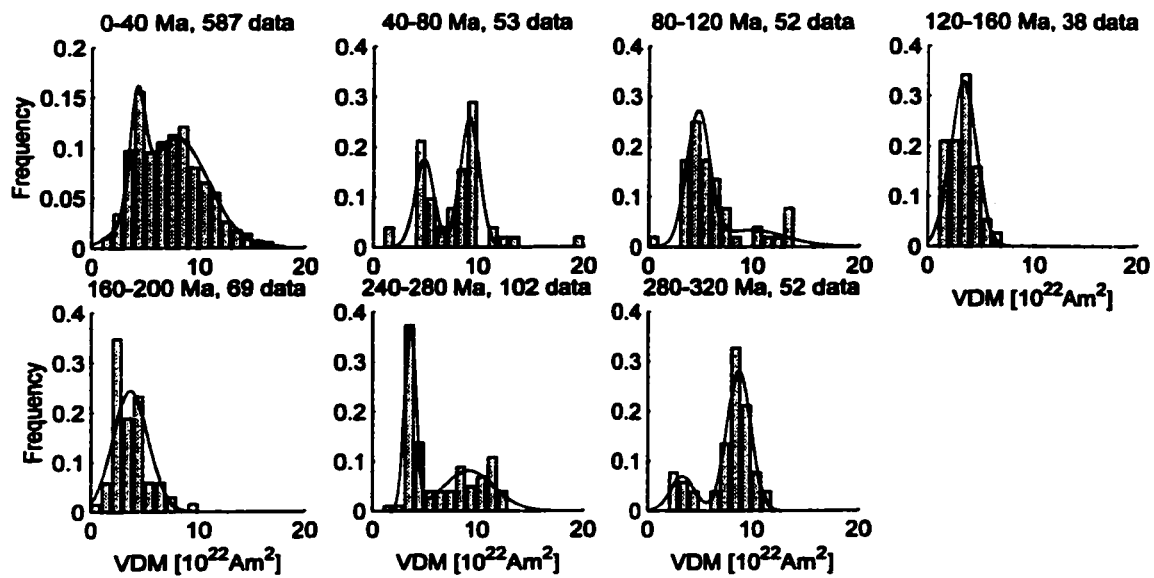


Figure D.4: Evolution of VDM data distribution for ages 0–320 Ma. Each histogram spans $\Delta t = 40$ Myr. Minimum and maximum ages as well as the number of data are given at the top of each histogram. Histograms 4 and 5 include a unimodal and all others a bimodal normal fit. Only VDM less than $20 \times 10^{22} \text{Am}^2$ are plotted.

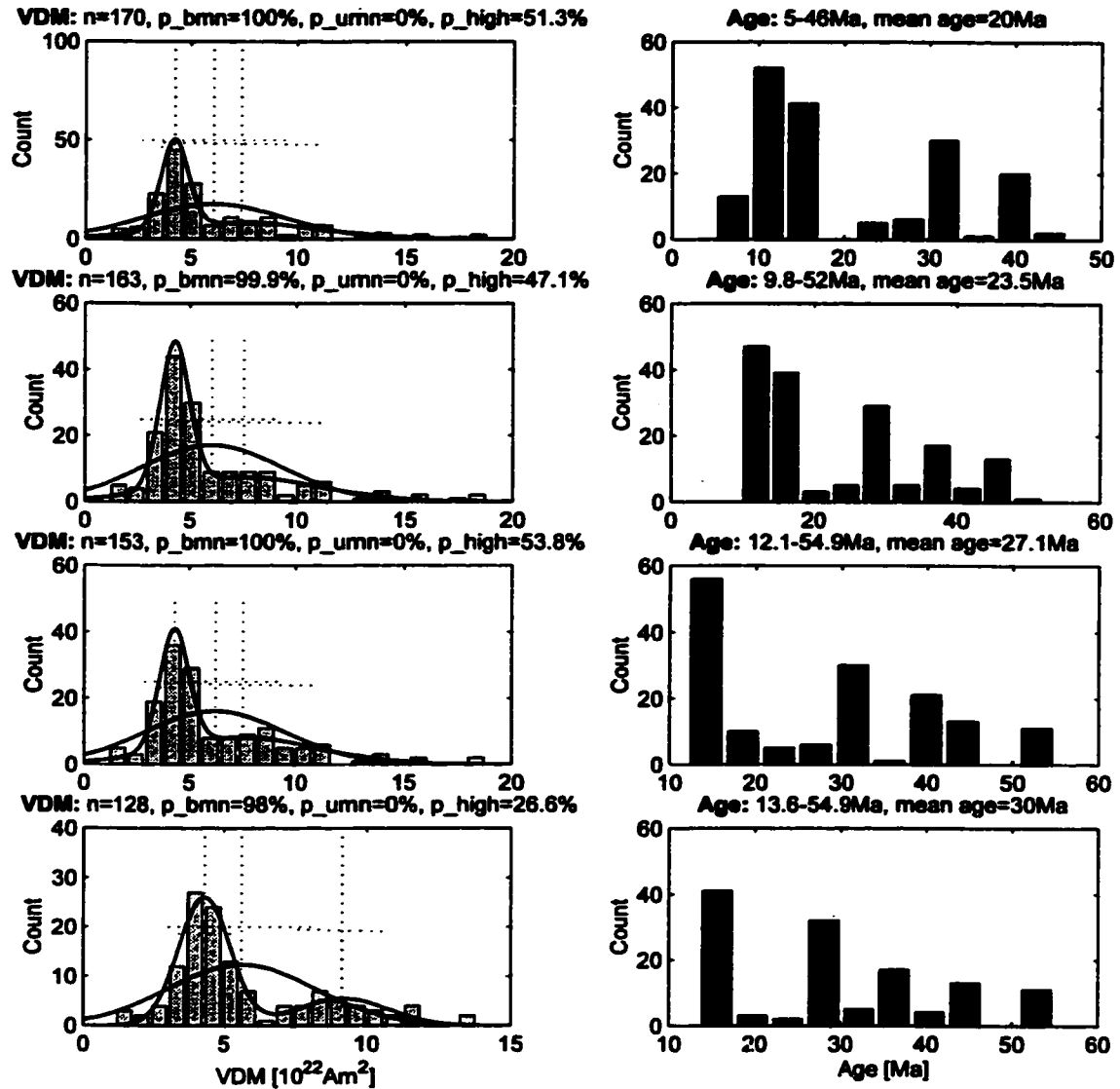


Figure D.5: Individual VDM data (left column) and corresponding age distributions (right column) for ages 5–320 Ma (part 1). Each VDM histogram spans at least $\Delta t_{min} = 40$ Myr and has a minimum of $N_{min} = 50$ VDM data. The data window is shifted by at least 20 data points between groups. The bimodal (unimodal) normal fit is shown as a black (grey) curve, bimodal high and low and unimodal means and standard deviations are indicated by dotted lines. At the top of the VDM histograms are given: n , the number of data points, the level of significance in the KS1 test for bimodal (p_{bmn}) and unimodal (p_{umn}) normal fit, and the percentage of the distribution due to the high intensity (p_{high}). At the top of the age histograms are given: Minimum and maximum ages as well as the mean age. Only VDM less than $20 \times 10^{22}Am^2$ are plotted.

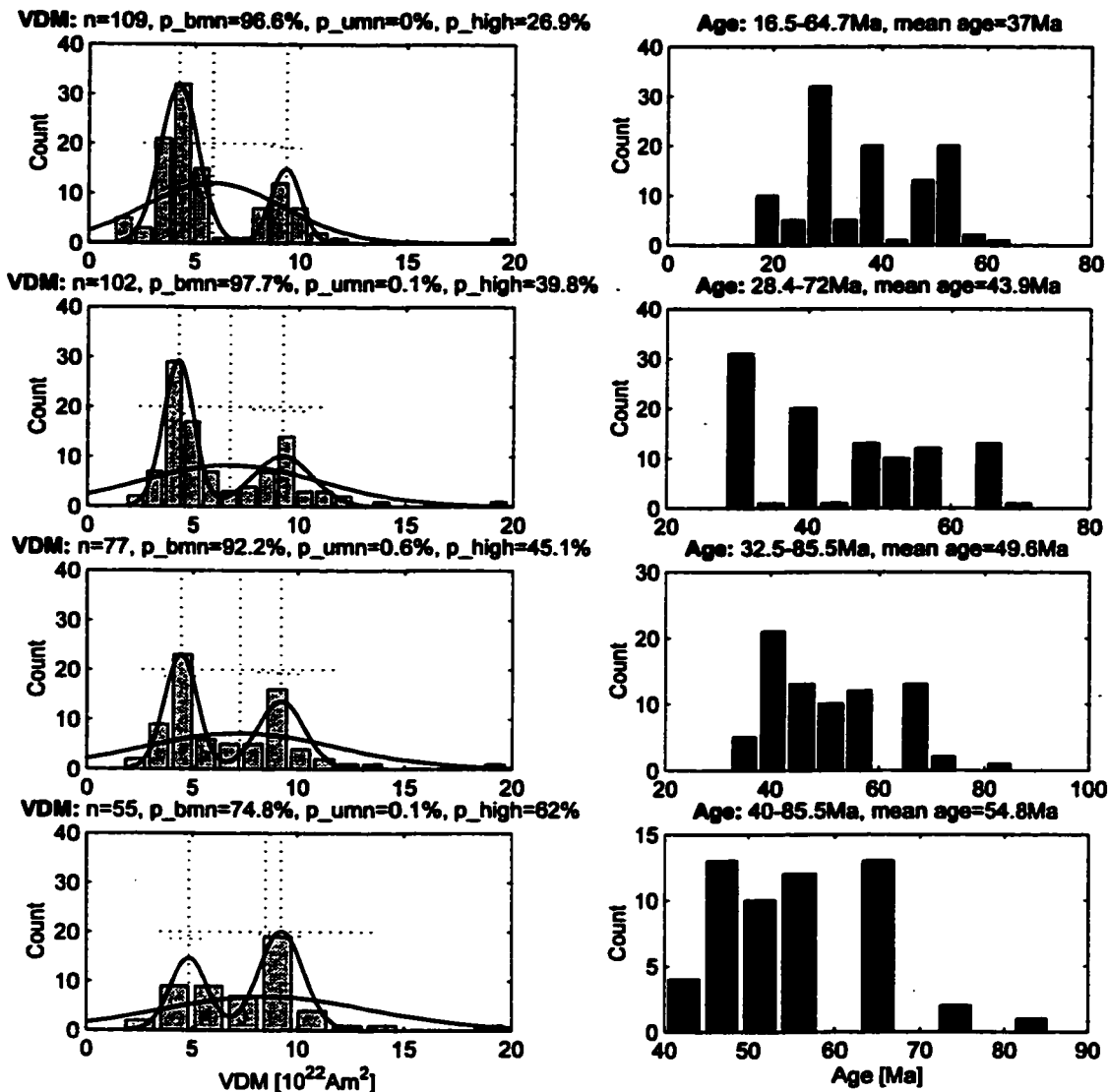


Figure D.6: Individual VDM data (left column) and corresponding age distributions (right column) for ages 5–320 Ma (part 2). Each VDM histogram spans at least $\Delta t_{\min} = 40$ Myr and has a minimum of $N_{\min} = 50$ VDM data. The data window is shifted by at least 20 data points between groups. The bimodal (unimodal) normal fit is shown as a black (grey) curve, bimodal high and low and unimodal means and standard deviations are indicated by dotted lines. At the top of the VDM histograms are given: n , the number of data points, the level of significance in the KS1 test for bimodal (p_{bmn}) and unimodal (p_{umn}) normal fit, and the percentage of the distribution due to the high intensity (p_{high}). At the top of the age histograms are given: Minimum and maximum ages as well as the mean age. Only VDM less than $20 \times 10^{22} \text{Am}^2$ are plotted.

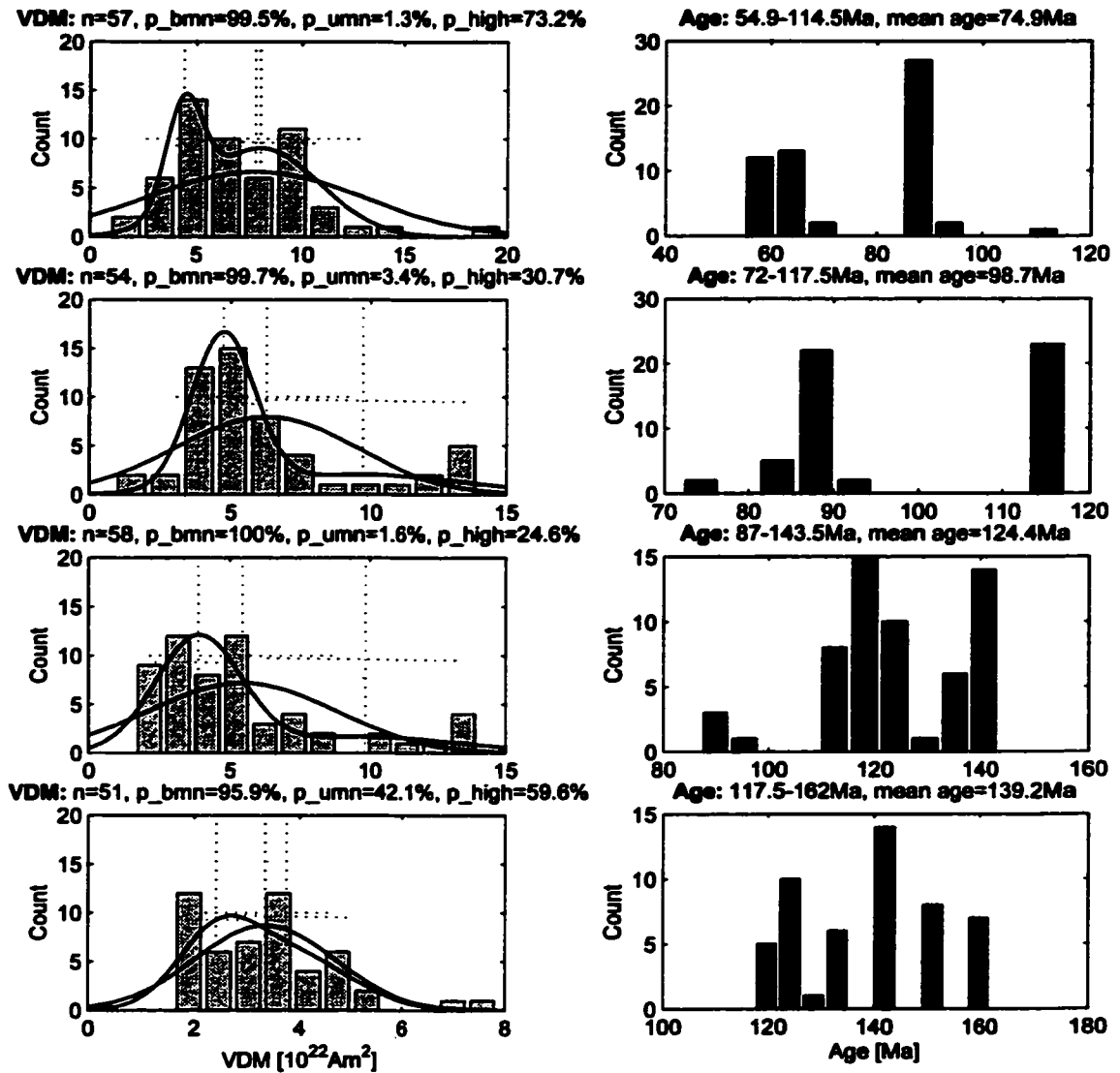


Figure D.7: Individual VDM data (left column) and corresponding age distributions (right column) for ages 5–320 Ma (part 3). Each VDM histogram spans at least $\Delta t_{\text{min}} = 40$ Myr and has a minimum of $N_{\text{min}} = 50$ VDM data. The data window is shifted by at least 20 data points between groups. The bimodal (unimodal) normal fit is shown as a black (grey) curve, bimodal high and low and unimodal means and standard deviations are indicated by dotted lines. At the top of the VDM histograms are given: n , the number of data points, the level of significance in the KS1 test for bimodal (p_{bmn}) and unimodal (p_{umn}) normal fit, and the percentage of the distribution due to the high intensity (p_{high}). At the top of the age histograms are given: Minimum and maximum ages as well as the mean age. Only VDM less than $20 \times 10^{22} \text{Am}^2$ are plotted.

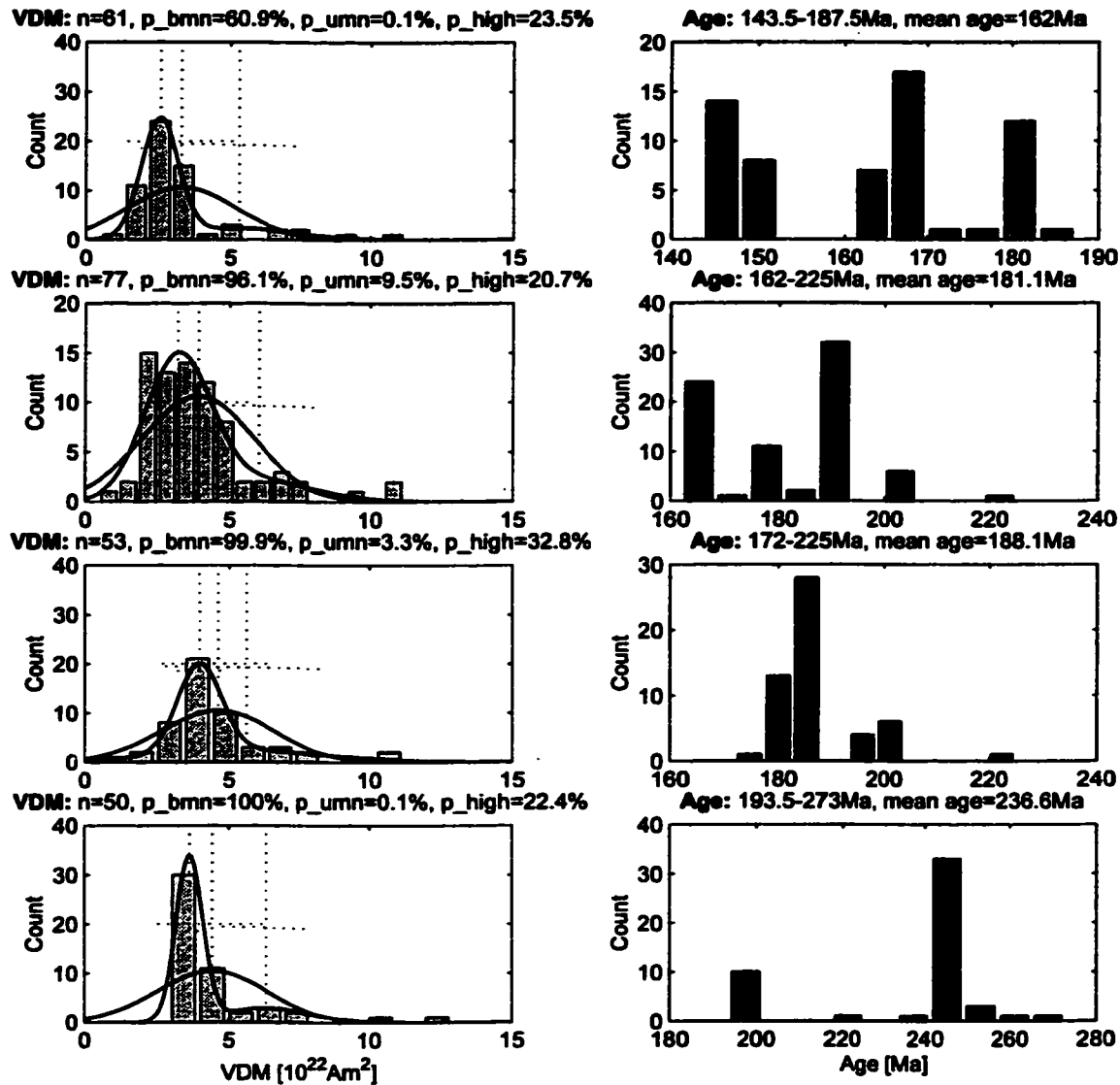


Figure D.8: Individual VDM data (left column) and corresponding age distributions (right column) for ages 5–320 Ma (part 4). Each VDM histogram spans at least $\Delta t_{\min} = 40$ Myr and has a minimum of $N_{\min} = 50$ VDM data. The data window is shifted by at least 20 data points between groups. The bimodal (unimodal) normal fit is shown as a black (grey) curve, bimodal high and low and unimodal means and standard deviations are indicated by dotted lines. At the top of the VDM histograms are given: n , the number of data points, the level of significance in the KS1 test for bimodal (p_{bmn}) and unimodal (p_{umn}) normal fit, and the percentage of the distribution due to the high intensity (p_{high}). At the top of the age histograms are given: Minimum and maximum ages as well as the mean age. Only VDM less than $20 \times 10^{22} \text{Am}^2$ are plotted.

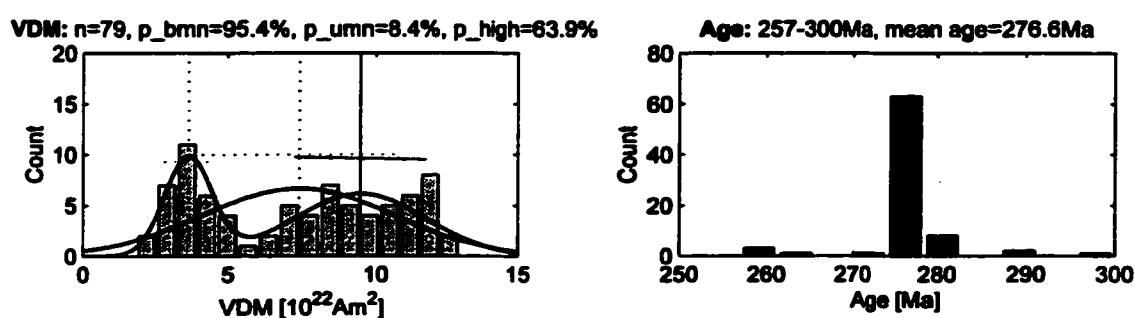


Figure D.9: Individual VDM data (left column) and corresponding age distributions (right column) for ages 5–320 Ma (part 5). Each VDM histogram spans at least $\Delta t_{\min} = 40$ Myr and has a minimum of $N_{\min} = 50$ VDM data. The data window is shifted by at least 20 data points between groups. The bimodal (unimodal) normal fit is shown as a black (grey) curve, bimodal high and low and unimodal means and standard deviations are indicated by dotted lines. At the top of the VDM histograms are given: n , the number of data points, the level of significance in the KS1 test for bimodal (p_{bmn}) and unimodal (p_{umn}) normal fit, and the percentage of the distribution due to the high intensity (p_{high}). At the top of the age histograms are given: Minimum and maximum ages as well as the mean age. Only VDM less than $20 \times 10^{22} \text{Am}^2$ are plotted.

VITA

Name: Rainer Heller

Date: December 20, 2001

Education

Diplom: Physics, Christian-Albrechts-Universität zu Kiel, Germany, 1996

Ph. D.: Earth and Space Sciences, University of Washington, 2001

Dissertation Title

Ph. D.: THE PALEOMAGNETIC FIELD'S LONG-TERM MEAN INTENSITY
AND SECULAR VARIATION